

1-1-2012

Structural Design Issues On GFRP-Reinforced Concrete Bridge Barriers

Ekaterina Tropynina
Ryerson University

Follow this and additional works at: <http://digitalcommons.ryerson.ca/dissertations>



Part of the [Civil Engineering Commons](#)

Recommended Citation

Tropynina, Ekaterina, "Structural Design Issues On GFRP-Reinforced Concrete Bridge Barriers" (2012). *Theses and dissertations*. Paper 1710.

This Thesis is brought to you for free and open access by Digital Commons @ Ryerson. It has been accepted for inclusion in Theses and dissertations by an authorized administrator of Digital Commons @ Ryerson. For more information, please contact bcameron@ryerson.ca.

STRUCTURAL DESIGN ISSUES ON GFRP-REINFORCED CONCRETE BRIDGE BARRIERS

BY

**Ekaterina Tropynina,
B.Sc., Ryerson University, Toronto, 2009**

A Thesis

Presented to Ryerson University

In partial fulfillment of the
Requirement for the degree of
Master of Applied Science

In the program of
Civil Engineering
Toronto, Ontario, Canada, 2012
Ekaterina Tropynina 2012©

AUTHOR'S DECLARATION FOR ELECTRONIC SUBMISSION OF A THESIS

I hereby declare that I am the sole author of this thesis. This is a true copy of the thesis, including any required final revisions, as accepted by my examiners.

I authorize Ryerson University to lend this thesis to other institutions or individuals for the purpose of scholarly research.

I further authorize Ryerson University to reproduce this thesis by photocopying or by other means, in total or in part, at the request of other institutions or individuals for the purpose of scholarly research.

I understand that my thesis may be made electronically available to the public.

ABSTRACT

In the era of bridge rehabilitation, glass fibre reinforced polymer (GFRP) bars are considered an alternative solution to steel reinforcement to eliminate steel corrosion. In this thesis, a new bridge barrier reinforcement layout was proposed incorporating GFRP bars with anchorage heads. However, it was observed that no design provisions or research data in the literature were found to design the anchorage at barrier-deck slab junction. As such, pullout tests were conducted on GFRP bars embedded in concrete slabs, to determine their pullout strength. Also, testing to-collapse of full-scale bridge barrier under static loading was conducted to determine its load carrying capacity. In addition, finite element analysis of the barrier wall and deck slab portion was performed in order to examine the level of accuracy of the specified factored applied moments due to vehicle impact at the barrier-deck junction. The experimental findings qualified the proposed GFRP-reinforced barrier detailing when subjected to simulated vehicle impact loading.

ACKNOWLEDGEMENTS

I would like to express my deep appreciation to Dr. Khaled Sennah for his continuous support throughout the project. Thanks to Mr. Nidal Jaalouk for his technical help during the experimental part of the thesis.

I would also like to thank other staff members of Civil Engineering department in Ryerson University for their assistance. I wish to thank Schoeck Canada limited for their financial support and encouragement.

TABLE OF CONTENTS

Abstract.....	iii
Acknowledgements.....	iv
Table of Contents.....	v
List of Tables.....	vii
List of Figures.....	viii
List of Symbols.....	xi
 Chapter 1: Introduction.....	 1
1.1 General.....	4
1.2 Problem Statement.....	5
1.3 Objectives.....	5
1.4 Scope of Work.....	5
1.5 Thesis Overview.....	6
 Chapter 2: Literature Review.....	 8
2.1 Fibre Reinforced Polymers Technology.....	8
2.1.1 Fibres	9
2.1.2 Resins.....	9
2.1.3 Manufacturing Process	11
2.1.4 Properties of FRP.....	11
2.1.5 Applications of FRPs in Structural Engineering	12
2.2 Background on Concrete Bridge Barrier Design.....	13
2.2.1 Traffic Barrier and Performance Levels.....	14
2.2.2 Crash Test Requirements.....	15
2.2.3 Barrier-deck Anchorage.....	16
2.2.4 Transverse moments in cantilever slabs due to railing loads.....	18
2.3. Previous Research on Concrete Barrier	20
2.4. Bond Mechanism.....	22
2.4.1 Bond Failure Modes.....	23
2.4.2 Determination of Bond Strength.....	25
2.4.3 Bond Strength and Development Length Equations in Design Codes.....	27
2.4.4 Development Length Equation of the Headed-End Bars.....	32
2.5. Previous Work on Pull Out tests.....	34
2.5.1 Effect of Properties of the FRP Bar on their bond behavior.....	35
2.5.2 Structural considerations.....	37
 Chapter 3: Pull out strength of GFRP bars.....	 40
3.1 General.....	40
3.2 Materials for the Pullout tests.....	41
3.3. Description of Slab Pull Out Specimens.....	44
3.4. Test setup for slab pull out test.....	45
3.5. Test Results and Discussions.....	49
3.6. Comparison to Code Predictions.....	57
3.6.1 CSA S806-02 Development Length.....	57

3.6.2 Development Length Equation Specified in CSA S06-06.....	58
3.6.3 Development Length Specified in ACI 440.1-06.....	59
3.6.4. Development Length of Headed Anchors according to CSA A23.3-04.....	60
3.7 Conclusions.....	61
Chapter 4: Experimental tests on GFRP-reinforced concrete barrier.....	62
4.1 General.....	62
4.2 Yield line Analysis.....	63
4.3 Proposed GFRP-Reinforced Barrier.....	65
4.4 Static Load Testing.....	66
4.5 Description of Test Samples.....	66
4.6 Test Setup.....	73
4.7 Test Results an Discussions.....	75
4.8. Discussion of Test Results and Correlations with CHBDC Design Values.....	83
4.9 Analytical Investigation of Punching Shear Failure of the Samples.....	93
4.9.1 Punching Shear Models.....	94
4.9.2 Comparison between Predicted and Experimental Results.....	96
Chapter 5: Finite-element modeling of barrier –deck system.....	97
5.1 General.....	97
5.2 Parametric Study.....	98
5.2.1 Key Parameters.....	98
5.3 FEM SAP2000 Modeling.....	99
5.4. FEA Results and Discussions.....	102
5.4.1 PL-3 Barrier.....	102
5.4.2 PL-2 barrier with tapered face and PL-2 Parapets with constant thickness	104
5.5 Summary of the Findings.....	105
Chapter 6: Conclusions	111
6.1 General.....	111
6.2 Conclusions.....	111
Appendix A.....	115
Appendix B.....	117
References.....	118

LIST OF TABLES

Table 1.1	Transverse moments in cantilever slabs due to horizontal railing loads in selected PL-3 and PL-2 barriers. (CHBDC Commentary, 2006).....	6
Table 2.1	Traffic Barrier Loads, from Figure 3.8.8.1, <i>CAN/CSA-S6-00</i>	16
Table 2.2	Summary of phases for the splitting and pullout modes of failure. (Ametrano, 2011).....	24
Table 2.3	Tension development length, l_d , for GFRP bars with ribbed surface for normal density concrete ($k_1 = 1$).....	34
Table 3.1	Nominal Diameter and Sectional Area of Schoeck ComBAR®.....	42
Table 3.2	Material properties of Straight ComBAR (Schoeck ComBAR Technical Information).....	42
Table 3.3	Dimensions and Anchorage Forces for ComBAR Heads.....	43
Table 3.4	Summary of test specimens	44
Table 3.5	Results from Slab Pullout Test	57
Table 3.6	Mean value of the maximum loads obtained from slab pullout tests	56
Table 3.7	Parameters for development length equation specified in CSA S806-02.....	58
Table 3.8	Development length results based on development Length Equation specified in CSA S806-02.....	58
Table 3.9	Parameters for the development length equation specified in CSA S06-06.....	59
Table 3.10	Required development length requirement based on CSA S06-06.....	59
Table 3.11	Parameters for the developable bar stress equation specified in ACI 440.1-06.....	59
Table 3.12	Development length requirement per ACI 440.1-06	60
Table 3.13	Parameters for the Equation 3.7 specified in CSA A23.3-04	61
Table 3.14	Embedment length of the headed anchor based on concrete breakout capacity	61
Table 4.1	Ratio of test result-to-predicted punching shear capacity.....	96
Table 5.1	Finite Element Results for PL-3 barrier.....	107
Table 5.2	Finite Element Results for PL-2 Barrier Wall.....	108
Table 5.3	Finite Element Results for PL-2 Parapet Wall.....	109
Table 5.4	Proposed design table for barrier-deck joint.....	110

LIST OF FIGURES

Figure 1.1	Corrosion-induced degradation of steel-reinforced bridge barrier wall.....	2
Figure 1.2	View of GFRP bars with cast heads.....	2
Figure 1.3	Conventional steel reinforced bridge barrier on the right and proposed GFRP reinforced bridge barrier on the left.	3
Figure 2.1	Various FRP Products Used For Reinforcement Of Concrete Structures. (Source: Newhook And Svecova, 2006).....	8
Figure 2.2	Schematic illustration of the pultrusion manufacturing process. (Technical Information ComBAR, Schoeck, 2011).....	11
Figure 2.3	Stress-strain curves of FRP (ACI 440-96).....	12
Figure 2.4.	Application of traffic design loads to traffic barriers, from Figure 12.5.2.4, <i>CAN/CSA-S6-00</i>	17
Figure 2.5	Cracking and damage mechanisms in bond: (a) End view showing splitting cracks between bars and concrete cover; (b) Side view of member showing shear crack and/or local concrete crushing due to bar pullout. (Source: ACI 408R-03).....	23
Figure 2.6	Bond stress versus slip. (Source: Harajli <i>et al.</i> , 2004).....	25
Figure 2.7	Possible Failure modes (Steel Rebar).....	25
Figure 2.8	Variation of bond force along length of rebar in reinforced concrete member subjected to bending: (a) cracked concrete member; (b) bond forces on rebar; (c) variation of tensile forces along rebar; (d) variation of bond force acting on reinforcing bar (Source: ACI 408R-03).....	26
Figure 3.1	GFRP bar head details (Schoeck, 2011).....	40
Figure 3.2	Views of the formwork for casting concrete slabs with embedded GFRP bars.....	45
Figure 3.3	Test setup for slab pullout testing.....	46
Figure 3.4	Views of steel grips used in pullout tests, clamping the bar from two opposite sides.....	47
Figure 3.5	View of (a) test setup with steel grips and (b) bar damage due to gripping on the bar during testing.....	47
Figure 3.6	Metal rope wrapped around a 12-mm diameter bar at the grip location.....	47
Figure 3.7	Views of the revised testup showing the added large grip shown in (b), clamping the bar from two oppsite sides	48
Figure 3.8	Views of bar rupture at the location of the large grip	48
Figure 3.9	Views of the manufactured grip with conical wedges clamping the bars from all sides.....	49
Figure 3.10	Views of the bar rupture at grip location during pullout tests	50
Figure 3.11	Views of the bar rupture along its free length during pullout tests.....	51
Figure 3.12	Views of the bar pullout from the concrete slab after the test showing concrete shearing	51
Figure 3.13	Views of the combined bar pullout and concrete breakout (conical failure) at top surface of concrete slab.....	52
Figure 4.1	LRFD yield-line analysis of barrier wall (AASHTO, 2004).....	64
Figure 4.2	Schematic diagram of the Reinforcement for the constructed barrier wall....	68

Figure 4.3 View of reinforcement in the constructed PL-3 barrier.....	68
Figure 4.4 Close-up view of the deck cantilever reinforcement and the GFRP bars with headed end to be embedded in the deck slab.....	69
Figure 4.5 View of the barrier after Construction.....	69
Figure 4.6 Schematics diagram of the barrier showing control joints and load locations	69
Figure 4.7 Front view of Sample 1.....	70
Figure 4.8 View of LVDT location in Sample 1: two LVDTs at the top of the wall oriented horizontally and 2 LVDTs at the bottom of the deck edge oriented vertically.....	70
Figure 4.9 Back view of Sample 2 showing 2 LVDTs at the top of the barrier oriented horizontally and 2 LVDTs at the bottom of the deck edge oriented vertically.....	71
Figure 4.10 View of back face of Sample 3 showing 5 LVDTs placed at the top of the wall and oriented horizontally and 3 LVDTs placed at the bottom of the deck edge and oriented vertically.....	71
Figure 4.11 View of back face of Sample 4 showing 5 LVDTs oriented horizontally at the top of the wall and 3 LVDTs oriented vertically at the bottom of the deck edge.....	72
Figure 4.12 View of back face of Sample 5 showing 5 LVDTs oriented horizontally at the top of the wall and 3LVDTs oriented vertically at the bottom of the deck edge.....	72
Figure 4.13 Schematic section of the test setup.....	73
Figure 4.14 Schematic plan view of the test setup.....	74
Figure 4.15 Views of the test setup and sensor location at (a) front and (b) back of the barrier wall at interior load location.....	74
Figure 4.16 Views of the test setup and sensor location at (a) front and (b) back of the barrier wall at end load location.....	74
Figure 4.17 Crack pattern in the side of Sample 1.....	75
Figure 4.18 Crack pattern in the front side of Sample 1.....	76
Figure 4.19 Crack pattern in side of Sample 2.....	77
Figure 4.20 Crack pattern in front of Sample 2.....	77
Figure 4.21 Crack pattern in the back face of Sample 3 at barrier end location.....	78
Figure 4.22 Crack Pattern at side of Sample 3 at barrier end location.....	79
Figure 4.23 Crack Pattern in front of Sample 3 and barrier end location.....	79
Figure 4.24 Cracks appeared at front face during testing at interior load location.....	80
Figure 4.25 Punching shear crack appeared at end of the test at interior load location...	80
Figure 4.26 Views of the punching shear failure at the end of the test of barrier segment loaded at control joint.....	81
Figure 4.27 Views of punching shear failure of barrier segment loaded at mid-length between two control joints	82
Figure 4.28 Load-deflection relationship of the 1m barrier wall	84
Figure 4.29 Load-deflection relationship of the barrier wall of 150-mm spacing between vertical bars at the front face.....	85
Figure 4.30 Views of (a) the projecting steel dowels from foundation wall that are (b) welded to deck cantilever steel reinforcement.....	85

Figure 4.31	Load-deflection relationship of the barrier wall loaded at end location.....	86
Figure 4.32	Load-deflection relationship of the deck cantilever of the barrier wall loaded at its end.....	87
Figure 4.33	Load-deflection relationship for the deck of barrier segment at control joint	88
Figure 4.34	Load-deflection relationship for the deck cantilever of barrier segment at control joint.....	89
Figure 4.35	Load-horizontal concrete strain relationship at the back face of the for barrier segment loaded at mid-length between two control joints.....	89
Figure 4.36	Load-deflection relationship for barrier segment loaded at mid-length between two control joints.....	91
Figure 4.37	Load-deflection relationship for the deck cantilever of barrier segment at mid-length between two control joints.....	91
Figure 4.38	Load-horizontal concrete strain relationship at the back face of the for barrier segment loaded at mid-length between two control joints.....	92
Figure 4.39	Critical perimeter at internal portion of the barrier wall.....	93
Figure 4.40	Critical perimeter at the end portion of the barrier wall.....	93
Figure 5.1	Elevation and Section of PL- 2 Parapet FE Model.....	100
Figure 5.2	Plan view of PL-2 Parapet FE Model.....	100
Figure 5.3	Elevation of PL-2 Barrier wall FE Model.....	101
Figure 5.4	Elevation of PL-3 Barrier Wall FE Model.....	101
Figure A.1	Moment Diagram for PL-2 Barrier Wall with load application at the end of the wall.....	122
Figure A.2	Moment Diagram for PL-2 Barrier Wall. Load application at inner portion of the wall.....	123
Figure B.1	16M bar position in concrete slab, casted for pullout tests and dimensions of the casted slab.....	124
Figure B.2	12M bar position in concrete slab, casted for pullout tests and dimensions of the casted slab.....	124

LIST OF SYMBOLS

- a** Depth of an equivalent rectangular stress block, mm
- A_b** Area of rebar,
- A_{cv}** = Area of concrete subjected to shear
- A_{frp}** = area of FRP bar, mm²
- A_s** = area of reinforcing bars on the flexural tension side of a member, mm²
- A_{vf}** = Dowel area cross shear plane
- A_{se}** = effective cross-sectional area of anchor
- A_{tr}** = Area of transverse reinforcement normal to the plane through the anchored bars, mm.
- b** = average width of the segment, mm
- d_b** = rebar diameter (mm);
- c** = cohesion factor = 0.52 MPa
- C** = The lesser of the cover to the center of the bar or one-half of the center-on-center spacing of the bars being developed;
- C/d_b** = Cover to diameter ratio. Should not be taken larger than 3.5.
- d** = effective depth (distance from the extreme compression fiber to the centroid of the tensile force), mm
- d_b** = Diameter of the bar, mm.
- d_{cs}** = The smaller of: (a) the distance from the closest concrete surface to the centre of the bar being developed; or (b) two-thirds of the centre-to-centre spacing of the bars being developed. The value shall not be taken greater than 2.5 d_b, mm.
- E_{FRP}** = Modulus of elasticity of FRP, MPa.
- E_s** = Modulus of elasticity of steel, 200x10 MPa.
- f'_c** = specified compressive strength of concrete, MPa
- √f'_c** = Square Root of Concrete Compressive Strength, MPa, max. permissible value should be 8MPa.
- f_s** = tensile strength in reinforcing bars, MPa
- f_F** = Design Stress in FRP tension reinforcement at Ultimate Limit State, MPa
- f_{FRP}** = Stress in FRP reinforcement, MPa.

f_{cr} = Flexural cracking strength of concrete, MPa. Equal to: (a) $0.4\sqrt{f'_c}$ for normal density concrete; (b) $0.34\sqrt{f'_c}$ for semi-low density concrete; (c) $0.3\sqrt{f'_c}$ for low density concrete. The value of $\sqrt{f'_c}$ used to compute f_{cr} must be less than 8MPa.

f_{ut} = specified tensile strength of an anchor

f_y = Yield stress of steel, Mpa.

h = height of the barrier, mm

h_{ef} = effective anchor embedment length

k = coefficient for factored concrete breakout resistance in tension

k_1 = Bar location factor: 1.3 for horizontal reinforcement placed so that more than 300 mm of fresh concrete cast in the member below development length or splice; 1.0 for all other cases.

k_2 = Concrete density factor: 1.3 for structural low-density concrete; 1.2 for structural semi- low-density concrete; 1.0 for normal density concrete.

k_3 = Bar size factor: 0.8 for $A_b < 300\text{mm}^2$; 1.0 for $A_b > 300\text{mm}^2$.

k_4 = Bar fibre factor: 1.0 for CFRP and GFRP; 1.25 for AFRP.

$k_{4(CHBDC)}$ = Bar surface factor representing the ratio of bond strength of FRP to that of steel rebar having the same cross-sectional area, but not greater than 1.0. In absence of manufacturer or test data, 0.8 shall be used.

k_5 = Bar surface profile factor. Can be taken as less than 1.0, but not less than 0.5, if this value has been shown by experiment. In the absence of direct experimental results the following values are used: 1.0 for surface-roughened or sand coated surfaces; 1.05 for spiral pattern surfaces; 1.0 for braided surfaces; 1.05 for ribbed surfaces; 1.80 for indented surfaces.

k_{tr} = transverse reinforcement index, mm

l = embedment length of rebar (mm);

L_c = critical wall length, mm

l_d = Development length of FRP bars in Tension, mm

l = Embedment length of bar in concrete, mm

L_t = Length of load application, mm

M = resisting moment, $N \times m$

M_b = Moment due to the top railing, if any, $N \times m$

M_c = Moment about horizontal axis, $N \times m$

M_w = Moment about the vertical axis, $N \times m$

n = Number of bars being developed or spliced.

n (A23.3-04) = number of anchors in the group

N_{br} = factored concrete breakout resistance in tension of a single anchor in cracked concrete.

N_{sr} = factored resistance of a single anchor or group of anchors in tension as governed by steel resistance.

P_c = Permanent compressive force = 8.02 N/mm

R = resistance modification factor

s = Spacing of transverse reinforcement, mm

Ø_c = resistance factor of concrete

Ø_s = resisting factor for reinforcing bars;

α = parameter defined by $0.85 - 0.0015f'_c \geq 0.67$;

k = Bar location factor: 1.5 for horizontal reinforcement placed above 300 mm of concrete; 1.0 for bars with less than 300 mm of concrete below.

μ = friction factor = 0.6

μ = average bond stress (MPa);

CHAPTER 1

INTRODUCTION

1.1 General

Bridges built prior to the 1970's did not use air-entrained concrete and coated reinforcing steel bars to protect from the effects of freeze-thaw cycles and the application of winter de-icing salt. This leads to corrosion-induced degradation in bridge elements as shown in Fig. 1.1. Accordingly, exposed bridge elements are all likely candidates for expensive replacement on the majority of these older bridges. It is estimated that over 40% of all bridges in Canada are older than 40 years and are in need of rehabilitation or replacement. The backlog of maintenance, rehabilitation and replacement of highway bridges is estimated at \$10 billion. The current traditional bridge rehabilitation/replacement systems in most situations are very time consuming and costly. The prohibitive costs needed to upgrade bridge structures require the development of innovative technologies to bridge replacement/repair; and provide sustainable bridge systems that prolong the service life of the structure (Sennah et al, 2011).

In November 2007, The Residential and Civil Construction Alliance of Ontario, Canada, (RCCAO, 2007) released a report on the state of Ontario bridges, entitled "Ontario's Bridges: Bridging the Gap." The report warns that the integrity of Ontario's municipal bridge infrastructure and public safety are at risk after years of deferred maintenance, irregular inspections, and lack of government oversight. Recent media coverage on bridge collapses in Laval, Quebec and Minneapolis, Minnesota, has highlighted the serious consequences of postponing actions to rehabilitate or reconstruct deteriorated bridges and the urgent need to take timely responsible action to safeguard the public from potential infrastructure failure. The study noted that many of Ontario's bridges were built in the 1950s and 1960s, and "it is expected that most bridges will require costly rehabilitation or replacement after 50 years of life." According to the Provincial Auditor's report in 2004, almost one-third of the approximately 2,800 provincial bridges under Ministry of Transportation of Ontario's (MTO) jurisdiction are in need of major rehabilitation or maintenance based on MTO's own figures. For the estimated 12,000 municipal bridges in Ontario, the RCCAO report stated that there is a lack of information on their conditions and a capital investment of at least \$2 billion will be required over the next five years to rehabilitate this aging infrastructure. The RCCAO report stated some recommendations



Fig. 1.1 Corrosion-induced degradation of steel-reinforced bridge barrier wall

to be made to promote the public's safety and the sustainability of Ontario's bridges. One of these recommendations includes promoting bridge engineering designs that improve the life expectancy and reduce maintenance costs of bridges. .



Fig. 1.2 View of GFRP bars with cast heads

Fibre-reinforced polymers (FRPs), as non-corrodible materials, are considered as an alternative to reinforcing steel bars in bridge decks and barrier walls to overcome steel corrosion-related problems. The GFRP bars used in this study have tensile strength of 1100 MPa, compared to 400 MPa yield strength of the reinforcing steel bars.

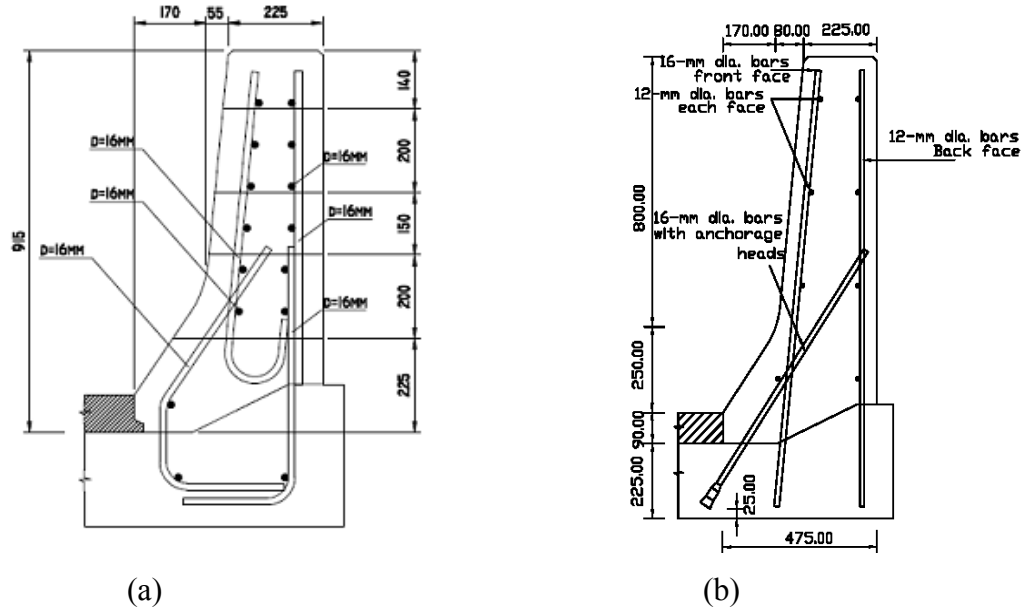


Fig. 1.3 Conventional steel reinforced bridge barrier on the right and proposed GFRP reinforced bridge barrier on the left.

The special “ribbed” surface profile of these bars, shown in Fig. 1.2, ensure optimal bond between concrete and the bar. Until recently, the installation of GFRP bars was often not convenient by the fact that bent bars have to be produced in the factory since GFRP bars cannot be bent at the site. Also, bent GFRP bars are much weaker than straight bars, due to the redirection of the fibres in the bend. As a result, number of bent GFRP bars is increased and even doubled at such locations where bar bents are required. This type of barrier configuration is shown in Fig. 1.3(a). The use of headed-end GFRP bars is intended to eliminate the unnecessary and expensive use of custom made bar bents. In the proposed GFRP bar arrangement in PL-3 bridge barrier shown in Fig. 1.3(b), GFRP bars with headed ends are used as straight bars at the inside face of the barrier walls with an end head at the bottom to reduce their development length in the deck slab, avoiding the use of hooks. This headed end is made of a thermo-setting polymeric concrete with a compressive strength far greater than that of normal grade concrete. It is cast onto the end of the straight bar and hardened at elevated temperatures. The concrete mix contains an alkali resistant Vinyl Ester resin, the same material used in the straight bars, and a mixture of fine aggregates. The outer diameter of the end heads is 2.5 times the diameter of the bar. The head of the 16-mm diameter bar is 100 mm long. It begins with a wide disk, which

transfers a large portion of the load from the bar into the concrete. Beyond this disk, the head tapers in five steps to the outer diameter of the blank head. This geometry ensures optimal anchorage forces and minimal transverse splitting action in the vicinity of the head.

1.2 Problem statement

Steel corrosion in reinforced concrete structures creates significant problems in terms of their strength and service life. An alternative use of GFRP reinforcement in bridge barriers was introduced to solve such problems. The design process of bridge barrier walls specified in the Canadian Highway Bridge Design Code, CHBDC, (CSA, 2006a; CSA, 2006b) is based on the AASHTO Guide Specification for bridge railings (AASHTO, 1989) and the AASHTO Guide for Selecting, Locating and Designing Traffic Barriers (AASHTO, 1977). CHBDC specifies that bridge barriers should be crash tested to comply with certain criteria for structural adequacy, occupant risk, and vehicle trajectory after collision. For barrier-to-deck slab anchorage, CHBDC specifies that if crash test results for the anchorage are not available, the anchorage and the deck should be designed for the maximum bending moment, shear and pullout loads that can be transmitted to them by the barrier wall. This can be achieved by the manual calculation using a generally established theory or evaluation of a full-scale prototype by a static load test. The latter is the subject of this thesis for the barrier-deck anchorage compliance with code design values in addition to the load carrying capacity of the barrier wall to resist simulated vehicle impact loading. In addition, there is no available data for pullout strength of the GFRP bars and therefore moment capacity of barrier-deck joint can be determined by experimental testing. Also, pullout tests of the reinforcing GFRP materials have to be performed in order to verify bonding properties between the bar and the surrounding concrete. For the design of the barrier-deck junction under bending moment resulting from vehicle impact, CHBDC Commentary (CSA, 2006b) specifies factored bending moments at this junction at interior location and end locations of the barrier as shown in Table. 1.1 to assist in the design of the amount of vertical reinforcement at the inside face of the barrier wall. However, CHBDC Commentary did not specify the transverse length of deck overhang on which barrier is located. It is believed that the length of transverse overhang should influence the factored design moment at the barrier-deck junction. There are different scenarios of barrier-deck configuration (i.e. fixed base simulating

the case of the barrier supported over thick voided or solid slab bridge superstructure and the case of barriers supported over deck slab cantilever of different length which is the case of deck slab-on-girder bridges). Therefore, finite element analysis needs to be performed in order to investigate whether the deck cantilever would change the factored design moment at the barrier-deck joint as opposed to the case of barrier wall full-fixed to virtually non-deformable thick slab.

1.3 Objectives

The objectives of this study include:

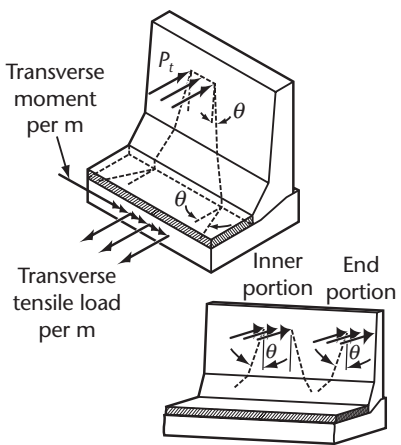
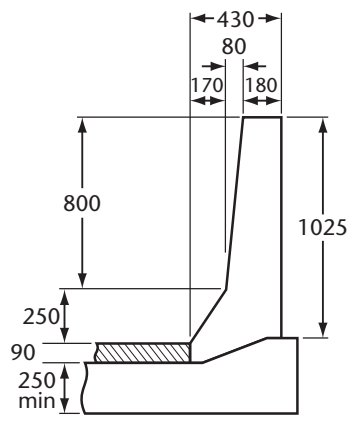
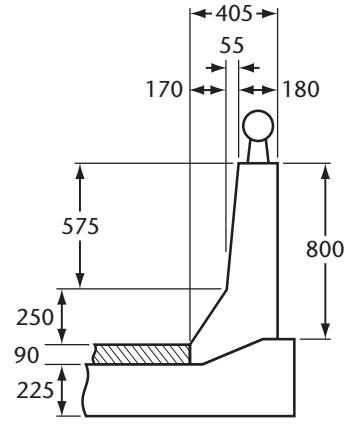
1. Investigating the pullout behavior of the GFRP bars with and without headed ends, embedded in concrete;
2. Evaluate, using finite-element modeling, the level of confidence of the specified CHBDC values of the factored applied moment at the barrier-deck junction due to vehicle impact; and
3. Testing to-collapse full-scale deck-barrier of the proposed GFRP-reinforcement detailing in PL-3 barrier wall to investigate its failure mode and load carrying capacities.

1.4 Scope of work

The scope of work of this study includes:

1. Performing pullout tests on GFRP bars with ribbed-surface, considering key parameters such as embedment length, bar size and end condition (i.e. with or without cast head), following by correlation of data with available code provisions for bar anchorage length.
2. Performing full-scale static tests on short-barrier length to investigate the failure mode and load carrying capacity of the barrier-deck joint and to correlate the experimental findings with code provisions for joint strength in flexure.
3. Performing full-scale static tests on long barrier wall to investigate failure modes and load carrying capacities due to transverse loading, then correlating the results with the available code provision for wall strength.
4. Conducting three-dimensional finite-element modeling of the barrier-deck cantilever system under transverse line loading at interior and end locations as shown in Table 1.1 and correlate the results with the CHBDC-specified factored applied load values shown in Table 1.1.

Table 1.1 Transverse moments in cantilever slabs due to horizontal railing loads in selected PL-3 and PL-2 barriers. (Table C5.4 in CHBDC Commentary, CSA 2006b)

Horizontal load or moment dispersion at inner portion of deck		Performance Level 3 barrier	Performance Level 2 barrier with rail
			
Factored horizontal load P_t (Clause 3.8.8.1)		357 kN	170 kN
Length of load application (Clause 12.5.2.4)		2400 mm	1050 mm
Height of load application above deck (Clause 12.5.2.4)		900 mm	700 mm
Moment in inner portions of deck per metre at face of barrier		83 kN-m/m	38 kN-m/m
Dispersal angle for barrier	Dispersal angle for deck	$\theta = 42^\circ$	$\theta = 47^\circ$
Tensile force in inner portion of deck at deck edge		144 kN/m	100 kN/m
Dispersal angle for barrier	Dispersal angle for deck	$\theta = 3^\circ$	$\theta = 10^\circ$
Moment in end portion of deck per metre at face of barrier		102 kN-m/m	52 kN-m/m
Dispersal angle for barrier	Dispersal angle for deck	$\theta = 48^\circ$	$\theta = 45^\circ$
Tensile force in end portion of deck at deck edge		161 kN/m	142 kN/m
Dispersal angle for barrier	Dispersal angle for deck	$\theta = 0^\circ$	$\theta = 0^\circ$
Dispersal angle for barrier	Dispersal angle for deck	$\theta = 8^\circ$	$\theta = 8^\circ$

1.5 Thesis Overview

This thesis is organized in six Chapters. Chapter 1 gives an overview of the research. Chapter 2 provides an understanding of the components, manufacturing, properties, mechanics, durability and applications of FRP materials. The parameters that affect the bond behavior of FRP bars in

concrete are also discussed in this section. Current design codes equations for bar development length and barrier load carrying capacities are explained. Chapter 3 describes the experimental study on pullout tests of GFRP bars. It also summarizes materials used in this research study and the methodologies of the experimental testing program. Moreover, it presents the experimental results and an analytical discussion on the findings. Chapter 4 describes the experimental study on full-scale static tests for the anchorage system between deck and the barrier wall and on the barrier wall at its interior and end locations. It also presents the experimental results, observations and analytical discussion on the findings. Chapter 5 describes the study, using the finite-element modeling, to investigate different case scenarios of deck-to-barrier connections. It includes description of finite-element models, description of deck-barrier joint configurations and description of loads used in modeling. Chapter 6 provides the conclusions and recommendations for future research.

CHAPTER 2

LITERATURE REVIEW

2.1 Fibre Reinforced Polymers Technology

Fibre reinforced polymers (FRP's) of various types and configurations have existed since the post world war II era (Tang, 1997). Their high strength to weight ratio have made them an attractive building and structural rehabilitation material. Advanced polymer technology allow structural engineers use FRPs as special internal / external reinforcement in concrete structures for rehabilitation or new construction.

Fibre reinforced polymers (FRPs) are composite materials consisting of high strength fibres embedded in a polymer matrix. Since FRPs are composed of two different materials, the properties of the FRP system depend on those of the individual components. The fibres provide strength and stiffness to the composite and carry most of the applied loads whereas the matrix acts to bond and protect the fibres and to transfer stress from fibre to fibre through shear stresses (ACI 440R-07). For structural engineering applications, the most common fibres used in FRPs are glass (GFRP), carbon (CFRP), and aramid (AFRP). FRP materials can be manufactured as sheets, plates and wraps for strengthening applications of existing structures or as bars, rods, and tendons for internal reinforcement of concrete in new construction or as a structural element itself. Figure 2.1 shows the typical FRP materials used for strengthening and rehabilitation of concrete structures.



Fig. 2.1 Various FRP products (Newhook and Svecova, 2006)

2.1.1 Fibres

Fibres provide the strength and stiffness of an FRP composite. Since fibres used in most structural applications are continuous and oriented in a specified direction, FRPs are orthotropic composites and they are much stronger and stiffer in the direction of the fibres. The selection of fibres for specific applications depends on several factors including the required strength, the stiffness, durability concerns, cost limitations, and the fibre availability. For structural applications, the three most commonly used fibres are glass, carbon and aramid.

Glass fibres generally are produced by direct melt process where the fibres are drawn from a glass melt with a diameter of 3-25 microns. Glass fibres are the most common for construction as it is more economical. Glass fibres are frequently used in the manufacturing of FRP bars, pultruded FRP structural sections and FRP wraps for seismic applications. Glass fibres are extensively used in structural engineering applications such as prestressing tendons for concrete, rehabilitation of infrastructure due to its non-corrosive nature and structural FRP wraps for restoration and strengthening of reinforced concrete beams, columns, and slabs. Carbon fibres made from a process called pyrolysis. The formation of carbon fibres requires processing temperatures above 1000 °C (ACI 440R-07), which makes it more expensive. Aramid fibres manufactured from a synthetic compound called aromatic polyamide in a process called extrusion and spinning (Newhook and Svecova, 2006). FRPs manufactured from aramid fibres have low compressive and shear strengths as a result of the anisotropic properties of the fibres. Some studies have indicated that the type of material can also influence the resistance to environmental exposure and in turn the durability. Tam and Sheikh (2008) tested the durability of various FRP materials to determine their resistance to environmental exposures. Aramid and carbon FRP reinforcing bars are seldom considered for use in reinforced concrete because of their significantly higher costs than standard steel. (Johnson David, 2009).

2.1.2 Resins

Selection of the proper matrix is very important in the manufacturing of FRPs. The physical and thermal properties of the matrix significantly affect the final mechanical properties as well as the manufacturing process of the FRP. In addition to coating and protecting the fibres from abrasion,

the role of the matrix is to transfer stresses between the fibres. The matrix transfers inter-laminar and in-plane shear stresses in the FRP, and provides lateral support to fibres against buckling when subjected to compressive loads (ACI 440.1R-07). Matrix materials for FRPs can be grouped into two general categories: thermoplastics and thermosetting resins. Thermoplastics include polymer compounds such as polyethylene, nylon, and polyamides whereas thermosetting materials include polyesters, vinyl esters, and epoxies. Typically for structural engineering applications, thermosetting materials are currently used. Thermoplastics matrix polymers are made from molecules in a linear structural form that are held in place by weak secondary bonds. The secondary bonds can be destroyed by heat or pressure and allow the thermoplastic to be reshaped although this could degrade its mechanical properties. Since thermoplastics display inferior thermal and physical properties when compared to thermosetting resins, they are not used as often as thermosetting resins, especially for structural engineering applications.

Thermosetting polymers are low molecular-weight liquids with very low viscosity and their molecules are joined together by chemical cross-links forming a rigid, three-dimensional structure once cured (ACI 440.1R-07). Once the resins have hardened, they cannot be reshaped by applying heat or pressure. Thermosetting resins have good thermal stability and chemical resistance and undergo low creep and stress relaxation. Thermosetting resins generally have good thermal stability at service temperatures, have good chemical resistance, and display low creep and relaxation properties in comparison with most thermoplastics. (Newhook and Svecova, 2006). Polyesters is the most widely used polymers due to their relatively low cost and ease of processing since their resins cure at ambient temperatures. Several specific types of polyesters are available for use with varying degrees of thermal and chemical stability, moisture absorption, and shrinkage during curing. Vinylesters is often categorized as a class of polyesters because of their similar processing procedures. Vinylesters are resistant to strong acids and alkalis therefore they are commonly used as reinforcing bars for concrete since they are in a highly alkaline environment within the concrete. Furthermore, vinylesters offer lower moisture absorption and shrinkage when compared to polyesters however are slightly more expensive. Epoxies are often used in wet lay-up applications of FRP plates and sheets due to their ability to cure at ambient temperature and exceptional adhesion characteristics. Epoxies have high strength, good dimensional stability, relatively good high-temperature properties, strong resistance to chemicals

(except acids), and superior toughness.

2.1.3 Manufacturing Process

The manufacturing of FRPs for structural applications is done by pultrusion. Pultrusion process is commonly used to fabricate FRP elements that have a constant cross-sectional profile such as bars, rods, tendons, plates, and structural sections including bridge beams and decks. This is a continuous process that combines fibre reinforcements and thermosetting resin and is fully automated. Reinforcement materials, such as raw fibres (rovings), mats or fabrics, are pulled through a resin bath where the material is thoroughly coated or impregnated with a liquid thermosetting resin. The saturated reinforcements are then pulled through a heated die. As the fibres pass through the die, the polymer matrix hardens into the shape of the die and therefore produces a structural component. The FRP component is pulled through the die from the cured end in a continuous process, which intern allows for FRP component for any length to be produced. Resulting from this process, the all of the fibres in the pultruded component are aligned in a single direction creating a unidirectional FRP. The process is driven by a system of caterpillar or tandem pullers located between the die exit and the cutoff mechanism (ACI 440R-07). Figure 2.2 shows a schematic of the pultrusion manufacturing process for a channel element.

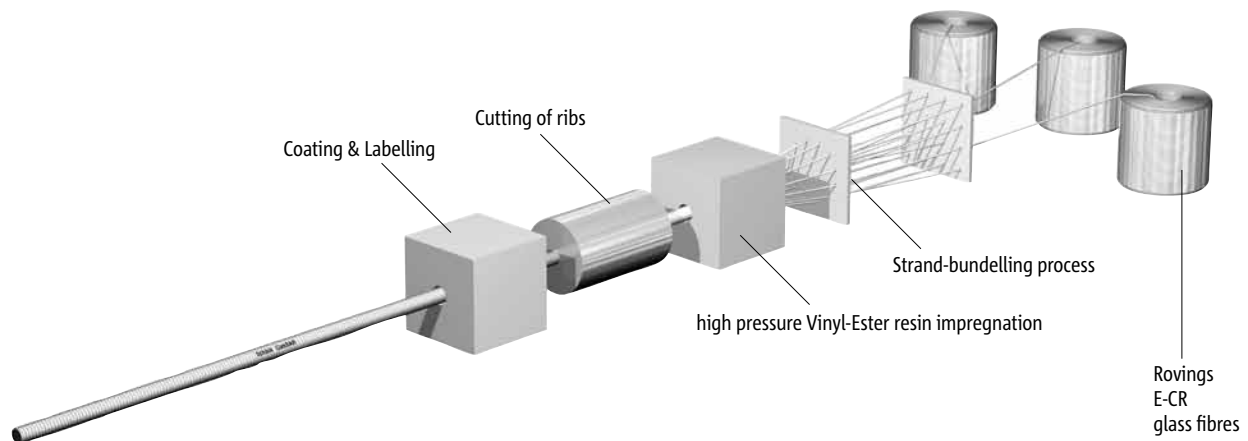


Fig. 2.2 Schematic illustration of the pultrusion manufacturing process (Schoeck, 2011).

2.1.4 Properties of FRP

The properties of FRP systems vary significantly depending on the relative proportions of fibre and matrix, the mechanical properties of the constituents, the fibre orientation within the matrix

and the manufacturing method. The mechanical properties of FRPs are highly directionally dependent, and the properties typically specified are in the direction of the fibres. All FRPs exhibit linear elastic tensile stress-strain behavior in the direction of the fibres with no yielding prior to failure. Figure 2.3 shows the linear elastic behavior of FRP from the typical stress-strain curve. The curves also show that FRP systems have a lower modulus of elasticity than that of steel, except for some CFRP systems. The strength of FRP materials depends on whether the force being applied is tensile or compressive. Most FRPs are significantly more effective under tension, therefore they are generally used as tensile reinforcement. The response of the FRP system depends on the failure strains of its fibres and matrix.

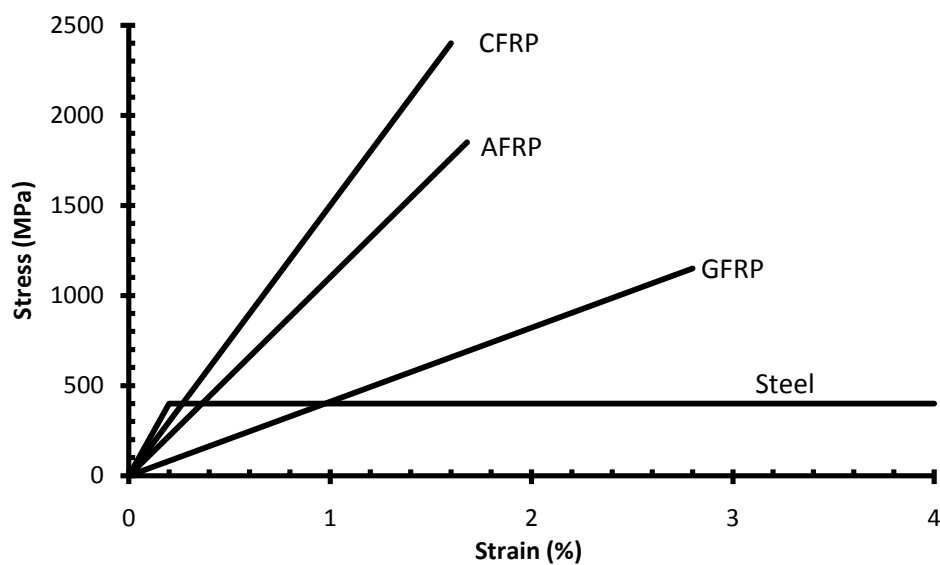


Fig. 2.3 Stress-strain curves of FRP (ACI 440.1R-07)

2.1.5 Applications of FRPs in Structural Engineering

FRPs are used in structural engineering in various forms. Entire structures or structural elements can be fabricated entirely of FRP such as pedestrian bridges, utility poles, bridge deck panels, and girders. FRPs can also be used for new construction as internal rebars and prestressing tendons. FRP rebars and reinforcing grids have been used successfully as internal reinforcement in concrete beams and slabs. Another application for FRPs is stay-in-place formwork. In these applications, the concrete formwork is fabricated from FRP and acts in a composite manner with the hardened concrete. The FRP formwork can be used as tensile reinforcement for slabs and

beams. Columns and beams made from concrete-filled FRP tubes are an example of the stay-in-place formwork, which has become popular recently. The FRP tube formwork provides both tensile and confining reinforcement to the concrete (Bisby, 2006). FRPs have also been used as a method for strengthening and rehabilitating concrete, steel, masonry and timber structures. FRPs have the ability to increase their existing flexural, shear, or confinement strength. Materials used for these applications are either prestressing tendons, pre-manufactured rigid FRP strips that are bonded to the surface of the structure with an adhesive, or wet lay-up sheets which are dry FRP sheets bonded to the surface using a polymer resin (Bisby, 2006). In addition, FRP strips, rods, and tendons can be inserted with an adhesive into grooves cut into structural members in applications called near-surface mounting (NSM).

2.2 Background on Concrete Bridge Barrier Design

The design process of bridge barrier walls specified in the Canadian Highway Bridge Design Code, CHBDC, (CSA, 2006a; CSA, 2006b) is based on the AASHTO Guide Specification for bridge railings (AASHTO, 1989) and the AASHTO Guide for Selecting, Locating and Designing Traffic Barriers (AASHTO, 1977). The requirements for the design of barriers are specified in Section 12 of CHBDC. Barriers on bridges receiving salt are exposed to a highly-corrosive environment. To ensure long-term performance, these barriers must either be made from materials that can withstand this environment or be protected by an adequate protective coating. The barriers are divided into four different types according to their function, namely: (i) traffic barrier; (ii) pedestrian barrier; (iii) bicycle barrier; and (iv) combination barrier. In the appraisal of a barrier the specific regulations, which will be mentioned in the following subsections, are not the only factors to consider. There also exist some general factors, which should not be underestimated. These factors are durability, ease of repair, snow accumulation on and snow removal from deck, visibility through or over barrier, deck drainage, future wearing surfaces, and aesthetics. Damaged barriers need to be repaired quickly with minimal disruption to traffic. Traffic barriers should be designed with features such as anchorages that are unlikely to be damaged or cause damage to the bridge deck during an accident and modular construction using prefabricated sections that allow damaged sections to be repaired quickly.

2.2.1 Traffic Barrier and Performance Levels

Traffic barriers should be provided on both sides of highway bridges to delineate the superstructure edge and therefore to reduce the consequences of vehicles leaving the roadway upon the occurrence of an accident. Crash tests are used to determine barrier adequacy in reducing the consequences of vehicles leaving the roadway. If a barrier has the same details as those of an existing traffic barrier the adequacy can be determined from an evaluation of the existing barrier's performance when struck by vehicles. The adequacy of a traffic barrier in reducing the consequences of a vehicle leaving the roadway is based on the level of protection provided to the occupants of the vehicle, to other vehicles on the roadway and to people and property beneath the bridge. This protection is provided by retaining the vehicle and its cargo on the bridge, by smoothly redirecting the vehicle away from the barrier and by limiting the rebound of the vehicle back into traffic.

Traffic barrier requirements vary from bridge site to bridge site and are based on the expected frequency and consequences of vehicle accidents at a bridge site. This procedure assumes that the frequencies and consequences of vehicle accidents at bridge sites are a function of many variables. The ranking system, used in CHBDC to determine the site conditions of a bridge site, are named Performance Level (PL) and are defined as follows:

Performance Level 1 (PL-1): The performance level for traffic barriers on bridges where the expected frequency and consequences of vehicles leaving the roadway are similar to that expected on low traffic volume roads. Crash test requirements require crash testing with a small automobile and a pickup truck in accordance with CHBDC-specified impact speed and impact angle.

Performance Level 2 (PL-2): The performance level for traffic barriers on bridges where the expected frequency and consequences of vehicles leaving the roadway are similar to that expected on high to moderate traffic volume highways. Crash test requirements require crash testing with a small automobile, a pickup truck, and a single unit truck in accordance with CHBDC-specified impact speed and impact angle.

Performance Level 3 (PL-3): The performance level for traffic barriers on bridges where the expected frequency and consequences of vehicles leaving the roadway are similar to that expected on high traffic volume highways with high percentage of trucks. Crash test

requirements require crash testing with a small automobile, a pickup truck, and a tractor- trailer truck in accordance with CHBDC-specified impact speed and impact angle.

Alternative Performance Levels, as mentioned in Section 12.5.2.1.1 in CHBDC, have to be approved by the Regularity Authority for the bridge and defined by specifying their crash test requirements. These levels shall be considered along with Performance Levels 1, 2, or 3 when determining the optimum performance level which is the one with the least costs. The optimal level of traffic barrier performance at a bridge site is assumed to be the level giving the least costs where costs includes the costs of supplying and maintaining a traffic barrier as well as the costs of the accidents expected with the use of the traffic barrier. The minimum barrier heights for PL 1, 2, and 3 traffic barriers are 0.68, 0.80, and 1.05 m, respectively. Traffic barrier height requirements are intended to prevent impacting vehicles from vaulting or rolling over a barrier. The higher the center of gravity of the impacting vehicle, the greater the required traffic barrier height needed to contain it. In addition, the geometry of the roadway face of a traffic barrier as well as the transition into the roadway face of the approach roadway traffic barrier shall have a smooth and continuous alignment, as laid out in Section 12.5.2.2 in CHBDC. Where a traffic barrier is located between the roadway and a sidewalk or bikeway, the sidewalk or bikeway face of the barrier should have a minimum height of 0.60 m measured from the surface of the sidewalk or bikeway.

2.2.2 Crash Test Requirements

With the defined Performance Level the crash test requirements, which should be in accordance with the crash test requirements of *AASHTO Guide Specifications for Bridge Railings*, are defined as mentioned in Section 12.5.2.3 in CHBDC. Those crash test requirements shall be satisfied along the entire length of a traffic barrier, especially at any changes in barrier type, shape, alignment, or strength that may affect the barrier performance. Alternative Performance Levels shall meet the crash test requirements of the optimum Performance Level or of a more severe Performance Level as considered. Under Section 12.5.2.3.2 of CHBDC, the crash test requirements for traffic barrier transitions are defined. They should meet the crash test requirements used for appraising the approach roadway traffic barrier, provided that it has been crash tested to requirements that test its geometry, strength, and behavior to an equivalent or

more severe level.

2.2.3 Barrier-deck Anchorage

The performance of the traffic barrier anchorage during crash testing is the basis for its capability. In case no significant damage occurs in the anchorage or deck during crash testing, the anchorage is considered to be acceptable. If there is no crash testing results for the anchorage available, the anchorage and deck shall be designed to resist the maximum bending, shear and punching loads that can be transmitted to them by the traffic barrier. As such, the initial design of the proposed PL-3 precast bridge barrier (Sennah et al., 2011) was carried out to meet the CHBDC design criteria specified for static loading at the anchorage between the deck slab and the barrier wall (Table 1.1). For PL-3 barriers, CHBDC specifies transverse, longitudinal and vertical loads of 210, 70 and 90 kN, respectively, that can be applied simultaneously over a certain barrier length. CHBDC specifies that transverse load shall be applied over a barrier length of 2400 mm for PL-3 barriers. Since transverse loading creates the critical load carrying capacity, both the longitudinal and vertical loads were not considered in the design of barrier wall reinforcement and anchorages between the deck slab and the barrier wall. It should be noted that CHBDC specifies a live load factor of 1.7. Thus, the design impact load on PL-3 barrier wall over 2.4 m length is 357 kN. Table 2.1 summarized CHBDC specified transverse, longitudinal and vertical loads used to design PL-1, -2 and -3 barriers under static loading. While Fig. 2.4 shows the locations of such loads on the barrier according to Section 12.5.2.4 of CHBDC. It should be noted that the transverse loading simulating vehicle impact is specified to be distributed over 1.2 and 1.05 m for PL-1 and PL-2 barriers, respectively. While the vertical load is specified to be distributed over 5.5 m for PL-1 and PL-2 barriers and over 12 m length for PL-3 barriers.

Table 2.1 Traffic Barrier Loads (CSA, 2006a)

Performance level	Transverse load, kN	Longitudinal load, kN	Vertical load, kN
PL-1	50	20	10
PL-2	100	30	30
PL-3	210	70	90

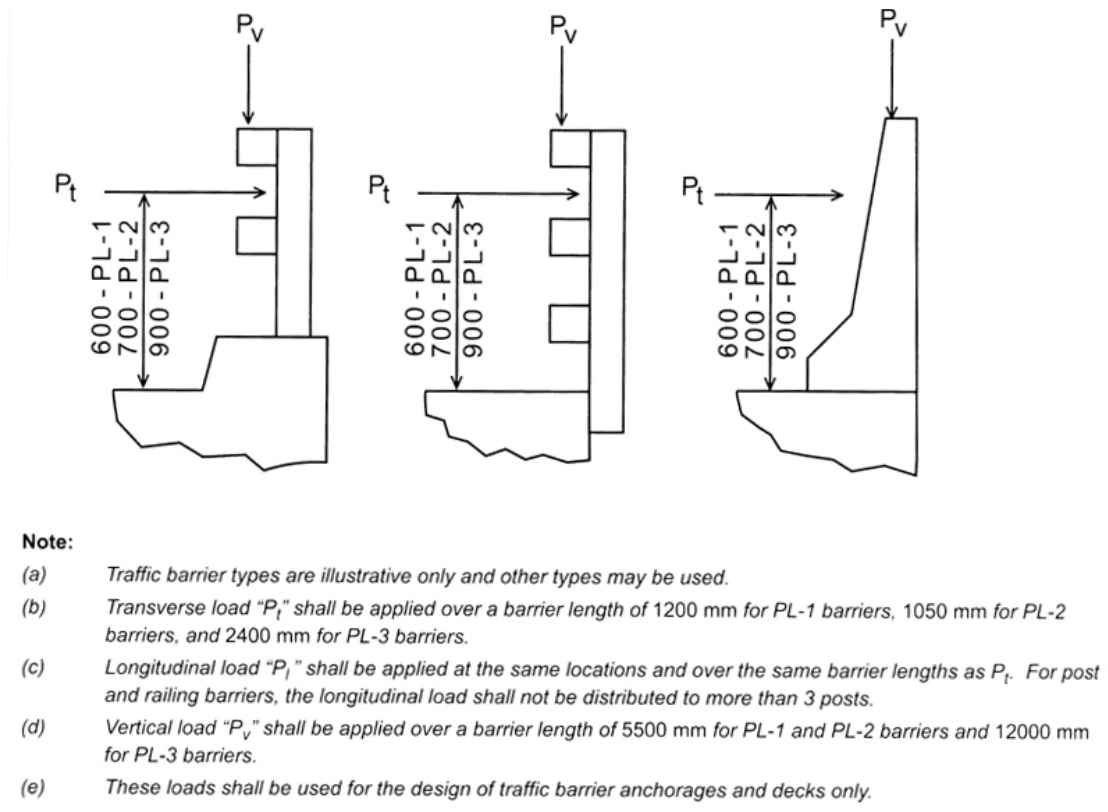


Fig. 2.4 Application of traffic design loads to traffic barriers (CSA, 2006a)

For the anchorage resistance of the GFRP bars embedded in the deck slab, Pahn (Pahn 2008) conducted pullout tests on 16 mm diameter GFRP bars provided with headed ends to determine their pullout capacity when they are embedded in concrete over bond lengths of 100 and 200 mm. The results from this testing formed the basis for the developed PL-3 barrier-deck joint. As for the design of the vertical and horizontal reinforcement in the barrier wall, the AASHTO-LRFD yield-line analysis were performed (Tropynina and Goremykin, 2009) on the ultimate flexural capacity of the concrete components as specified in the AASHTO-LRFD Bridge Design Specifications (AASHTO, 2012). In the analysis, it was assumed that the yield-line failure pattern occurs within the barrier wall only and does not extend into the deck slab. This means that the deck slab must have sufficient resistance to force the yield-line failure pattern to remain within the barrier wall. The LRFD yield-line analysis is also based on the assumption that sufficient longitudinal length of barrier wall exists to result in the desired yield-line failure pattern.

Such design work for the PL-3 bridge barrier proposed the use of 16 mm and 12 mm diameter GFRP bars as vertical reinforcement in the barrier front and back faces, respectively, with 12 mm diameter GFRP bars as horizontal reinforcement in case of PL-3 barrier wall, all at 300 mm spacing. The connection between the deck slab and the barrier wall utilized the GFRP headed end bars for proper anchorage. Figure 1.3 shows a schematic diagram of the GFRP reinforcement on the designed barrier wall which is now the subject of study in this thesis. Two full-scale PL-3 barrier models of 1200 mm length were erected and tested to-collapse to determine their ultimate load carrying capacities and failure models (Tropynina and Goremykin, 2009). The first barrier was a control one with reinforcing steel bars, while the second barrier model was reinforced with GFRP bars with headed ends. Based on the data generated from the experimental study, it was concluded that GFRP bars with headed anchorage could be safely used in bridge barrier walls to resist the applied vehicle impact load specified in CHBDC at the barrier wall-deck slab anchorage. However, CHBDC Clause 12.4.3.4.4 specifies crash testing for the design of the barrier wall itself (i.e. both vertical and horizontal reinforcement). Results of vehicle crash test on the proposed barrier shown in Fig. 1.3 can be found elsewhere (Sennah et al., 2011).

Barrier design involved several assumptions. The primary assumption is that the yield-line failure pattern occurs within the parapet and does not extend into the deck. Design approach also assumes the development of the nominal moment strength of the barrier wall in the transverse and longitudinal directions. Another assumption is that the negative and positive wall restraining moments are equal and the negative and positive beam resisting moments are also equal. Design of the barrier reinforcement requires the calculation of the nominal resistance, R_w and the comparison of the obtained value to the accepted one according to the Canadian Standards. Details of AASHTO-LRFD yield-line equations are presented in Chapter 4 in this thesis.

2.2.4 Transverse moments in cantilever slabs due to railing loads

The magnitudes of the unfactored loads that are to be applied to various performance level barrier and/or railing systems to determine the force effects in the deck slab and barrier anchorage are specified in Clause 3.8.8.1 of CHBDC. The length of load application on the barrier and the location or height of load application above the roadway is specified in Clause 12.4.3.5 of CHBDC as shown in Fig. 2.4. Horizontal loads in the transverse and longitudinal

directions specified to be applied simultaneously with vertical loading on the barrier or rail. The force effects in the deck due to horizontal loads alone can be determined and superimposed on the analysis results of the deck slab for vertical loads applied to the barrier. Simplified methods of analysis were presented in CHBDC The determination of moments in the deck slab due to concentrated horizontal railing loads (see Table 1.1). A constant length of slab at the exterior edge or face of barrier equal to 1.50 m was used for determining moment intensity resulting from horizontal concentrated loads on barriers. This length was increased by a linear dispersion equal to 0.8 times the distance between the longitudinal line of deck section being analyzed and the face of the barrier, representing an angle of dispersal equal to 21° for an inner portion of deck. This angle of dispersal was probably conservative for most cases. However, the magnitudes of the design loads in previous codes were much lower than the present load requirements for performance level barriers. This necessitates the use of more refined methods of analysis to determine the dispersal of combined horizontal and vertical loads that are applied over specified lengths on performance level barriers and rails.

The results of finite-element analysis for horizontal loading on selected PL-3 and PL-2 barriers used in some Canadian provinces are shown in Table C5.4 (Clause C5.7.1.6.3) of CHBDC which is Table 1.1 in this thesis. The factored loads are shown with the length of the load application at the point of loading on the barrier. Transverse moment intensity (kN-m/m) at the face of barrier and transverse tensile load intensity (kN/m) in the deck at the barrier-deck intersection are shown for both inner and end portions of the deck. The end portion of the deck is located at the discontinuous end of a deck or barrier, such as found at a transverse expansion joint. The width of an end portion in the longitudinal direction of the bridge deck is approximately equal to 1.5 to 2.0 times the height of load application above the deck. Additional transverse deck reinforcement is usually placed in this region to resist the increased moment intensity.

The analysis results show lines of dispersion for distribution of moment and tensile load intensities. This is the classic concept used for load dispersion in previous codes and is only shown here (see Table 1.1) to indicate the approximate nature of moment and load dispersal. The actual dispersal depends on the stiffness and geometry of the barrier and deck elements and the load location relative to the supporting elements. Also, as shown in Table 1.1, the actual lines of

dispersion are not linear but vary from element to element. The results of this analysis would be superimposed on the separate analysis for the effects of vertical loading on the barrier as specified in Clause 12.4.3.5 of CHBDC. This combined analysis would be used for determining the length and size of cantilever deck reinforcement that may be required to resist barrier or railing loads. These requirements are independent of the case required to resist vertical wheel loads as specified in Clause 5.7.1.6.1 of CHBDC and are considered separately. The loading case that determines the maximum amount of reinforcement will then govern. The magnitude and distribution of force effects resulting from vertical barrier loading depend greatly on the location of beam lines in the deck cross-section. However, the magnitude of maximum moment intensity resulting from horizontal barrier loading is not as sensitive to this geometrical feature. Regardless, this geometrical feature has an influence on the dispersal of moment intensity in the deck resulting from horizontal load on the barrier.

2.3 Previous Research on Concrete Barriers

Most of the research regarding the GFRP reinforcement of bridge barriers was performed by Sherbrooke University in collaboration with MTQ and by Ryerson University in collaboration with MTO. The reports were based on the use of GFRP reinforcement as an alternative to the conventional steel. Tests were focused on comparing the general behavior and cracking patterns of barriers reinforced with GFRP bars with those of identical geometry reinforced with conventional steel under the static and impact loads. Based on the test results, the behavior of PL-2 and PL-3 barriers, reinforced with GFRP bars, subjected either to static or impact loads were similar to that of the identical barriers reinforced with the steel bars.

Tropynina and Goremykin (2009) performed tests on full-scale PL-3 barriers reinforced with GFRP bars with bar arrangement shown in Fig. 1.3. The objective of these tests was to check the adequacy of the calculated amount of GFRP reinforcement in terms of strength at the deck-barrier junction. Sennah et al. (2011) conducted vehicle crash test on such barrier wall shown in Fig. 1.3 to determine its structural adequacy under vehicle impact. Crash test results showed that the developed barrier contained and redirected the vehicle. The vehicle did not penetrate, underide or override the parapet. No detached elements, fragments, or other debris from the barrier were present to penetrate or show potential for penetrating the occupant compartment, or

to present undue hazard to others in the area. No occupant compartment deformation occurred. The test vehicle remained upright during and after the collision event.

The evaluation of vehicle crashworthiness has involved numerous full-scale crash tests of the vehicle and highway hardware to verify the compliance with regulatory requirements (Alberson et al., 2005; Plaxico et al. 2000; Pfeifer and Sicking, 1997). Specific crash testing on bridge barriers was reported elsewhere (among them: Bielenberg et al., 2003; Buth, et al., 2000; Mak, et al., 1994). Few authors conducted pendulum impact testing as an alternative to vehicle crash testing (El-Gamal et al, 2007; El-Salakawy, et al., 2005; El-Salakawy, et al., 2003; Bank, et al., 1997). Computer simulation tools are increasingly being used for the upfront assessment of crashworthiness without going through multiple-cycles of prototype testing and iterative design changes. Computer simulation of vehicle collisions has improved significantly over the past few years. With advances in computer technology and explicit large-displacement non-linear finite-element (FE) software, full-scale models and simulations of such sophisticated collisions are becoming ever more possible. Many authors worked on the validation of these FE vehicle models by correlating the results of the finite-element simulation with those obtained from existing vehicle crash tests (among them: Zaouk, et al., 1998). Few types of software for large displacement, inelastic, dynamic, finite-element crash analysis are commercially available (LSDYNA, MADYMO, and ABAQUS/ Explicit software). Several authors dealt with finite-element computer simulation of flexible highway barriers (Ranzo and Bonin, 2005; Plaxico, et al., 1998; Uddin and Hackett, 1998; Ross, et al., 1993), while others dealt with finite-element computer simulation of existing guardrail terminals (Wekezer et al., 2000; Ray and Patzner, 1997). Few authors dealt specifically with impact simulation, using finite-element modeling and multi-body dynamics, of rigid concrete bridge barrier and bridge railing (Marzougui, et al., 2008; Consolazio, et al., 2003; Itoh, et al., 2000; Thomson et al., 1999). Other authors dealt specifically with crash testing of transitions from roadway guardrail to concrete bridge barrier (Buth, et al., 2000).

Few authors dealt with the use of fiber reinforced polymers, FRP's, in concrete barriers. Maheu and Bakht (1994) developed a new barrier wall using FRP (GFRP) NEFMAC grids, with connection to the deck slab by means of double-headed tension bars of steel spaced at 300 mm. This new barrier

wall system was adopted in the CHBDC of 2000. El-Salakaway et al. (2003) tested to-collapse PL-2 and PL-3 barrier walls reinforced with GFRP bars. They conducted pendulum impact testing (Elsalakaway, 2005) on the developed barriers in lieu of vehicle crash testing. In 2007, El-Gamal et al. (2007) conducted pendulum impact testing on PL-2 and PL-3 barrier walls reinforced with new GFRP bars produced by Pultrall Inc. of Quebec, with lower tensile strength and bigger modulus of elasticity than those used in the earlier pendulum impact testing. Using this new type of GFRP bars is expected to lead to considerable savings in the cost of bridge barriers reinforced with FRP bars. conducted finite-element modeling of the pendulum impact tests conducted above as well as FEA modeling incorporating material and geometric non-linearity of such barriers under increasing monotonic loading to-collapse. The developed FEA models verified by results from these pendulum impact tests and to be used in a further stage to examine different scenarios of FRP detailing and material properties with an ultimate goal of reaching better cost-effective design of GFRP reinforced bridge barrier walls.

Deitz et al. (2004) focused on the behavior of bridge deck overhangs in the event of a barrier wall impact, leading to a combination of flexure, shear, and axial tension. The objective of their investigation was to evaluate deck overhangs under these forces. Three bridge deck reinforcing schemes were considered in the study, namely: all epoxy-coated steel ECS, all GFRP, and hybrid made up of a top mat of GFRP ebars and a bottom mat of ECS bars. Laboratory testing of nine specimens was performed. Results showed that all three reinforcing schemes meet the AASHTO requirements. Results showed that the ECS specimens provided warning through the apparent yielding of the reinforcement, while the GFRP and hybrid specimens provided warning through large crack widths and large displacements. The ECS specimen failure was attributed to an anchorage failure beneath the barrier wall, indicating an inadequate development length. However, a change in development length was not recommended. The specimens meet the code requirements for development length based on the nominal bar strength, and testing showed that the barrier wall system could resist the design load.

2.4 Bond Mechanism

In a reinforced concrete flexural member, the tension force carried by the reinforcement balances the compression force in the concrete. The tension force is transferred to the reinforcement

through the bond between the reinforcement and the surrounding concrete. Bond stresses exist whenever the force in the tensile reinforcement changes. Bond between FRP reinforcement and concrete is developed through a mechanism similar to that of steel reinforcement and depends on FRP type, elastic modulus, surface deformation, and the shape of the FRP bars (Tighiouart et al., 1998; Al-Zaharani et al. 1996).

2.4.1 Bond Failure Modes

Bond failures are divided into either splitting or pullout failure. Splitting failure mode occurs when the concrete surrounding the reinforcing bar develops transverse splitting cracks (Figure 2.5a). Splitting failure results in cracking along planes that are both perpendicular and parallel to the reinforcement. As the reinforcing bars are loaded they exert radial pressure on the surrounding concrete. If the surrounding concrete and/or the transverse reinforcement are not adequate to resist this pressure, a splitting crack initiates at the concrete-rebar interface and propagates towards the surface leading to the failure of the concrete by concrete cover splitting. Pullout failure mode occurs when the rebar pull out of the concrete when the cover, bar spacing or transverse reinforcement is sufficient to prevent or delay a splitting failure. Pullout failure occurs when the radial forces from the loaded reinforcing bar are lower than what the surrounding concrete and/or transverse reinforcement can resist and the tangential forces are higher than what the concrete can resist. Pullout failure results in a shearing along a surface at the top of the ribs around the bars (Figure 2.5 b).

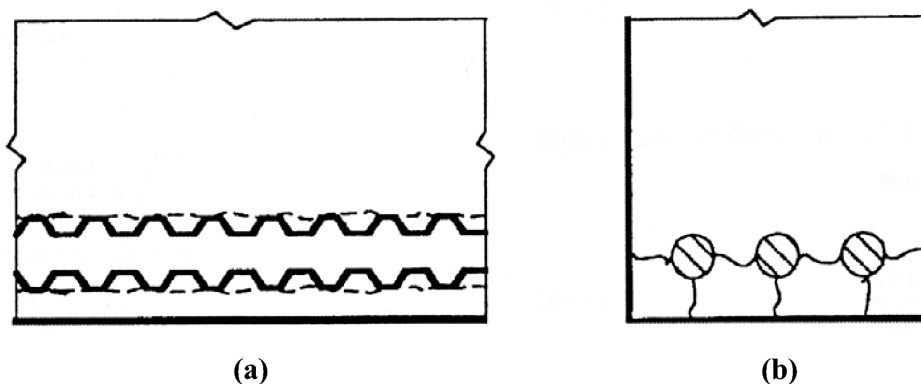


Fig. 2.5 Cracking and damage mechanisms in bond: (a) End view showing splitting cracks between bars and concrete cover; (b) Side view of member showing shear crack and/or local concrete crushing due to bar pullout. (Source: ACI 408R-03)

It is common for both splitting and pullout failures to observe crushed concrete in a region adjacent to the bearing surfaces of some of the deformations. Furthermore, both bond failures are related to the slip of the rebar relative to the concrete. In the pullout mode of failure, higher bond strength is achieved than in the splitting mode of failure since the concrete is well confined and therefore, the radial splitting cracks need more energy to reach the surface of the concrete. Bond force-slip and bond stress-slip curves can be used to better understand the nature of bond response and can be used to determine the required embedment length for the rebar to achieve its desired strength prior to bond failure. Harajli et al. (2004) studied the effect of confinement of bond strength between steel bars and concrete and produced a splitting and pullout failure bond stress-slip envelop for steel rebar (Figure 2.6) in confined and plain concrete. For both failure modes, the stress- slip envelopes consist of four phases that explain the bond behavior during static loading. Table 2.2 summarizes the phases for the splitting and pullout modes of failure.

Table 2.2 Summary of phases for the splitting and pullout modes of failure (Ametrano, 2011)

Phase	Failure Mode	
	Splitting	Pullout
First	First phase ends when an increase in the residual stress component of the bond force results in the development of splitting tensile cracks and the bond stress-slip relationship deviates from the pull out behaviour at s_{α}	First phase ends when the bond force is constant at a peak bond stress (u_1).
Second	Second phase ends when the crack has propagated to the surface and the splitting of the cover occurs indicating a complete deterioration of the bond (s_{max} , u_{max}).	The second phase is a constant bond following the peak bond stress (s_1 to s_2).
Third	The third phase shows significant drop in bond stress. (u_{max} to u_{ps} for confined concrete and u_{max} to βu_{max} plain concrete)	Third phase shows a significant drop in stress from s_2 to s_3 .
Fourth	Fourth phase ends at zero bond stress and is a continuation of the third phase.	The fourth phase a constant bond for $s > s_3$.

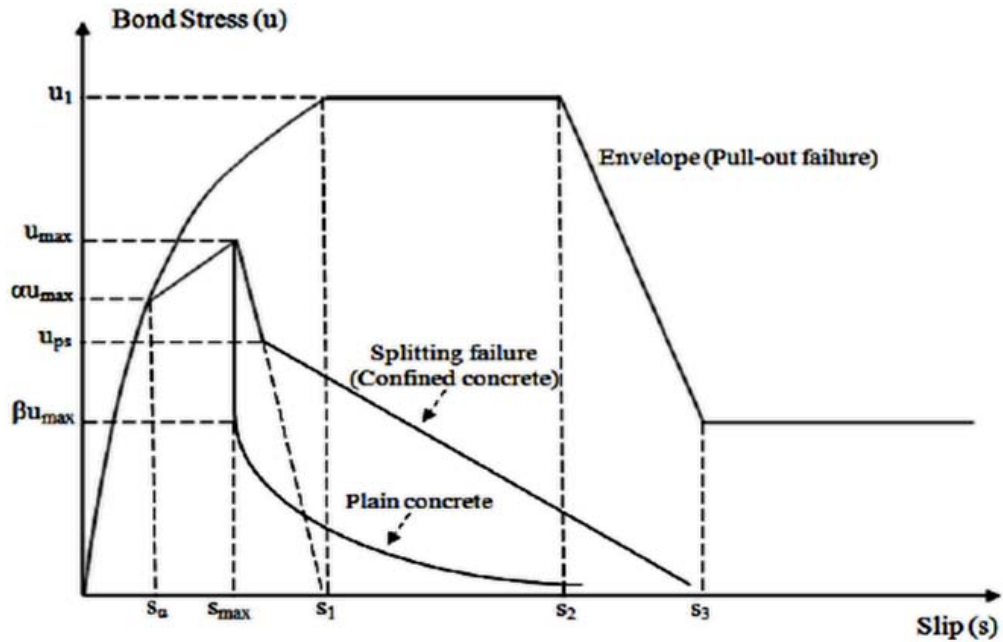


Fig. 2.6 Bond stress versus slip. (Harajli et al., 2004)

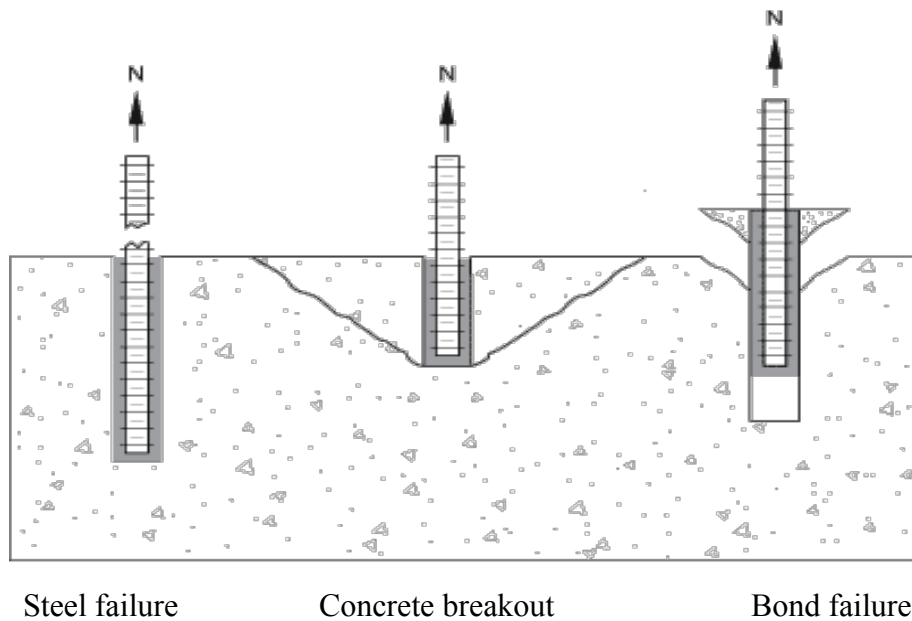


Fig. 2.7 Possible failure modes (steel rebar)

2.4.2 Determination of Bond Strength

For several years, bond strength was represented in terms of the shear stress at the interface between the reinforcing bar and the concrete, essentially treating bond as a material property (ACI 408R-03). It is now understood that bond, anchorage, development, and splice strength are

structural properties that are dependent on not only the materials, but also on the geometry of the reinforcing bar and the structural member itself. The bond force, U , is defined as the change in tensile force per unit length. The tensile force in the bar, T , varies from a relatively high value at the location of cracks to a low value between cracks. When the concrete cracks around the rebar, the rebar carries the complete tensile load at the location of the crack. At the uncracked locations, the tensile load is shared between the concrete and the rebar, thus causing the force in the bar to be lower. The real distribution of bond forces along the length of the bar cannot be determined because they depend on the location of the flexural cracks as the amount of tensile load shared by the concrete – neither of which can be evaluated. Figure 2.8 illustrates the variation of bond forces along the length of a rebar. Since the main focus of design is to ensure that the rebar is adequately anchored so that failure will not occur due to bond, it is convenient and realistic for design purposes to assume bond forces are uniform over the anchored, developed or spliced length of the reinforcement (ACI 408R-03).

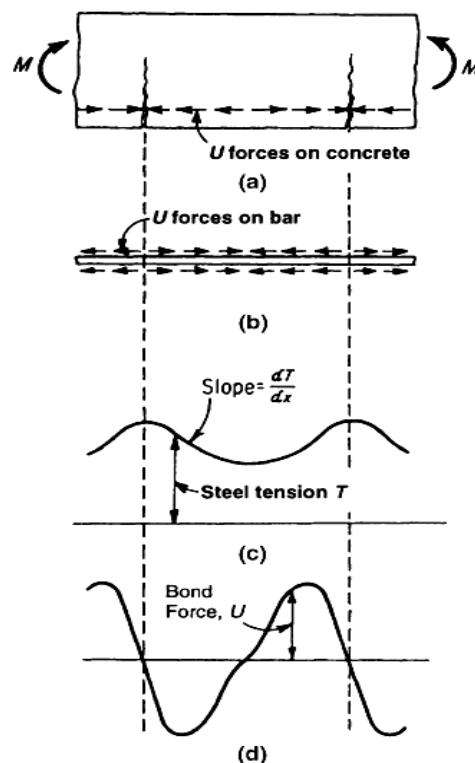


Fig. 2.8 Variation of bond force along length of rebar in reinforced concrete member subjected to bending: (a) cracked concrete member; (b) bond forces on rebar; (c) variation of tensile forces along rebar; (d) variation of bond force acting on reinforcing bar (ACI 408R-03)

Assuming a uniform distribution of stress, the force on the rebar is resisted by an average bond stress acting on the surface of the rebar. Therefore, an equilibrium condition can be established for a rebar embedded in concrete with a length:

$$l\pi d_b \mu = A_b f_s \quad (2.1)$$

Where l = embedment length of rebar (mm); d_b = rebar diameter (mm); μ = average bond stress (MPa); A_b = area of rebar; and f_s = stress in rebar (MPa).

From Equation 2.1, the average bond strength can be expressed as:

$$\mu = \frac{A_b f_s}{l\pi d_b} = \frac{d_b f_s}{4l} \quad (2.2)$$

2.4.3 Bond Strength and Development Length Equations in Design Codes

When used in design, development length and splice length are understood to represent the length of embedded reinforcement required to develop the design strength of reinforcement at a critical section (ACI 318-02). Design codes always specify the development length required to develop the design stress in the rebar because it is easier to apply by engineers. The development length can be related to the bond strength by using Equation 2.1. The following sections discuss the development length equations for FRP bars provided by CSA.S806-02, CSA.S6-06 and ACI 440.1R-07.

CSA.S806-02

The Canadian Standards Association CSA.S806-02 (CSA, 2002) recommends the use of the following equation to determine the development length of the FRP bars:

$$l_d = 1.15 \frac{k_1 k_2 k_3 k_4 k_5}{d_{cs}} \frac{f_F}{\sqrt{f'_c}} A_b \quad (2.3)$$

Where:

l_d = Development length of FRP bars in Tension, mm;

k_1 = Bar location factor: 1.3 for horizontal reinforcement placed so that more than 300 mm of fresh concrete cast in the member below development length or splice; 1.0 for all other cases;

k_2 = Concrete density factor: 1.3 for structural low-density concrete; 1.2 for structural semi- low-density concrete; 1.0 for normal density concrete;

k_3 = Bar size factor: 0.8 for $A_b < 300\text{mm}^2$; 1.0 for $A_b > 300\text{mm}^2$;

k_4 = Bar fibre factor: 1.0 for CFRP and GFRP; 1.25 for AFRP;

k_5 = Bar surface profile factor. Can be taken as less than 1.0, but not less than 0.5, if this value has been shown by experiment. In the absence of direct experimental results the following values are used: 1.0 for surface-roughened or sand coated surfaces; 1.05 for spiral pattern surfaces; 1.0 for braided surfaces; 1.05 for ribbed surfaces; 1.80 for indented surfaces;

d_{cs} = The smaller of: (a) the distance from the closest concrete surface to the centre of the bar being developed; or (b) two-thirds of the centre-to-centre spacing of the bars being developed.

The value shall not be taken greater than $2.5 d_b$, mm;

f_F = Design Stress in FRP tension reinforcement at Ultimate Limit State, MPa;

$\sqrt{f'_c}$ = Square Root of Concrete Compressive Strength, MPa, max. permissible value should be 8 MPa; and

A_b = Area of an individual bar, mm^2 .

Substitution of Equation 2.3 into Equation 2.2 gives the following expression for the average bond:

$$\mu = \frac{d_{cs} \sqrt{f'_c}}{1.15 k_1 k_2 k_3 k_4 k_5 \pi d_b} \quad (2.4)$$

From Equation 2.4, it is apparent that the bond stress is a function of the concrete cover, the compressive strength of concrete, the bar diameter, the bar location, the concrete density, the fibre type, and the bar surface profile.

CSA.S6-06

The Canadian Highway and Bridge Design Code, CSA.S6-06 (CSA, 2006) modified the development length equation for steel by multiplying the transverse reinforcement index by the

modular ratio of FRP to steel bars to determine the development length of FRP bars. The development length equation for an FRP bar is given as follows:

$$l_d = 0.45 \frac{k_1 k_4}{\left[d_{cs} + k_{tr} \frac{E_{FRP} u}{E_s} \right]} \left[\frac{f_{FRP} u}{f_{cr}} \right] A \quad (2.5)$$

Where:

l_d = Development length of FRP bars in tension, mm;

k_1 = Bar location factor: 1.3 for horizontal reinforcement placed so that more than 300 mm of fresh concrete is cast in the member below the development length or splice; 1.0 for all other cases;

k_4 = Bar surface factor representing the ratio of bond strength of FRP to that of steel rebar having the same cross-sectional area, but not greater than 1.0. In absence of manufacturer or test data, 0.8 shall be used;

d_{cs} = The smaller of: (a) the distance from the closest concrete surface to the centre of the bar being developed; or (b) two-thirds of the centre-to-centre spacing of the bars being developed, mm;

E_{FRP} = Modulus of elasticity of FRP, MPa;

E_s = Modulus of elasticity of steel, 200,000 MPa;

f_{FRP} = Stress in FRP reinforcement, MPa;

f_{cr} = Flexural cracking strength of concrete, MPa. Equal to: (a) $0.4\sqrt{f'_c}$ for normal density concrete; (b) $0.34\sqrt{f'_c}$ for semi-low density concrete; (c) $0.3\sqrt{f'_c}$ for low density concrete. The value of $\sqrt{f'_c}$ used to compute f_{cr} must be less than 8MPa;

A_{frp} = area of FRP bar, mm²; and

k_{tr} = transverse reinforcement index, mm, that can be calculated as follows.

$$k_{tr} = \frac{A_{tr} f_y}{10.5 s n} \quad (2.6)$$

$$\left(d_{cs} + k_{tr} \frac{E_{frp}}{E_s} \right) \leq 2.5 d_b \quad (2.7)$$

Where:

A_{tr} = area of transverse reinforcement normal to the plane through the anchored bars, mm^2 ;

f_y = yield stress of steel, MPa;

s = spacing of transverse reinforcement, mm; and

n = number of bars being developed or spliced.

Combining Equation 2.7 with Equation 2.2 gives the following expression for average bond strength:

$$\mu = \frac{\left(d_{cs} + k_{tr} \frac{E_{frp}}{E_s}\right) f_{cr}}{0.45 k_1 k_4 \pi d_b} \quad (2.8)$$

Equation 2.8 shows that CSA S6-06 considers the bond strength of FRP bars to be a function of the concrete cover, the confinement provided by transverse reinforcement, the modulus of elasticity of the FRP, flexural compressive strength – which is related to the concrete density and compressive strength, the bar location, bar surface and the bar diameter.

ACI 440.1R-07

The bond strength specified by the American Concrete Institute (ACI) Guide for the Design and Construction of Concrete Reinforced with FRP Bars, ACI 440.1R-07 (ACI, 2007) is based on research from Wambeke and Sheild (2006). A relationship for the bond strength of FRP bars was developed similar to the way that Orangun *et al.* (1977) developed an equation for the bond strength of steel bars and concrete. Wambeke and Shelid compiled a database of 269 beam bond tests, mostly consisting of GFRP specimens and a few AFRP specimens, which was limited to beam-end tests, notch- beam tests, and splice tests whose compressive strength ranged from 28 to 45 MPa. A linear regression of the normalized average bond stress versus the normalized cover and embedment length resulted in the following relationship:

$$\mu = \left(0.33 + 0.025 \frac{c}{d_b} + 8.3 \frac{d_b}{l_e}\right) \sqrt{f'_c} \quad (2.9)$$

Where:

C = the lesser of the cover to the center of the bar or one-half of the center-on-center spacing of the bars being developed;

d_b = diameter of the bar, mm;

l_e = embedment length of bar in concrete, mm; and

f'_c = compressive strength of concrete, MPa. In the database, the bar surface (spiral wrap versus helical lug) did not appear to affect the results, nor did the presence of transverse reinforcement, however it was concluded that the affect of confinement should be further investigated.

Wambeke and Sheild developed a subset of their full data base to determine a factor of safety having embedment lengths of at least $19d_b$. The C/d_b ratio was limited to 3.5 so that the same for use with their equations. This database included both splitting and pullout failure so that specimens' equation could be used to predict developable bar stresses for both failure modes. This limit was decided upon because specimens in the database that had a C/d_b greater than 3.5 and embedment lengths greater than $19d_b$, the failure modes were always pullout. The following equation was developed for predicting the developable bar stress for a given cover and embedment length:

$$f_{frp} = \frac{0.83\sqrt{f'_c}}{\alpha} \left(13.6 \frac{l_e}{d_b} + \frac{C}{d_b} \frac{l_e}{d_b} + 340 \right) \quad (2.9)$$

Where:

C/d_b = Cover to diameter ratio. Should not be taken larger than 3.5;

α = Bar location factor: 1.5 for horizontal reinforcement place above 300 mm of concrete; 1.0 for bars with less than 300 mm of concrete below;

l_e = Embedment length of bar in concrete, mm;

f'_c = Compressive strength of concrete, MPa; and

f_{frp} = Design tensile stress of FRP, MPa

Based on Wambeke and Shild's results, the bond of AFRP bars is similar to GFRP. There was no data for CFRP bars, however it is anticipated that the much larger stiffness of the CFRP bars will

likely decrease the required development length – resulting in a lower material modification factor. A material factor of 1.0 recommended for CFRP bars. It can be seen the bond between FRP bars and concrete according to ACI 440.1R-07 is dependent on the concrete cover, bar diameter, the embedment length and the concrete compressive strength and bar location.

The bond relationship presented in Wamebeke and Shield’s study was developed primarily on GFRP bars. Very few of the test specimens in the data base contained transverse reinforcement therefore its effectiveness is difficult to judge based on a few results. Furthermore, the bond relationship was developed using specimens with concrete compressive strengths ranging from 28 to 45 MPa. No limits have been placed on the concrete compressive strength as there are in the other codes. Therefore it is still necessary to further investigate the suitability of ACI 440.1R-07 equation for bond by studying the effects of transverse reinforcement and effect of concrete strength.

2.4.4 Development Length Equation of the Headed-End Bars

CSA A23.3-04

The Canadian Standard CSA A23.3-04 “Design of Concrete Structures” specifies the following procedure in Annex D to calculate the capacity of steel headed anchor:

1. **Steel resistance of anchor in tension.** The factored resistance of an anchor in tension as governed by the steel, N_{sr} , shall be evaluated by calculations based on the properties of the anchor material and the physical dimensions of the anchor.

$$N_{sr} = \phi_s n A_{se} f_{ut} R \quad (2.10)$$

N_{sr} = factored resistance of a single anchor or group of anchors in tension as governed by steel resistance;

ϕ_s = steel embedment material resistance factor for reinforcement;

n = number of anchors in the group;

A_{se} = effective cross-sectional area of anchor;

f_{ut} = specified tensile strength of an anchor; and

R = resistance modification factor.

2. **Concrete breakout resistance of anchor in tension.** The factored breakout resistance of an anchor in tension in cracked concrete shall not exceed:

$$N_{br} = k\phi_c\sqrt{f'_c}h_{ef}^{1.5}R \quad (2.11)$$

N_{br} = factored concrete breakout resistance in tension of a single anchor in cracked concrete;

k = coefficient for factored concrete breakout resistance in tension; and

h_{ef} = effective anchor embedment length.

3. **Pullout resistance of anchor in tension.** The pullout resistance of a single headed stud, shall not exceed:

$$N_{pr} = 8A_{bh}\phi_cf'_cR \quad (2.12)$$

Where A_{bh} = bearing area of the head of the stud.

When designing anchors, consideration must be given to the capacity of both the steel anchor and the embedded portion of the anchor. The 45° cone method utilizes a 45° conical failure surface in the determination of the concrete breakout capacity. The results in design expressions that are based on the square of the embedment depth, (i.e. h_{ef}^2). The CCD method however, considers fracture mechanics (size effect) in utilizing a 35° projected failure surface for the embedment portion of the anchor. This results in expressions with the embedment depth raised to the power of 1.5 (i.e. $h_{ef}^{1.5}$)

To have a sense of the change in the development length of GFRP bars with ribbed surface to the concrete strength and bar size, the author of this thesis calculated the development length based on CSA-S806 equation for bars with headed ends for long term applications. The results are listed in Table 2.3 below.

Table 2.3 Tension development length, l_d , for GFRP bars with ribbed surgance for normal density concrete ($k_1=1$)

BAR SIZE	NORMAL DENSITY CONCRETE -LONG TERM APPLICATION-100YRS									
	$f_c = 20$	$f_c = 25$	$f_c = 30$	$f_c = 35$	$f_c = 40$	$f_c = 45$	$f_c = 50$	$f_c = 55$	$f_c = 60$	$f_c = 64$
12	315	288	268	253	240	230	221	214	207	202
16	365	337	316	300	287	277	268	260	253	248
32	1206	1090	1003	936	882	838	800	767	739	718

1. Values are calculated based on CSA Standard S806-02, Clause 9.3.2. , Clause 9.3.4. and CHBDC S6-06, Clause 16.5.3, 16.8.4.2.

$$l_{d\text{bar}} = 1.15 \left(\frac{k_1 \cdot k_2 \cdot k_3 \cdot k_4}{d_c} \right) \cdot \left(\frac{f_{\text{ComBAR}} - f_{\text{head}}}{f_c} \right) \cdot A_b$$

$l_{d\text{ head}}$:

- FOR 12MM BAR = 60mm
- FOR 16 MM BAR = 100mm
- FOR 32 MM BAR = 100mm

$$L_d \text{ TOTAL}(\text{value in the table}) = l_{d\text{ bar}} + l_{d\text{ head}}$$

2. Design stress in ComBAR tension reinforcement $f_{\text{ComBAR}} = 1100\text{MPa}$ (Ultimate Tensile Stress)* 0.5 (Resistance factor, CHBDC S6-06)

3. $k_2 = 1$, $k_4 = 1$, $k_3 = 0.8$ for bar sizes M12, M16 and for size M32 - $k_3 = 1$

4. Multiply value L_d by k_2 , when this differs from 1.0

5. Concrete Density Factor:

$k_2 = 1.3$ for structural low density concrete

$k_2 = 1.2$ for semi-low density concrete

$k_2 = 1.0$ for normal density concrete

2.5 Previous work on Pullout Tests

Few bond test studies have been done with FRP bars. Most of these studies used the direct pullout method. This method consists of embedding rebar at a specific distance into a concrete cylinder of 150 mm diameter and 300 mm length or a concrete block. Once cured, the bar is pulled out using a universal testing machine or hydraulic ram, while displacements and applied loads are measured.

The bond behavior of FRP bars and concrete is not the same as that of steel bars because of the

distinct differences in the force transfer and failure mechanisms of steel and FRP bars. Their different behavior is attributed to the differences in material properties and their interaction mechanisms with concrete (Chaallal and Benmokrane, 1993). Steel is an isotropic, homogeneous, and elasto-plastic material, whereas FRP is an anisotropic, non-homogenous and linear elastic material. The anisotropic nature of the FRP rebar is due to the resin influence on its shear and fibers influence its tensile properties. Material anisotropy leads to different physical and mechanical properties in both longitudinal and lateral directions. Therefore, the anisotropic behavior of FRP bars needs to be considered in the development of design equations and in the understanding of failure mechanisms (ACI 440.1R-07). The surface texture of FRP bar is created by epoxy, fibres or sand coating and causes the bars to be non-homogeneous. The non-uniform composition of FRP bars results in a reduction in their bond performance. As a result, it has been observed that for FRP bars, the main force transfer mechanisms between the FRP bar and concrete are through adhesion and friction (Tighiouart *et al.*, 1998; Conseza *et al.* 1997; Benmokrane *et al.*, 1996).

There are several factors, which affect the bond between FRP reinforcing bars and concrete. These factors include bar properties, structural characteristics, and concrete properties. The bar properties effect includes bar size, fibre type, bar modulus, and bar surface condition. The structural characteristics effect includes concrete cover, bar spacing, embedment length, bar cast position and transverse reinforcement (Ametrano, 2011).

2.5.1 Effect of Properties of the FRP Bar on their bond behavior

The relationship between bar size and bond strength of FRP bars in concrete has been investigated by Larralde and Silva Rodriguez (1993), Benmokrane and Masmoudi (1996), Tighiouart *et al.* (1998), Achillides and Pilakoutas (2004), Okelo and Yuan (2005), Aly *et al.* (2006), Okelo (2007), Baena *et al.* (2009), and Hao *et al.* (2009). Their research indicates similar results obtained for steel bars which is that the bond strength increases with the decrease in the bar diameter. Tighiouart *et al.* (1998) explained that the cause of decreasing bond strength with the increase in bar diameter is due to increased amount of bleed water trapped beneath the rebar which in turn creates more voids than would form under a smaller bar. The presence of voids decreases the contact area between the bar and the surrounding concrete and therefore reduces

the bond strength. Achillides and Pilakoutas (2004) suggested that the reason for the decrease in bond strength for larger bars is because they develop less adhesion with the surround concrete than smaller bars. Baena *et al.* (2009) suggests that the Poisson's effect may also influence the bond properties of FRP bars since the diameter reduces when the bar is under tension. The diameter reduction increases with bar size, indicating that the Poisson's effect has a greater influence on larger bars with larger diameters, leading to a reduction in frictional and mechanical locking stresses.

Aly *et al.* (2005, 2006) and Aly and Benmokrane (2005) found that the bond strength of the FRP bars was related to the square root of the longitudinal modulus of the FRP bars. The Canadian Bridge design Code determines the required development length for a FRP bar by modifying the formula used for steel bars. The transverse reinforcement index is multiplied by the modular ratio of FRP to steel bars. Therefore, the greater ratio will result in greater bond strength of the FRP bar. This indicates that a higher FRP modulus will yield a smaller development length needed. CSA S806-02, and ACI 440.1R-07 do not take into account the modulus of elasticity of the FRP bar being developed. Very limited work has been done thus far and therefore, the effect of the bar modulus should be further investigated.

FRP reinforcing bars are manufactured with different surface textures such as sand coated, spiral wrapped, helical lugged/ribbed, and indented. Similar to steel bars, it is evident that deformed bars produce a significantly higher bond than plain bars due to the mechanical interlocking between the surface of the bar and the surrounding concrete (Alunno Rossetti *et al.* 1995; Cosenza *et al.* 1997). CSA S806-02 provides modification factors for taking into account the different surface profiles of the FRP bars. A modification factor of 1.0 is assigned for roughened, sand-coated or braided surfaces; 1.05 is assigned to spiral patterned or ribbed surfaces; 1.80 for indented surfaces. This indicates that roughened, sand-coated and braided surfaces provide the highest bond strength followed by spiral patterned and ribbed surfaces, and lastly, indented surfaces with the weakest bond strength. Although CSA S806-02 suggests that the surface profile affects the bond strength of the FRP bar, Mosley *et al.* (2008) suggest the opposite. Mosely *et al.* (2008) investigated the bond strength of FRP reinforcement through three series of beam tests using GFRP and AFRP and showed that the deformation/surface texture of the FRP

reinforcement did not significantly affect the bond strength or crack widths. Hao *et al.* (2009) performed tests on 90 pullout specimens to study the behaviour of GFRP bars with ribbed surfaces with varying rib geometries in 28.7 MPa concrete. The research showed that when the rib height was kept constant at 5 or 6% of the rebar diameter, rib spacing equal to the rebar diameter was superior to rib spacing ranging from 0.5 to 3 times the rebar diameter. The research also showed that a rib spacing of the bar diameter, a rib height of 6% of the rebar diameter was superior to rib heights ranging from 3 to 9%. Research from Baena *et al.* (2009) concluded that when the bond failure is occurring at the rebar-concrete surface interface, the rebar surface treatment has a significant effect on the bond strength. Failure at the rebar surface occurs when the concrete strength is greater than 30 MPa. The influence of rebar surface treatment on bond strength is less important in the low concrete strength than in the high concrete strength. It is difficult to conclude that a definite relationship has been established for the effect of bar surface on the bond strength. Therefore the effect of bar surface should be further investigated as more information becomes available.

2.5.2 Structural considerations (embedment length, clear cover, position of the bar within the structural element)

The splitting and pullout modes of failure depend on the amount of concrete cover (Untrauer, 1965; Tepfers, 1973; Orangun *et al.*, 1977; Eligehausen, 1979; Darwin *et al.* 1996). For small cover and bar spacing, it is likely that splitting tensile failure will occur whereas for large cover and bar spacing, it is possible to obtain a pullout failure mode resulting in higher bond strength (ACI 408R-03). Ehsani *et al.* (1996) conducted a test program with a total of 102 specimens with GFRP bars. The research showed that concrete cover had a significant effect on the type of bond failure. If the test specimen had a concrete cover of one bar diameter ($c = 1d_b$), the splitting mode of failure occurred. If the test specimen had a cover of equal to or exceeding two bar diameters ($c \geq 2d_b$), a pullout failure or rebar fracture was observed. Orangun *et al.* (1977) conducted splice tests on 62 unconfined and 54 confined specimens that all failed due to splitting. An equation was developed that related the average bond stress normalized by the square root of the concrete compressive strength to the normalized cover to the center of the bar and the normalized splice length using linear regression. This methodology was used by Wambeke and Shield (2006) to evaluate compiled database of FRP bars using beam-end tests, notch-beam tests, and splice tests.

A linear regression of the normalized average bond stress versus the normalized cover and embedment length shows that an increase in cover was accompanied by an increase in the bond strength. Furthermore, their relationship shows that the effect of concrete cover and bar spacing on the bond strength is nonlinear. ACI 440.1R-07 uses Wambeke and Shield's relationship to determine the bond strength of a FRP bar which includes the effect of concrete cover. Similarly, CSA.S6-06, CSA.S806-02 design codes all incorporate the effect of the concrete cover and bar spacing in the determination of bond strength for a FRP bar.

Increase in embedment Length or splice length of a reinforcing bar will increase its bond capacity. However, this increase in capacity is not directly proportional to the increase in bonded length. This is a result of the bond forces not being uniformly distributed along the length of the bar. Bond failure tends to be incremental, initiating in the area with the highest bond force per unit length. The effect of embedment length of FRP bars on the average bond stress in concrete was studied by Larralde and Silva-Rodriguez (1993), Ehsani *et al.* (1995), Benmokrane *et al.* (1996), Sheild *et al.* (1997), Cosenza *et al.* (1997), Tigiouart *et al.* (1997, 1998), Achillides and Pilakoutas (2004), Aly *et al.* (2006), and Okelo (2007). Their research showed that the maximum average bond strength decreases with increasing embedment lengths which is similar to the behavior of steel bars. This was attributed to the non-uniform distribution of the bond stress along the length of the bar. For longer embedment lengths, Ehsani *et al.* (1995) reported that there is an increase in the initial tensile load and the initial stiffness of the bond stress- slip curve. Achillides and Pilakoutas (2004) found out that the rate of bond stress increase is greater for smaller embedment lengths than for larger embedment lengths and attributed this behavior to the non-uniform distribution of the bond stresses on the bar. Research by Okelo (2007) shows that for longer embedment lengths with higher compressive strengths, bar fracture, or concrete splitting or shear compression failure takes place. The study also shows that for short embedment lengths with low compressive strengths and small bar sizes, pullout of the bar occurs.

It has been observed that bar position during concrete placement plays an important role in the bond strength between concrete and reinforcing bars. The effect of bar casting position on the bond behavior of FRP bars was investigated by Challal and Benmokrane (1993), Eshani *et al.* (1993), Alunno Rossetti *et al.* (1995), Benmokrane and Masmoudi (1996), Tigiouart *et al.* (1998)

and Wambeke (2003). It was observed that top cast bars showed weaker bond strength compared to bottom cast bars. This was attributed to that during the placement of concrete, air, water and fine particles migrate upwards and become trapped below the surface of the rebar. This causes a significant decrease in the bond strength under horizontally placed bars near the top of the concrete surface due to the decreased contact area between the surrounding concrete and the bottom half of the rebar. Top cast bars generally refers to horizontal reinforcement with more than 305 mm of concrete below (ACI 440.1R-06). Tests from Ehsani et al. (1996) have shown that the bond strength of top bars is 66% of the bond strength of bottom bars. A decrease in the bond strength requires an increase in the required development length of the FRP bars. therefore, a modification factor is needed to account for the bar location when calculated the development length. ACI 440.1R-03 recommends a modification factor of 1.3 based on the available data from work by Chaallal and Benmokrane (1993) and Ehsani et al. (1996). ACI 440.1R-07 later revised its modification factor from 1.3 to 1.5 based on work done from Wambeke and Shield (2006). CSA.S806-02 and CSA.S6-06 design codes recommend a bar location modification factor of 1.3.

The use of transverse reinforcement provides confinement to developed and spliced bars by limiting the progression of splitting cracks and therefore increases the bond force needed to cause failure (Tepfers 1973; Orangun *et al.* 1977; Darwin and Graham 1993). Transverse reinforcement added beyond what is need to provide the transition from splitting to pullout failure becomes less effective and eventually provides no increase in the bond strength (Orangun *et al.* 1977).

CHAPTER 3

EXPERIMENTAL STUDY ON PULLOUT STRENGTH OF PRE- INSTALLED GFRP BARS IN CONCRETE

3.1 General

Steel bars have been the primary means of reinforcing in concrete for more than 100 years. Steel reinforcing bars have performed quite well in most applications except where members have been subjected to corrosive environment. Some examples of structures subjected to corrosive environments include bridge deck and barriers due to use of de-icing salt in winter times. Several approaches have been taken to control the corrosion problem. One of these methods is to coat steel bars with epoxy. Epoxy-coated steel bars have been widely used in bridges. However, there have been discoveries of premature corrosion of epoxy-coated steel bars that have led to concerns about long-term performance of such steel bars. Thus, the use of FRP technology has become another alternative to address the corrosion problem. In this research, GFRP bars are utilized as main reinforcement in bridge barrier as shown in Fig. 1.3.

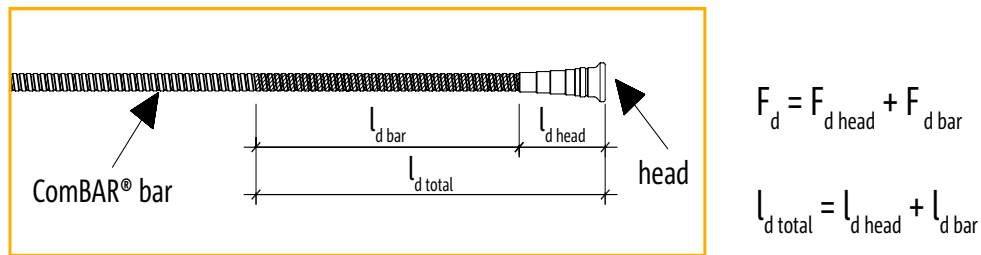


Fig. 3.1 GFRP bar head details (Schoeck, 2011)

The design procedure of the GFRP-reinforced bridge barrier shown in Fig. 1.3 requires information about the pullout capacity of the GFRP bars embedded in the concrete deck slab. It should be noted that the pullout capacity of straight and headed GFRP bars embedded in concrete is as yet unavailable. The development length specified in CHBDC, ACI 440 and CSA S806 can be applied to beams rather than anchorage in case of bridge barrier. As such, the objective of this research is to conduct experimental tests on full-scale concrete specimen to

determine the pullout capacity of GFRP bars with different embedment lengths, namely: 150, 200 and 250 mm, and with straight or headed ends. The results from these tests will determine the proper embedment length of the GFRP bar in the bridge deck slab to transfer its tensile capacity to concrete.

According to the previous research on direct pullout cube tests of the bars, there is a concern that tests results are not conservative due to additional confinement of the concrete around the bar. Ehsani, et al. (1997) conducted a study that compared bond behavior of FRP using the direct pullout method to FRP. Eighteen pullout specimens with varying rebar sizes (No. 3, 6, and 9 FRP bars), and embedment lengths were tested, and compared to 48 beam tests. Their direct pullout specimens consisted of casting three bars in 1219x762x406 mm concrete block. After curing (28 days), they applied load directly to the block through a hydraulic ram and read live and free end measurements with dial gauges. Upon comparison of the results, Ehsani, et al. (1997) found that the direct pullout method on concrete cubes yielded non-conservative development lengths. Analyzing a sampling of their data, they found the ultimate bond stresses increased by an average of 13% when the direct pullout test was used. In order to address a concern of non-conservative bond strength with the cube pull out tests, concrete slabs were used to promote bar pullout rather than concrete splitting. The variable parameters that were used to determine the GFRP bar pullout force include bar diameter, headed or straight bar and embedment length. The following sections describe the experimental program and results.

3.2 Materials for the Pullout tests

ComBAR® GFRP bars with ribbed surface manufactured by Schoeck Inc. (Schoeck, 2011) were used in this study. It has a special ribbed and coated surface. The matrix VEU resins were composed of modified vinyl ester with a maximum volume fraction of 25%. The fibre reinforcement was comprised of continuous ECR-glass fibres with a minimum volume fraction of 75%. Two bar diameters were considered in this study, namely: 12 and 16 mm diameter. Table 3.1 summaries geometrical characteristics of the bars. While Table 3.2 summarizes their material properties. ComBAR® bars behave linearly elastic up to failure. For all bar diameters, tensile rupture occurs at stresses well above 1,000 MPa. As a result of the comparatively low

modulus of elasticity of the bars (≥ 60 GPa), their failure in concrete members is preceded by large deflections.

Table 3.1 Nominal diameter and sectional area of GFRP bars with ribbed surface

US size	Metric size	Core diameter, mm	Exterior diameter, mm	Area, mm ²
#4	13	12	13.5	113
#5	16	16	18	201

Table 3.2 Material properties of straight GFRP bars with ribbed surface (Schoeck, 2011)

properties	terms	values	comments
ultimate tensile strength	f_u	$> 1,000$ MPa	all bar diameters
1,000 hour tensile strength ¹⁾	$f_{Fk1000h}$	950 MPa	5th percentile
logarithmic temporal slope ¹⁾	R_{10}	< 15 %	5th percentile
modulus of elasticity	E_f	> 60 GPa	64 GPa for ϕ 16mm bars ²⁾
ultimate elongation	ϵ_{Fu}	2.61%	ϕ 16mm bar ²⁾
bond stress	τ_f	12.2 MPa	ϕ 16mm bar
bar surface profile factor (bond)	k_s	≤ 1.0 ³⁾	(CSA S806 9.3)
bond coefficient	k_b	0.6 ³⁾	(CHBDC 16.8.2.3)
bar surface factor	k_4	≤ 0.8 ³⁾	(CHBDC 16.8.4.1)
transverse shear strength ⁴⁾	t	150 MPa	acc. CSA / ACI
min. concrete cover	min. c	$d_b + 10$ mm/ $d_b + 5$ mm (pre-cast)	min. cover for load transfer

¹⁾ values for determination of design value of tensile strength according to durability concept of fib defining time-to-failure lines (see page 15)

²⁾ values for 16mm ComBAR® bars (certification of compliance with ISIS specifications, University of Toronto)

³⁾ value determined for ComBAR® bars of all diameters

⁴⁾ values in tests according to CSA / ACI not for design of dowels

⁵⁾ Tests have shown that bond properties of ComBAR® bars are at least as good as those of steel rebar. Final tests are in progress.

ComBAR® bar end heads have been developed to produce ComBAR® double headed bolts (DHBs). These can be used as shear reinforcement in beams and punching shear reinforcement in slabs. Bar end heads can also be used to reduce the development length of straight bars wherever geometric constraints do not allow for the development of the plain bar (single headed bolts - SHB). ComBAR® bar end heads are made of polymeric concrete cast on the ribbed surface of the bar end. Their long-term behaviour / durability is governed by the behaviour of the bar. Long-term pull-out tests have been performed on bar end heads cast into highly alkaline

concrete cubes. The heads were subjected to constant loads until failure occurred. The concrete cubes were heated to 60°C and saturated with water over the duration of the tests. The time-to-failure line for the headed bars was established using the results of a large number of tests at different load levels. The characteristic value of the anchorage strength of the headed ends was determined for applications with a maximum effective temperature of 40°C (for projects in Canada and Central Europe). Figure 3.1 shows a schematic diagram of the GFRP bar with headed end. The total developed force of a ComBAR® bar with a headed end is the sum of the force anchored by the head and the additional force developed along the bar. Analogously, the total development length is the sum of the length of the head and the additional development length along the bar. Schoeck (2011) produced Table 3.3 for marketing, on which the capacity of the bar head is specified as 100 kN for the 16-mm diameter bar and 50 kN for the 50 mm diameter bar. However, it was not clear whether the capacity is for the length of the head or for a longer embedment length. As such, the experimental study reported in this thesis intends to investigate the pullout capacity of such bars embedded in concrete with different lengths, namely, 150, 200 and 250 mm. Such embedment length include the length of the head which is 100 and 60 mm for the 16- and 12-mm diameter bars. The results expects to ensure that the head-end GFRP bar and the GFRP bar with straight end, shown as main reinforcement in the front face of the proposed barrier wall in Fig.1.3, will transmit the tensile capacity of the bar into the deck slab through a 200 mm length of embedment.

Table 3.3 Dimensions and anchorage forces for GFRP bars with end heads (Schoeck, 2011)

diameter bar (mm)	length head (mm)	ext. diam. head (mm)	$F_{head,k}$ short term (kN)	$F_{head,k}$ long-term (100 yrs.) (kN)
12	60	30	50	25
16	100	40	100	59
32	100	64	137	98

Table 3.4 summarizes the text matrix of the test specimens. GFRP bars with 12- and 16-mm diameters were used to determine the effect of the bar diameter on the pullout strength. The effect of embedment length on pullout strength was also investigated by varying the embedment length to be 150, 200 and 250 mm. Two types of bars ends were considered, namely: headed and

without head (i.e straight end). For each bar configuration, 5 identical samples were cast to provide more reliable data to get the average pullout capacity of the bars.

Table 3.4 Summary of test specimens

Bar Size	Bar type	Embedment length	# of cubes samples	# of samples in slab
12	Straight	150	5	5
12	Straight	200	5	5
12	Straight	250	5	5
12	Headed	150	5	5
12	Headed	200	5	5
12	Headed	250	5	5
16	Straight	150	5	5
16	Straight	200	5	5
16	Straight	250	5	5
16	Headed	150	5	5
16	Headed	200	5	5
16	Headed	250	5	5

3.3 Description of Slab Pullout Specimens

Concrete slabs of 30-m length, 1.35-m width and 300 mm depth, were cast at off-campus facility using ready mix concrete of minimum strength of 30 MPa. The slab was reinforced with top and bottom reinforcement made of 15M steel bars spaced at 300 mm each direction to represent the actual condition in bridge decks. GFRP bars were embedded in a concrete slab at different embedment lengths of 150, 200 and 250 mm. A total of 60 single bars were embedded in the slabs. Distances between adjacent bars was maintained 1000 mm to accommodate the loading setup. Appendix A shows schematic diagrams of the concrete slabs, slab reinforced and GFRP arrangements. Figure 3.2 shows views of the formwork for casting the concrete slab with embedded GFRP bars. Concrete cylinders were tested to check the 28th day concrete strength. The concrete strengths resulted from cylinder tests were 35.7, 33.34, 28.31, 26.84 and 24.27 MPa. Thus, the average concrete strength was 29.69 MPa.



Fig. 3.2 Views of the formwork for casting concrete slabs with embedded GFRP bars

3.4 Test Setup for Slab Pullout Tests

A test setup shown in Fig. 3.3, in accordance with the requirements of the ASTM E-488-96 (ASTM, 1996) was used. The jacking system, load cell and bar grips rest over two HSS steel beams that rest on HSS steel beams. The latter were 1-m apart in order to avoid any confinement of the concrete around the bar. Test set up has to be disassembled and moved to the next bar every test. Hydraulic jack was placed on the steel beams. Then the load cell was placed on top of it separated by steel plate and rubber pads. The bar grips were placed on top of the load cell separated also by steel plate with rubber pads. Rubber pads were used in order to avoid damage on the load cell at the sudden failure of the samples and steel plate.

A critical issue in testing GFRP reinforcing bars is its low transverse strength; therefore, the bars could be damaged due to the gripping forces at the contact surface between the bar and the grips. For this study, the available steel grip shown in Fig. 3.4 was utilized. The grip used in this study consisted of two grooved halves, which encompass the rebar and then bolted together using high-strength steel bolts. The grips were secured together using a torque gun powered by compressed air. The amount of torque applied was limited such that the transverse strength of the GFRP bar could not be exceeded. The grip was designed to apply clamping forces along the length of the grip and at bar contact surface on opposite sides of the bars. Such grip system is shown with the test setup in Fig. 3.5(a). This gripping system was successful in testing the 12-mm diameter bars

of different embedment lengths. However, for the 16-mm bars, especially with deeper embedment, bar crushing and local damage occurred at the grip location as depicted in Fig. 3.5(b). As such, other grip system available in the structures laboratory, shown in Fig. 3.7(b) was used. This grip system was good for the 16-mm diameter bars according to the hole dimension that accommodate the bar. However, for 12-mm diameter bars, additional 3 – 5-mm diameter metal strand was used to wrap the bar between its ribs, as shown in Fig. 3.6, to distribute the clamping load evenly at the grip location. Figure 3.7(a) shows view of such grip in the test setup. However, in few loading cases, the GFRP ruptured and the steel strands smashed as shown in Fig. 3.8. As such, it was decided to use a grip system shown in Fig. 3.9. This grip system incorporated conical wedges to be inserted in a conical hole that accommodate the GFRP bar. These wedges ensure that the clamping force is distributed all around the bar perimeter and over a bar length of 75 mm. This gripping system proved successful in testing the rest of the bars except the 16-mm diameter headed bars with 250-mm embedment length.



Fig. 3.3 Test setup for slab pullout testing

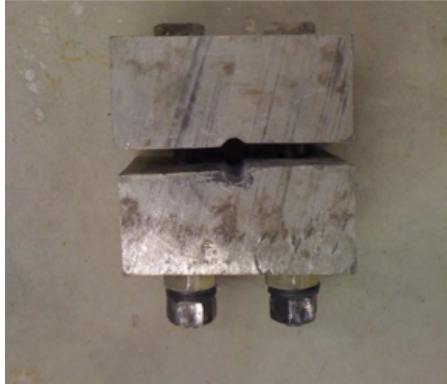


Fig. 3.4 Views of steel grips used in pullout tests, clamping the bar from two opposite sides



(a)



(b)

Fig. 3.5 View of (a) test setup with steel grips and (b) bar damage due to gripping on the bar during testing



Fig. 3.6 Metal rope wrapped around a 12-mm diameter bar at the grip location



(a)



(b)

Fig. 3.7 Views of the revised testup showing the added large grip shown in (b), clamping the bar from two opposite sides



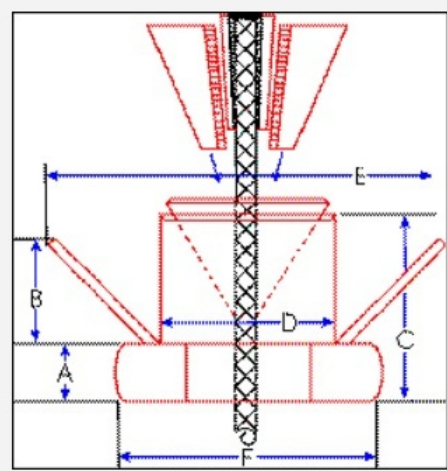
Fig. 3.8 Views of bar rupture at the location of the large grip



(a)



(b)



RING	BAR SIZE	A	B	C	D	E	F	WEIGHT
RS	#4 thru #8	1-1/2"	3"	4-1/2"	4"	7"	5-1/2"	20 lbs.
RL	#9 thru #18	2"	3"	5"	6"	9-3/4"	7-3/4"	43 lbs.

(c)

Fig. 3.9 Views of the manufactured grip with conical wedges clamping the bars from all sides

3.5 Test Results and Discussions

Like the steel anchors, if the embedment depth of the GFRP bar is small, the concrete cone breakout failure would occur. However, if the embedment depth of the GFRP bar is deeper, combined concrete/bond failure would occur. The combined failure includes a shallow concrete cone with a bond failure below the cone. In some cases, radial cracks may occur dividing the cone into pieces instead of one piece cone. The bond failure may occur at the concrete/bar interface by shearing concrete or by shearing the ribs. As mentioned earlier, some of the GFRP bars failed at the grip location. However, other GFRP bars failed due to bar tensile rupture along the free length of the bar between the grip and the top surface of the concrete slab. Figure 3.10 shows views of the bar tensile rupture just outside the grip location, while Fig. 3.11 shows views of the bar tensile rupture along the length of the bar. In any case, the dominating type of bar failure was pullout failure. Pulled-out bar left perfect hole in the concrete without any additional

concrete conical failure or cracks as shown in Fig. 3.12. In some pullout tests, a shallow concrete cone with a bond failure below the cone occurred as shown in Fig. 3.13. In pullout failure, it was observed that the bar sheared the concrete surrounding the bar. The ultimate bond force was dictated by the shear strength of the concrete surrounding the bar.

Table 3.5 summarizes the test results in the form of bar designation, bar embedment length, maximum slip at failure and failure mode. While Table 3.6 shows the average pullout capacity of bars that were pulled out from concrete. Generally, it can be observed that the pullout capacity increases with increase in embedment length for example the pullout capacity of the 12-mm diameter bars were 22kN, 24kN and 72kN for bar embedment length of 150-mm, 200-mm and 250-mm, respectively. One may observe that the rate of increase of pullout capacity with increase in embedment length is not linearly proportional. This may be attributed to the fact that some bars may have been connected to the steel mesh for stability during concrete casting, this increasing shear resistance of concrete to bar pullout. The use of transverse reinforcement in the slabs provides confinement to anchored bars to limit splitting cracks and therefore increases bond strength. By inspection of the results, one may observe that the presence of bar head generally increases the pullout capacity. However, the scatter in the data for bars with larger embedment slightly supports this conclusion. As for the effect of bar diameter, one may observe that the increase in bar diameter increase the pullout capacity.



Fig. 3.10 Views of the bar rupture at grip location during pullout tests

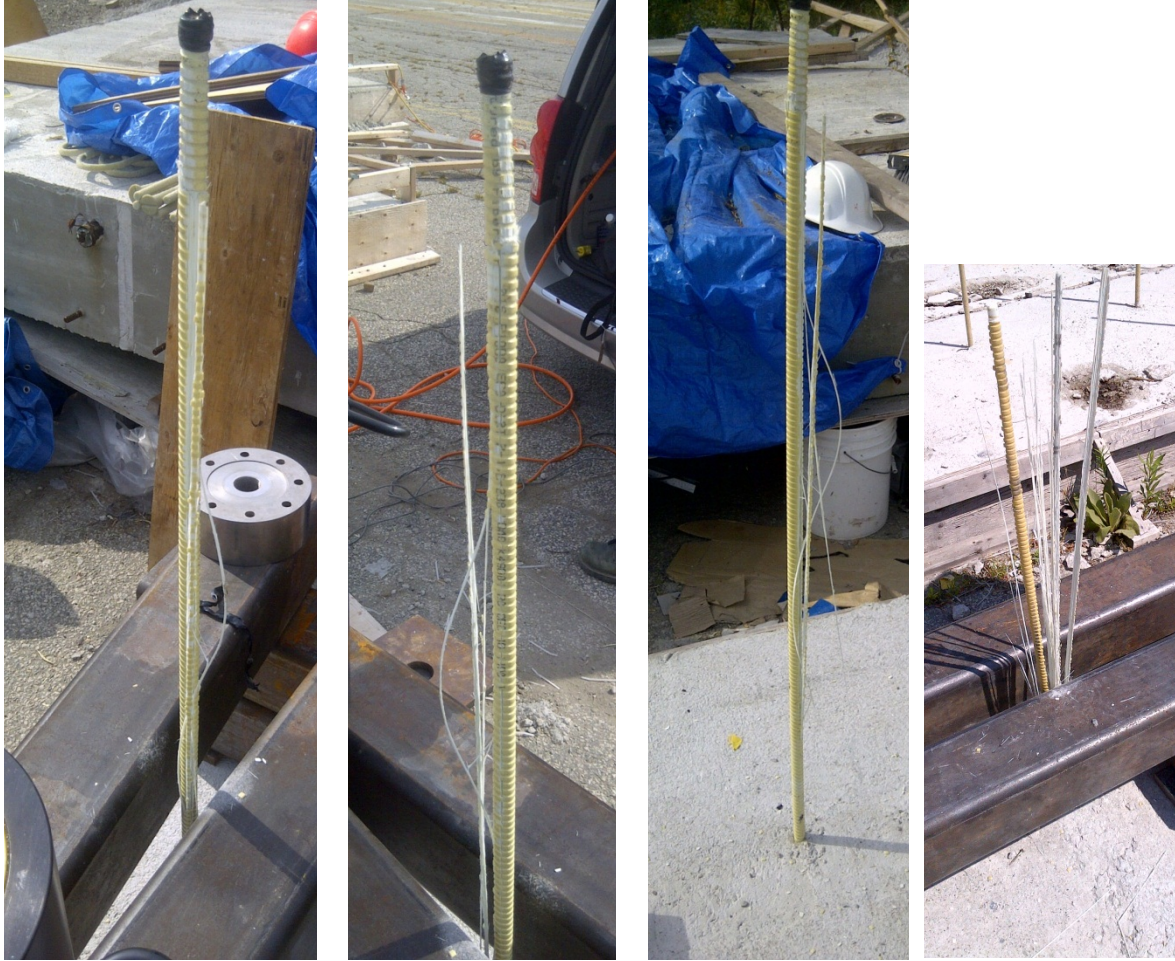


Fig. 3.11 Views of the bar rupture along its free length during pullout tests



Fig. 3.12 Views of the bar pullout from the concrete slab after the test showing concrete shearing



(a)



(b)



(c)



(d)



(e)



(f)



(g)



(h)

Fig. 3.13 Views of the combined bar pullout and concrete breakout (conical failure) at top surface of concrete slab

Table 3.5 Results from slab pullout tests

Test No.	Bar type	Embedment length, mm	Ultimate load, kN	LVDT maximum reading, mm	Failure mode
1	12D-Straight-1	150 mm	28	-1.74	Pulled out
2	12D-Straight-2	150 mm	22	-2.68	Pulled out
3	12D-Straight-3	150 mm	20	-1.11	Pulled out
4	12D-Straight-4	150 mm	16	-1.69	Pulled out
5	12D-Straight-5	150 mm	22	-1.06	Pulled out
6	12D-Straight-1	200 mm	25	-2.68	Pulled out
7	12D-Straight-2	200 mm	22	-1.03	Pulled out
8	12D-Straight-3	200 mm	24	-1.93	Pulled out
9	12D-Straight-4	200 mm	23	-0.99	Pulled out
10	12D-Straight-5	200 mm	26	-2.47	Pulled out
11	12D-Straight-1	250 mm	21	-1.51	slipped from grip
12	12D-Straight-1a	250 mm	24	-1.7	slipped from grip
13	12D-Straight-1b	250 mm	79	-3.23	Pulled out
14	12D-Straight-2	250 mm	65	-3.64	Pulled out
15	12D-Straight-3	250 mm	70	-2.76	Pulled out
16	12D-Straight-4	250 mm	66	-3.52	Pulled out
17	12D-Straight-5	250 mm	81	-3.96	Pulled out
18	12D - Headed-1	150 mm	28	-2.41	Bar broken at the grip
19	12D - Headed-2	150 mm	40	-4.2	Bar broken at the grip
20	12D - Headed-3	150 mm	51	-5.19	Pulled out
21	12D - Headed-4	150 mm	47	-4.06	Pulled out
22	12D - Headed-5	150 mm	48	-4.32	Pulled out
23	12D - Headed-1	200 mm	54	-4.93	Pulled out
24	12D - Headed-2	200 mm	53	-5.06	Pulled out
25	12D - Headed-3	200 mm	49	-5.74	Pulled out
26	12D - Headed-4	200 mm	37	-3.63	Bar broken at the grip
27	12D - Headed-5	200 mm	55	-5.44	Pulled out

28	12D - Headed-1	250 mm	54	-4.93	Pulled out
29	12D - Headed-2	250 mm	53	-5.06	Pulled out
30	12D - Headed-3	250 mm	85	-4.03	Pulled out
31	12D - Headed-4	250 mm	50	-1.53	Pulled out
32	12D - Headed-5	150 mm	76	-3.07	Pulled out
33	16D-Straight-1	150 mm	29	-1.64	Pulled out
34	16D-Straight-2	150 mm	22	-0.84	bar slipped from grip
35	16D-Straight-2a	150 mm	20	-0.81	bar slipped from grip
36	16D-Straight-2b	150 mm	21	-0.44	bar slipped from grip
37	16D-Straight-2c	150 mm	32	-2.22	Pulled out
38	16D-Straight-3	150 mm	48	-3.29	Pulled out
39	16D-Straight-4	150 mm	36	-1.86	Pulled out
40	16D-Straight-5	150 mm	36	-2.04	Pulled out
41	16D-Straight-1	200 mm	42	-0.5	Pulled out
42	16D-Straight-2	200 mm	44	-3.82	Pulled out
43	16D-Straight-3	200 mm	46	-2.33	Pulled out
44	16D-Straight-4	200 mm	47	-2.67	Pulled out
45	16D-Straight-5	200 mm	53	-2.77	Pulled out
46	16D-Straight-1	250 mm	141	-2.9	Pulled out
47	16D-Straight-2	250 mm	136	-1.59	pulled out
48	16D-Straight-3	250 mm	132	-3.72	Pulled out
49	16D-Straight-4	250 mm	117	-1.49	Pulled out
50	16D-Straight-5	250 mm	126	-2.6	Pulled out
51	16D-Headed-1	150 mm	93	-1.76	Pulled out
52	16D-Headed-2	150 mm	102	-2.77	Bar broke at the grip
53	16D-Headed-3	150 mm	128	-3.58	Pulled out
54	16D-Headed-4	150 mm	78	-2.68	Pulled Out
55	16D-Headed-5	150 mm	88	-0.98	Bar broke at the grip
56	16D-Headed-1	200mm	119	-1.64	Bar broke at the grip
57	16D-Headed-2	200mm	111	-2.77	Bar broke at the grip
58	16D-Headed-3	200mm	121	-1.58	pulled out

59	16D-Headed-4	200mm	122	-2.48	pulled out
60	16D-Headed-5	200mm	117	-2.93	Bar broke at the grip
61	16D-Headed-1	250 mm	50	-2.86	Bar broken at the grip
62	16D-Headed-2	250 mm	63	-2.88	Bar broken at the grip

Table 3.6 Mean value of the maximum loads obtained from slab pullout tests

Group No.	Bar type	Embedment length, mm	Mean value, kN
1	12-STRAIGHT	150	22
2	12-STRAIGHT	200	24
3	12-STRAIGHT	250	72
1	12-HEADED	150	49
2	12-HEADED	200	53.5
3	12-HEADED	250	65
1	16 - STRAIGHT	150	36
2	16 - STRAIGHT	200	46
3	16 - STRAIGHT	250	130
1	16 – HEADED	150	100
2	16 - HEADED	200	121.5

The tensile capacity of the bar is the multiplication of the bar cross-section areas, the tensile strength of GFRP material and the resistance factor of GFRP. CHBDC specified the GFRP resistance factor as 0.5. Given the material tensile strength of 1000 MPa as provided by the manufacturer, the tensile capacity of the 12- and 16-mm diameter GFRP bars are 56.5 and 100 kN, respectively. Based on the experimental findings, the pullout capacity of the headed GFRP bars were 65 and 121.5 kN for the 12- and 16-mm diameter bars with 250-mm and 200-mm embedment length respectively. As such the proposed configuration shown in Fig. 1.3 for the GFRP-reinforced barrier is adequate with respect to anchorage capacity. Still the straight bars with no heads can be adequate to transfer the tensile capacity of the bar to concrete through the

250-mm embedment length. This is evident from the pullout capacities of 72 and 130 kN recorded experimentally for the 12- and 16-mm diameter bars, respectively.

3.6 Comparison to Code Predictions

The design provisions and recommendations evaluated in this study are CSA S806-02, CSA S6-06, ACI 440.1R-06 and CSA A23.3-04. The development lengths provided by the codes are then compared with the approved-experimentally 250-mm embedment length of either of straight or headed GFRP bars. It should be noted that the development lengths specified in the above-mentioned codes, as presented in the following subsections, were based on beam test configurations in terms of bar size, concrete strength, concrete cover and reinforcement properties, except CSA A23.3-04 that depends on the concrete breakout capacity of headed steel bars embedded in concrete.

3.6.1 CSA S806-02 Development Length

The development length requirement for FRP bars provided by CSA S806-02 is shown in Equations 3.1. Table 3.7 shows the values of the parameters used in Equation 3.1 for each bar size and concrete. While Table 3.8 shows the corresponding development length of the GFRP bar.

$$ld = 1.15 \frac{k_1 k_2 k_3 k_4 k_5}{d_{cs}} \frac{f_F}{\sqrt{f'_c}} A_b \quad (3.1)$$

It can be observed that the development lengths are 348 and 464 mm for the 12- and 16-mm diameter bars which are far greater than the 250-mm embedment length that was proved adequate experimentally for the proposed barrier configuration shown in Fig. 1.3.

Table 3.7 Parameters for development length equation specified in CSA S806-02

Parameter	12-mm GFRP bar	16-mm GFRP bar
k_1	1	1
k_2	1	1
k_3	0.8	0.8
k_4	1	1
k_5	1	1
d_{cs}	30	40
f_{frp}	500 MPa	500 MPa
$\sqrt{f_c}$	5.477	5.477
A_b	113 mm ²	201 mm ²

Table 3.8 Development length results based on development Length Equation specified in CSA S806-02

f_c , MPa	d_b , mm	L_d , mm
30	12	348
30	16	464

3.6.2 Development Length Equation Specified in CSA S06-06

The development length requirement for FRP bars provided by CSA S06-06 is shown in Equation 3.2. Table 3.9 shows the values of the parameters used in Equation 3.2. While Table 3.10 shows the development length for the tested bars.

$$l_d = 0.45 \frac{k_1 k_4}{\left[d_{cs} + K_{tr} \frac{E_{FRPu}}{E_s} \right]} \left[\frac{f_{FRPu}}{f_{cr}} \right] A \quad (3.2)$$

It can be observed that the development lengths are 386 and 516 mm for the 12- and 16-mm diameter bars which are far greater than the 250-mm embedment length that was proved adequate experimentally for the proposed barrier configuration shown in Fig. 1.3.

Table 3.9 Parameters for the development length equation specified in CSA S06-06

PARAMETER	12mm GFRP bar	16mm GFRP bar
k_1	1	1
k_4	1	1
f_{frp}	500 MPa	500 MPa
f_{cr}	2.1908	2.1908
A_b	113	201

Table 3.10 Required development length requirement based on CSA S06-06

f_c , Mpa	d_b , mm	f_{frp} , MPa	l_d , mm
30	12	500	386
30	16	500	516

3.6.3 Development Length Specified in ACI 440.1-06

The development length requirement for FRP bars provided by ACI 440.1-06 is determined by solving for l in Equation 3.3.

$$f_{frp} = \frac{0.83\sqrt{f'_c}}{\alpha} \left(13.6 \frac{l_e}{d_b} + \frac{C}{d_b} \frac{l_e}{d_b} + 340 \right) \quad (3.3)$$

Table 3.11 shows the parameters used in Equation 3.3 for each bar size and Table 3.12 shows the development length. It can be observed that the development lengths are 500 and 721 mm for the 12- and 16-mm diameter bars which are far greater than the 250-mm embedment length that was proved adequate experimentally for the proposed barrier configuration shown in Fig. 1.3.

Table 3.11 Parameters for the developable bar stress equation specified in ACI 440.1-06

Parameter	12-mm GFRP bar	16-mm GFRP bar
f_{frp}	500 MPa	500 MPa
α	1	1
C/d_b	3.5	3.5
A_b	113	201

Table 3.12 Development length requirement per ACI 440.1-06

f_c , MPa	d_b , mm	f_{frp} , MPa	l_d , mm
30	12	500	500
30	16	500	721

3.6.4 Development Length of Headed Anchors according to CSA A23.3-04

According to the CSA A23.3-04 standard, steel headed anchor pullout capacity depends on three possible failure modes as follows:

1. Tension capacity of the rod

$$N_{sr} = \phi_s n A_{se} f_{ut} R \quad (3.4)$$

2. Tensile concrete breakout capacity

$$N_{cbr} = 10 \phi_c \sqrt{f'_c} h_{ef} \quad (3.5)$$

3. Pullout capacity of the head

Pullout capacity of tested bar depends mainly on bond strength between head and the bar. The first failure mode of GFRP rebar is not an option here as code limits maximum design strength of the bar to 50%. However, it is possible to use the tensile concrete breakout capacity equation to calculate for embedment length, which would be required to use full capacity of the head pullout strength. For a 12-mm diameter bar, and considering the maximum tensile capacity of the GFRP bar of 56.5 kN, the required development length would be:

$$l_d = \sqrt[1.5]{\frac{N_{br}}{10 \phi_c \sqrt{f'_c}}} \quad (3.6)$$

Table 3.13 summarizes the parameters used to calculate the development length. While Table 3.14 summarizes results of embedment length required for each bar size in order to reach full capacity of the head specified in the GFRP bar manufacturer's brochure. It can be observed that the development lengths are 130 and 200 mm for the 12- and 16-mm diameter bars. This means that CSA A23.3 procedure for concrete breakout capacity gives realistic results as compared to

experimental finding despite the use of GFRP bars in lieu of steel bars and concrete breakout capacity in lieu of bar pullout. CSA 23.3 gives better predictions than other Standards due to different testing methods used to predict development lengths in ACI440 and CHBDC. CSA 23.3 equation was based on results from direct pullout tests and equation from CHBDC and ACI440 was based on beam test method.

Table 3.13 Parameters for the Equation 3.7 specified in CSA A23.3-04

Parameter	12 mm GFRP bar	16 mm GFRP bar
ϕ_c	0.65	0.65
N_{rb}	50 kN	100 kN
f'_c	30 MPa	30 MPa

Table 3.22 Embedment length of the headed anchor based on concrete breakout capacity

f'_c , Mpa	d_b , mm	N_{rb} , kN	l_d , mm
30	12	50	130
30	16	100	200

3.7 Conclusions

Results from pullout tests of GFRP bars embedded in wide concrete slabs revealed that 200-mm embedment length of both headed and straight GFRP bars embedded in concrete deck slabs in the proposed barrier configuration shown in Fig. 1.3 is adequate. Results showed general trend of increase in pullout capacity with increase in bar size and embedment length. However, it is advisable to repeat some of these tests with different concrete strength and using the grip system shown in Fig. 3.9 to reach a data base from which an imperial equation for the pullout capacity of such bars can be developed.

CHAPTER 4

EXPERIMENTAL TESTS ON GFRP-REINFORCED PL-3 CONCRETE BARRIER

4.1 General

The design process of bridge barriers is specified in the Canadian Highway Bridge Design Code. CHBDC Clause 12.4.3.5 specifies that the suitability of a traffic barrier anchorage to the deck slab shall be based on its performance during crash testing of the traffic barrier. For an anchorage to be considered acceptable, significant damage shall not occur in the anchorage or deck during crash testing. CHBDC also specifies that if crash testing results for the anchorage are not available, the anchorage and deck shall be designed to resist the maximum bending, shear and punching loads that can be transmitted to them by the barrier wall. As such, the initial design of the proposed PL-3 bridge barrier (Sennah et al., 2010) was carried out to meet the CHBDC design criteria specified for static loading at the anchorage between the deck slab and the barrier wall. CHBDC specifies transverse, longitudinal and vertical loads of 210, 70 and 90 kN, respectively, that can be applied simultaneously over a certain barrier length in case of PL-3 barrier. It also specifies that transverse load shall be applied over a barrier length of 2400 mm for PL-3 barriers. Since transverse loading creates the critical load carrying capacity, both the longitudinal and vertical loads were not considered in the design of barrier wall reinforcement and anchorages between the deck slab and the barrier wall. It should be noted that CHBDC specifies a live load factor of 1.7. Thus, the design impact load on PL-3 barrier wall over 2.4 m length is 357 kN.

In spite the fact that the AASHTO-LRFD yield-line failure equations were developed for barriers reinforced with steel bars, they were applied herein for preliminary design of GFRP-reinforced barrier. As such, the design of the vertical and horizontal reinforcement in GFRP-reinforced barrier wall was conducted (Sennah et al., 2010) using the yield-line failure equations specified in the AASHTO-LRFD Bridge Design Specifications. This results in the barrier configuration shown in Fig. 1.3(b). Then, experimental tests on full-scale barrier wall were conducted as reported in this Chapter to verify the preliminary design by correlating the experimental failure load with the CHBDC factored design loads. This Chapter presents the AASHTO-LRFD yield-

line failure equations, the experimental program and experimental results on full-scale bridge barrier subjected to difference scenarios of static loading simulating vehicle impact.

4.2 Yield-Line Analysis

The yield-line analysis conducted herein was based only on the ultimate flexural capacity of the concrete components as specified in the AASHTO-LRFD Bridge Design Specifications. In the analysis, it was assumed that the yield-line failure pattern occurs within the barrier wall only and does not extend into the deck slab. This means that the deck slab must have sufficient resistance to force the yield-line failure pattern to remain within the barrier wall. If the failure pattern extends into the deck, the equations for resistance of the barrier wall will not be valid. The LRFD yield-line analysis is also based on the assumption that sufficient longitudinal length of barrier wall exists to result in the desired yield-line failure pattern. For short lengths of barrier walls, a single yield-line may form along the juncture of the barrier wall and the deck slab. Such a failure pattern is permissible, and the barrier wall resistance should be computed using appropriate analysis. Moreover, the LRFD yield-line analysis is based on the assumption that the negative and positive wall resisting moments are equal and that the negative and positive beam resisting moments are equal.

AASHTO-LRFD assumes two yield-line failure patterns based on the location of the truck collision with the barrier wall, as shown in Fig. 4.1. A force F_t distributed over a length L_t as shown in the figure produces the first yield-line failure pattern caused by a truck collision within a wall segment. This interior yield-line pattern is assumed to have three yield lines as shown in Fig. 4.1a. Two of the yield lines have tension on the inside face of the barrier wall and one yield line has tension on the outside face of the barrier wall. The latter is a vertical crack along the height of the barrier wall at the location of vehicle impact. The second yield-line failure pattern occurs at the end of the barrier wall as produced by a force F_t distributed over a length L_t as shown in Fig. 4.1b. In this case, there is only one diagonal yield line that produces tension on the inside face of the barrier. This type of yield-line pattern is assumed to occur at bridge barrier ends and at locations of deflection joints and expansion joints. A solution is obtained for the barrier wall load carrying capacity (i.e. nominal barrier wall resistance) by equating the external work due to the applied loads to the internal work delivered by the resisting plastic moments

along the yield lines. The resisting moment along the yield line is a resultant of the moment about the vertical axis from the longitudinal reinforcement (M_w) and the moment about the horizontal axis from the transverse reinforcement (M_c). The angle of the inclined yield lines can be expressed in terms of the critical length L_c as shown in Fig. 4.1. The applied force F_t is then minimized with respect to the length L_c to get the least value of this upper bound solution. As such, the following equations are introduced in AASHTO-LRFD Specifications.

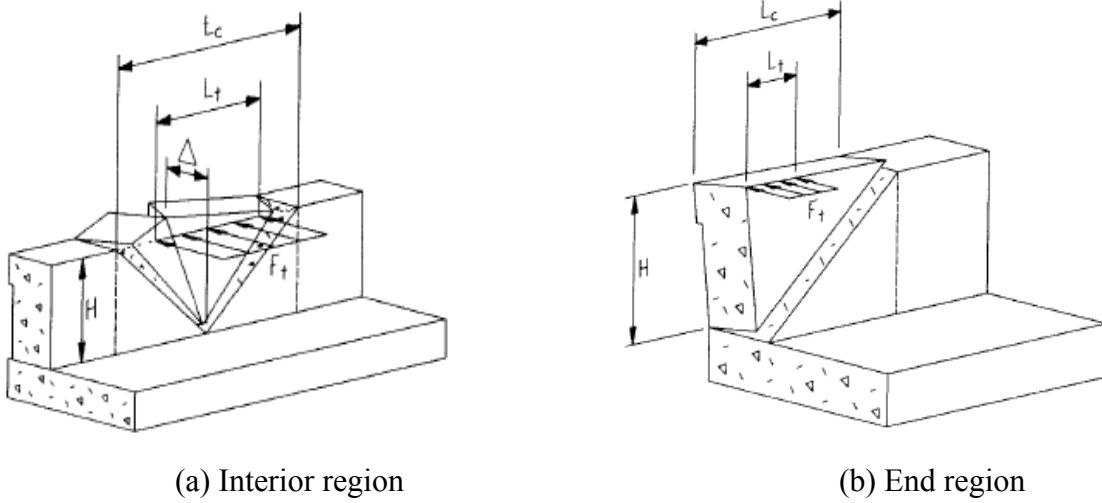


Fig. 4.1 LRFD yield-line analysis of barrier wall (AASHTO, 2012)

For impacts within the barrier segment:

The critical barrier wall length over which the yield line mechanism occurs can be taken as:

$$L_{ci} = \frac{L_t}{2} + \sqrt{\left(\frac{L_t}{2}\right)^2 + \left(\frac{8HM_{bint} + M_{wint}H}{M_{cint}}\right)} \quad (4.1)$$

The nominal barrier wall resistance to transverse load may be determined as:

$$R_{wi} = \left(\frac{2}{2L_{ci} - L_t}\right) \left(8M_{bint} + 8M_{wint}H + \frac{M_{cint}L_{ci}^2}{H}\right) \quad (4.2)$$

For impacts at end of wall or at joint:

The critical barrier wall length over which the yield line mechanism occurs can be taken as:

$$L_{ce} = \frac{L_t}{2} + \sqrt{\left(\frac{L_t}{2}\right)^2 + H\left(\frac{M_{bend} + M_{wend}H}{M_{cend}}\right)} \quad (4.3)$$

The nominal barrier wall resistance to transverse load may be determined as:

$$R_{we} = \left(\frac{2}{2L_{ce} - L_t}\right) \left(M_{bend} + M_{wend}H + \frac{M_{cend}L_{ce}^2}{H}\right) \quad (4.4)$$

Where: L_{ci} = critical length of interior yield line failure pattern; L_{ce} = critical length of exterior yield line failure pattern; L_t = longitudinal length of distribution of impact force F_t ; H = height of barrier wall; M_{bint} = flexural resistance of the cap beam; M_{wint} = flexural resistance of the wall about its vertical axis; M_{cin} = flexural resistance of the wall about a horizontal axis; and R_{wi} = total transverse resistance of the barrier wall.

4.3 Proposed GFRP-Reinforced Barrier

As for the design of the vertical and horizontal reinforcement in the barrier wall, the yield-line analysis was conducted (Sennah et al., 2010) to determine the ultimate flexural capacity of the concrete components as specified in the AASHTO-LRFD Bridge Design Specifications for different GFRP bar size and spacing. Such design work for the PL-3 bridge barrier proposed the use of 16 mm and 12 mm diameter GFRP bars as vertical reinforcement in the barrier front and back faces, respectively, with 12 mm diameter GFRP bars as horizontal reinforcement in case of PL-3 barrier wall, all at 300 mm spacing. The connection between the deck slab and the barrier wall utilized the GFRP headed end bars for proper anchorage. Figure 1.3 shows a schematic diagram of the GFRP reinforcement on the designed barrier wall. Two full-scale PL-3 barrier models of 1200 mm length were erected and tested to-collapse to determine their ultimate load carrying capacities and failure models (Sennah et al., 2010). The first barrier was a control one with reinforcing steel bars, while the second barrier model was reinforced with GFRP bars with headed ends. Based on the data generated from the experimental study, it was concluded that GFRP bars with headed anchorage can be safely used in bridge barrier walls to resist the applied vehicle impact load specified in CHBDC at the barrier wall-deck slab anchorage. However, CHBDC Clause 12.4.3.4.4 specifies crash testing for the design of the barrier wall itself (i.e. both

vertical and horizontal reinforcement). As such, vehicle crash testing was recently conducted (Sennah et al., 2011) to qualify the proposed barrier for use in Canadian bridges. The constructed barrier to perform the crash test was further investigated by conducting static load tests at interior and end locations as presented in the following sections.

4.4 Static Load Testing

A 40-m long barrier wall was built at Texas Transportation Institute with the cross-section configuration and GFRP bar arrangement shown in Fig. 4.2. It should be noted that the diagonal GFRP bar at the lower tapered surface of the barrier wall has a headed end embedded in the bridge deck slab to increase its pullout strength due to tensile force resulting from the bending moment at the barrier-deck slab junction. Figures 4.3 and 4.4 show views of the GFRP bars forming the barrier wall as well as the steel reinforcement of the cantilever deck slab projecting from an existing foundation at the test site. Figure 4.5 shows view of the barrier wall before conducting the recent vehicle crash testing (Sennah et al., 2011). After the crash testing, the barrier wall was tested under increasing static load to-collapse to determine its structural behavior, crack pattern and ultimate load carrying capacity under equivalent static load simulating vehicle impact. Figure 4.6 shows elevation of the barrier wall with 6 control joints, 6 m apart. To simulate the two load scenarios specified in AASHTO-LRFD Specifications, shown in Fig. 4.1, it was decided to load the barrier wall at its end with a horizontal line load at a height of 900 mm from the top surface of the asphalt and over 2400 mm length as shown in Fig. 4.6. As for loading the barrier internally, it was decided to load the barrier with a line load over 2400 mm length centered between the first and second control joints as shown in Fig. 4.6. In addition, to examine the effect of the control joint of barrier strength, it was decided to repeat this test in such a way that the line load is centred at the fourth control joint as shown in Fig. 4.6.

4.5 Description of Test Samples

Figure 4.6 shows schematics elevation of the barrier wall indicating the five load locations, which will be named here in this thesis as five test samples. Shape of the samples was according to the CHBDC requirements. Concrete cylinders taken during concrete casting resulted in concrete characteristic compressive strength of 32 MPa at the time of the testing which was 3 months after casting.

Sample 1: This sample represents a one-meter long PL-3 barrier wall located in the middle of the constructed barrier wall. The barrier wall was saw-cut to form this barrier segment. Figure 4.7 shows view of this inner portion of the barrier wall that has vertical GFRP bars at the barrier front face spaced at 300 mm center-to-center. Line load was applied over 1-m length of the sample at a height 900 mm measured from the top of the asphalt layer. Two LVDTs were placed horizontally at the top of the barrier wall to measure transverse deflection and 2 LVDTs were placed at the bottom of the deck and oriented vertically to measure deflection of the deck cantilever during load application. Figures 4.7 and 4.8 show views of the test setup at the front face and the LVDT arrangement at the back face of the barrier wall, respectively.

Sample 2: This sample represents a 1-meter long PL-3 barrier wall located at the end of the barrier where vertical GFRP bars at the barrier front face spaced at 150 mm center-to-center. The barrier wall was saw-cut to form this barrier segment. This sample is identical to sample 1 with respect to location of LVDTs and test setup. Figure 4.9 shows view of the test setup at the front face and the LVDT arrangement at the back face of the barrier wall for sample 2.

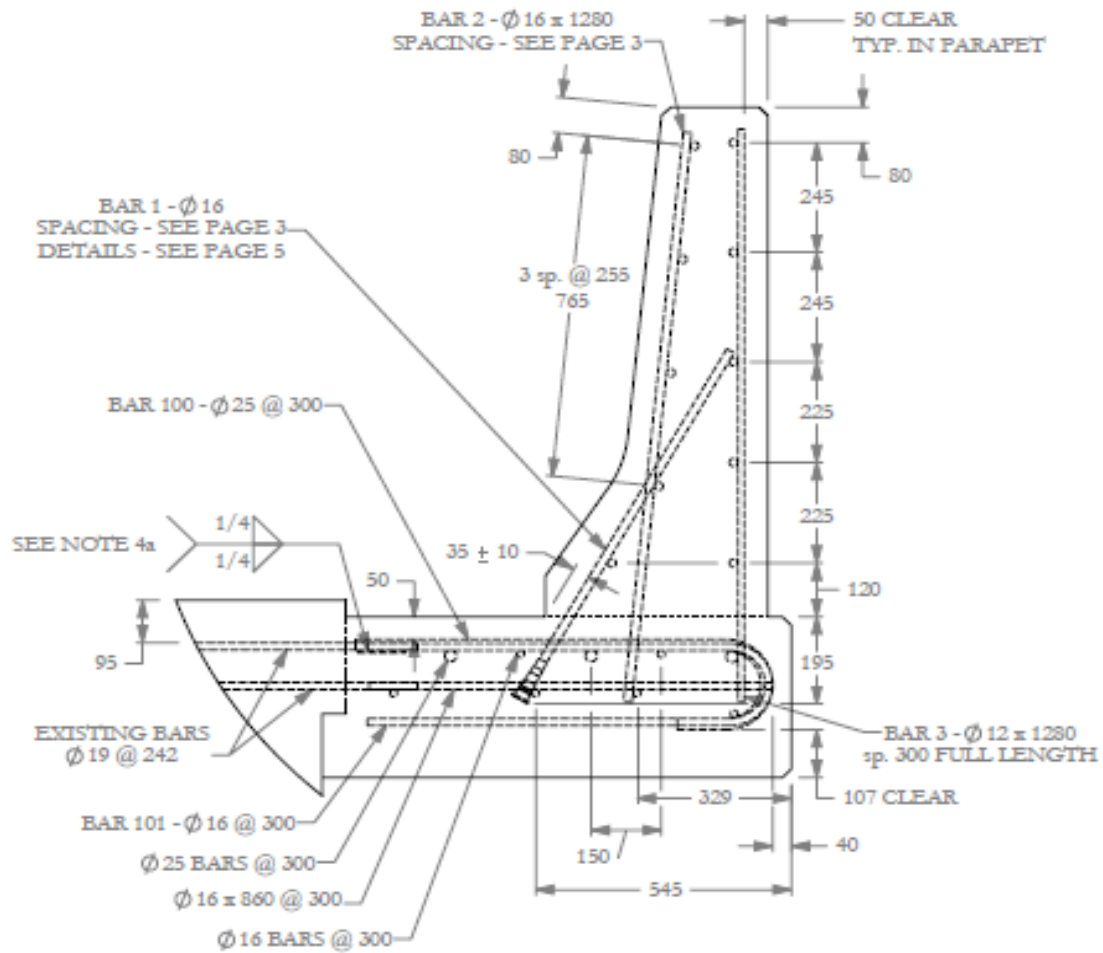


Fig. 4.2 Schematic diagram of the Reinforcement for the constructed barrier wall



Fig. 4.3 View of reinforcement in the constructed PL-3 barrier

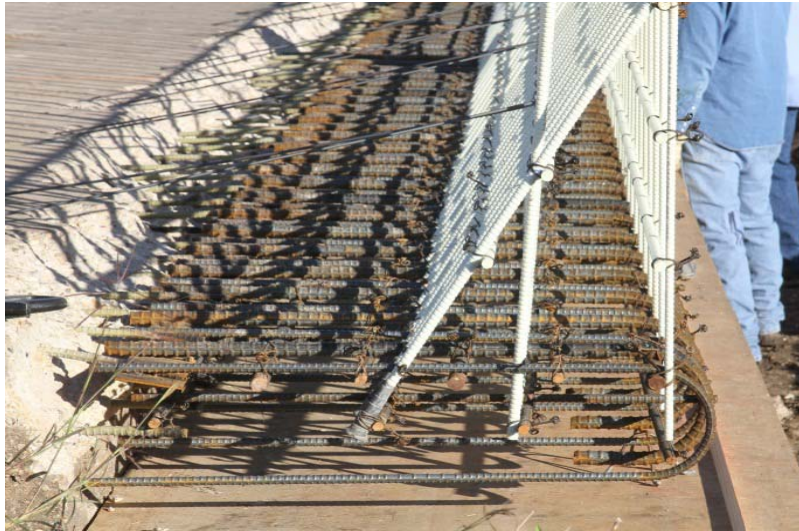
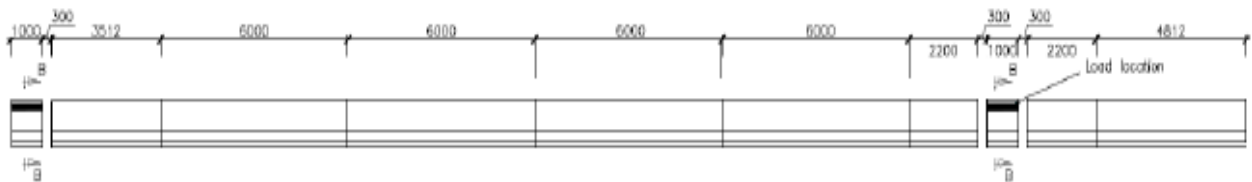


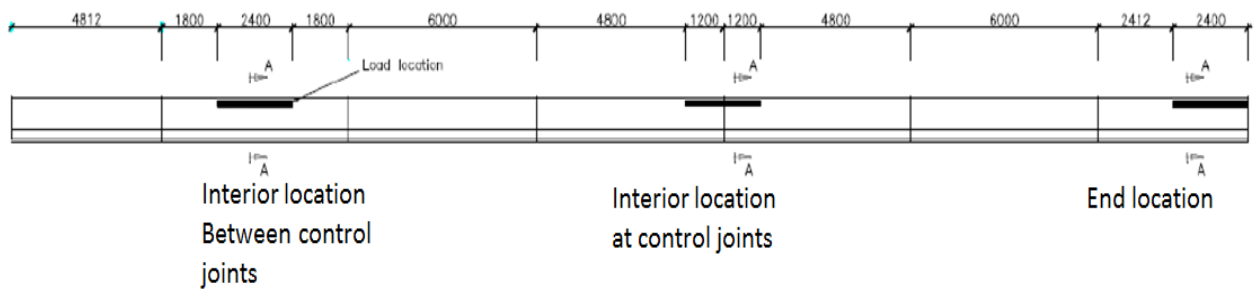
Fig. 4.4 Close-up view of the deck cantilever reinforcement and the GFRP bars with headed end to be embedded in the deck slab



Fig. 4.5 View of the barrier after Construction



(a) Samples 1 and 2



(b) Samples 3, 4 and 5

Fig. 4.6 Schematics diagram of the barrier showing control joints and load locations



Fig. 4.7 Front view of Sample 1

Sample 3: it represents the barrier wall segment located at the end of the constructed barrier wall as shown in Fig. 4.6b. This end portion of the barrier wall had vertical bars spaced at 150 mm center-to-center for a longitudinal length of the barrier equal to 2.25 m. Line load was applied over 2.4 m length of the sample at height of 900 mm measured from the top of the asphalt layer. As shown in Fig. 4.10, five LVDTs were placed at the top of the barrier wall at 1200 mm spacing to measure barrier lateral deflection, while three LVDTs were placed at the bottom of the deck and oriented vertically to measure deck cantilever deflection during load application process.



Fig. 4.8 View of LVDT location in Sample 1: two LVDTs at the top of the wall oriented horizontally and 2 LVDTs at the bottom of the deck edge oriented vertically



Fig. 4.9 Back view of Sample 2 showing 2 LVDTs at the top of the barrier oriented horizontally and 2 LVDTs at the bottom of the deck edge oriented vertically

Sample 4: it represents the barrier wall segment located in the middle of the constructed barrier wall and centered at the control joint. Line load was applied over 2.4-m length of the sample at height of 900 mm measured from the top of the asphalt layer. As depicted in Fig. 4.11, five LVDTs were placed at the top of the barrier wall and oriented horizontally to measure lateral deflection of the barrier wall at the level of the applied load, while three LVDTs were placed at the bottom of the deck to measure its vertical deflection during load application process.



Fig. 4.10 View of back face of Sample 3 showing 5 LVDTs placed at the top of the wall and oriented horizontally and 3 LVDTs placed at the bottom of the deck edge and oriented vertically



Fig. 4.11 View of back face of Sample 4 showing 5 LVDTs oriented horizontally at the top of the wall and 3 LVDTs oriented vertically at the bottom of the deck edge

Sample 5: this sample is identical to sample except that is centered at the mid-distance between two consecutive control joints. Figure 4.12 shows view of the sample 5 with LVDT arrangement. Comparing test results of samples 4 and 5 would indicate whether the presence of the control joint at the center of the applied transverse loading would affect its ultimate load carrying capacity.



Fig. 4.12 View of back face of Sample 5 showing 5 LVDTs oriented horizontally at the top of the wall and 3LVDTs oriented vertically at the bottom of the deck edge.

4.6 Test Setup

All five samples were tested with the same test setup shown in Figs. 4.13 and 4.15. The load was applied using a jacking load of 2500 kN capacity. The jacking load was applied on a steel I-beam oriented horizontally, that transferred that load to two spread beams to form a line load over 2400 mm length of the barrier wall. A trapezoidal timber wedge was inserted between the tapered face of the barrier and the spread beam to ensure that the transferred load acted horizontally on the barrier wall. This load transfer system ensured that a uniformly distributed line load was applied on the barrier wall. The hydraulic jack was rest on a steel curved plate attached to a steel column and the push steel beams were rest on a steel table on the front size of the barrier wall as shown in Figures 4.15 and 4.16.

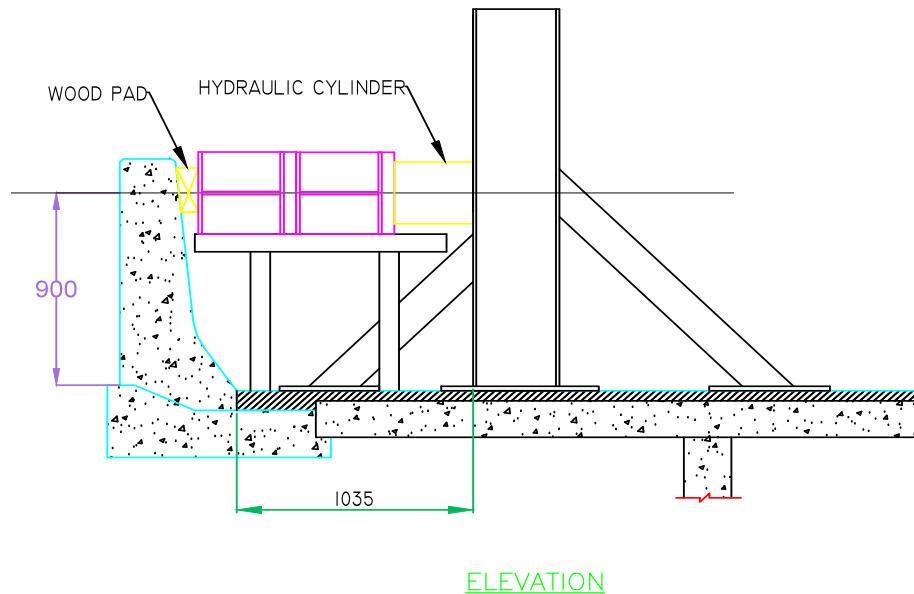


Fig. 4.13 Schematic section of the test setup

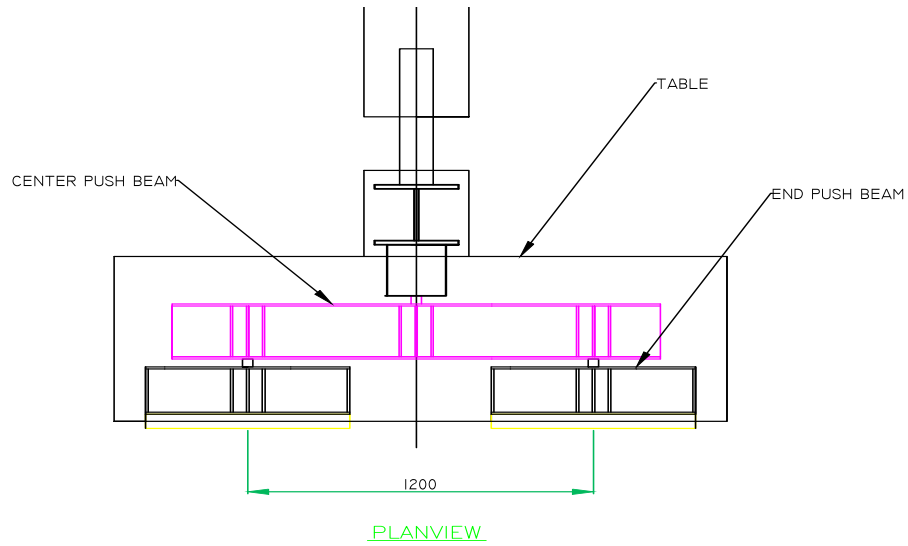


Fig. 4.14 Schematic plan view of the test setup



Fig. 4.15 Views of the test setup and sensor location at (a) front and (b) back of the barrier wall at interior load location



Fig. 4.16 Views of the test setup and sensor location at (a) front and (b) back of the barrier wall at end load location

4.7 Test Results and Discussions

Each barrier location was subjected to increasing static load using the jacking system and steel frame. At a load increment of 25 kN, the barrier wall was inspected to mark crack propagation until collapse. The barrier was considered failed when the sensors continued to record increasing deflections with no increase in applied load (i.e. the barrier could not absorb an increase in the applied load).

Sample 1: the first visible flexural crack appeared at the front side of the barrier-deck junction at 75-kN jacking load. The second flexural crack appeared at 105 kN load along the intersection of the two tapered portions of the barrier front face. These cracks propagated through barrier thickness with increase in the applied load as depicted in Figs. 4.17 and 4.18. Also, other flexural cracks appeared at the front face of the barrier wall and propagated through the barrier wall thickness with load increase. When the applied load reached 150 kN, extensive cracks appeared in deck slab portion under the barrier wall due to anchorage and diagonal compression, leading to failure of the sample at 165 kN formation inside the slab. Figure 4.17 and 4.18 show views of the crack pattern at failure for sample 1.



Fig. 4.17 Crack pattern in the side of Sample 1



(a) Left side



(b) Right side

Fig. 4.19 Crack pattern in side of Sample 2

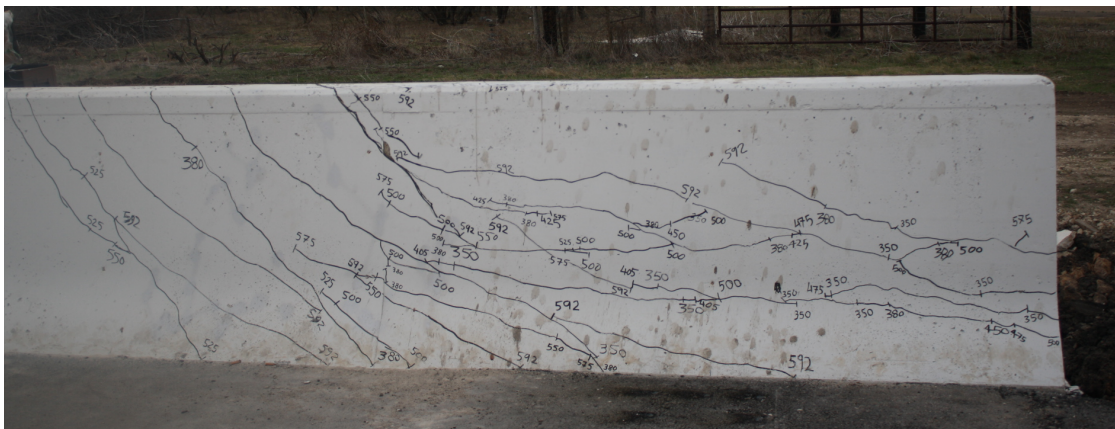


Fig. 4.20 Crack pattern in front of Sample 2

Sample 3: In this test, the barrier wall was loaded at its end with a line load over 2400 mm length. Figures 4.21 through 4.23 show views of the crack pattern after failure. It was observed that with increase in load, horizontal crack appeared at the front side of the barrier wall-deck slab junction. Other horizontal cracks appeared on the tapered part of the front side of the barrier wall



Fig. 4.22 Crack Pattern at side of Sample 3 at barrier end location



(a) Front face



(b) Side view

Fig. 4.23 Crack Pattern in front of Sample 3 and barrier end location

Sample 4: In case of loading the barrier internally at the control joint, Figure 4.24 and 4.25 show views of the barrier wall during testing. While Fig. 4.26 shows views of the crack pattern after failure. It was observed that with increase in load, horizontal crack appeared at the front side of the barrier wall-deck slab junction. Other horizontal cracks appeared on the tapered part of the front side of the barrier wall at a load of 350 kN. These cracks appeared within the 2400 mm length of the line load, extending diagonally outside the loading region and reaching the top surface of the barrier wall at a load of 425 kN. These cracks showed that the barrier wall behaved as a cantilever wall within the 2400 mm length of the line load, while the two-way slab action appeared outside this region (on the left and right side of the line load) in the form of diagonal cracks extending to the top surface. However, punching shear crack appeared on the left side of the line load at a load greater than 575 kN and propagated through the barrier thickness and to the other side of the line load at an ultimate load of 602 kN. The sudden punching shear failure at the line load location may be attributed to the GFRP bar low stiffness, bond characteristics, elastic response till failure, low strength under compression and shear stresses. The barrier could not absorb any increase in load beyond 607 kN.



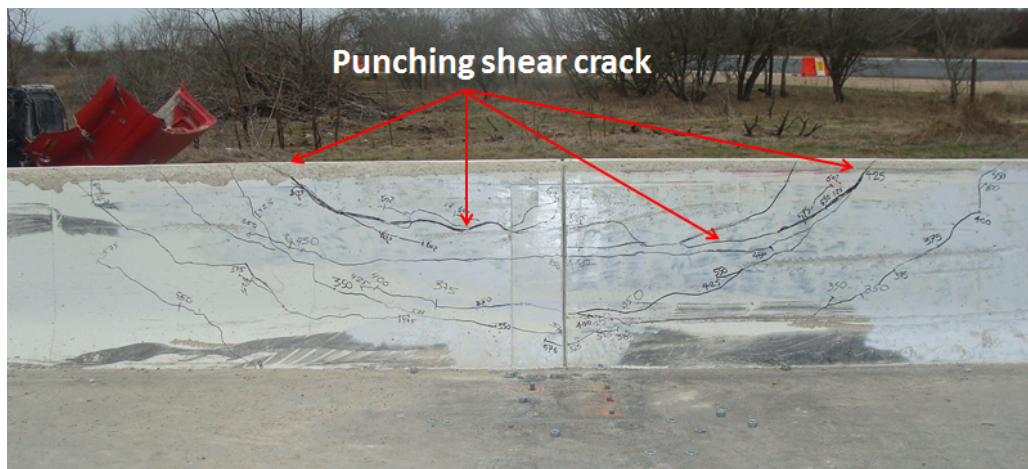
Figure 4.24 Cracks appeared at front face during testing at interior load location



Figure 4.25 Punching shear crack appeared at end of the test at interior load location



(a) Side view



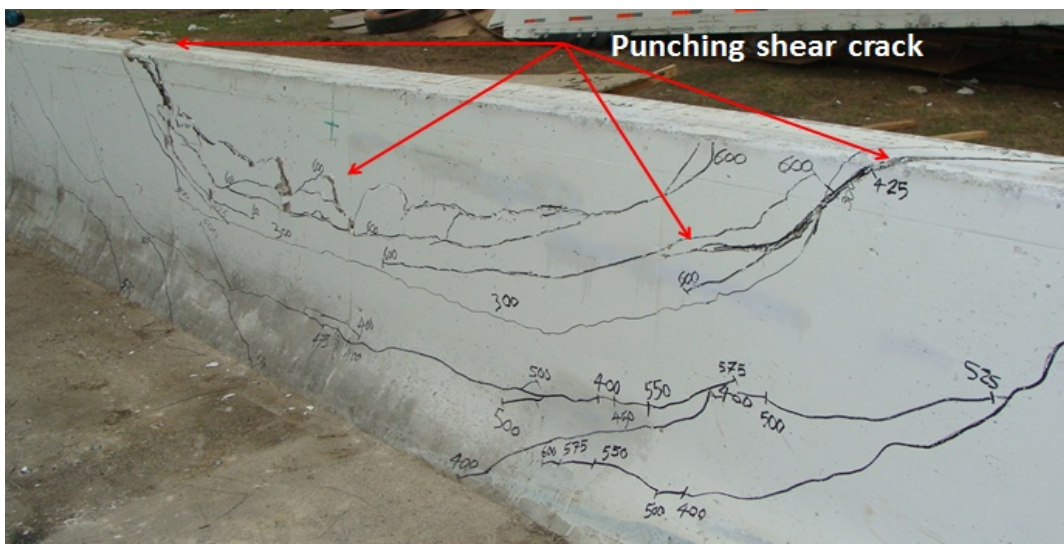
(b) Front face



(c) Back face

Fig. 4.26 Views of the punching shear failure at the end of the test of barrier segment loaded at control joint

Sample 5: As for loading the barrier wall at the mid-length between the first and the second control joints shown in Figure 4.6, similar behavior to the loading at the control joint mentioned above was observed. Figure 4.27 shows views of the crack pattern and failure mode due to punching shear. It was observed that with increase in load, horizontal crack appeared at the front side of the barrier wall-deck slab junction. Other horizontal cracks appeared on the tapered part of the front side of the barrier wall at a load of 300 kN. These cracks appeared within the 2400 mm length of the line load, extending diagonally outside the loading region and reaching the top surface of the barrier wall at a load of 350 kN. These cracks showed that the barrier wall behaved as a cantilever wall within the 2400 mm length of the line load, while the two-way slab action appeared outside this region (on the left and right side of the line load) in the form of diagonal cracks extending to the top surface. However, punching shear crack occurred at the line load location and propagated through the barrier thickness at a load of 600 kN. The barrier could not absorb any increase in load beyond 621 kN.



(a) Front face



(c) Top surface



(c) Back face

Fig. 4.27 Views of punching shear failure of barrier segment loaded at mid-length between two control joints

4.8. Discussion of Test Results and Correlations with CHBDC Design Values

Sample 1. Sample 1 was intended to examine the flexural capacity of the barrier wall at the bottom of the barrier as well as the anchorage capacity of the barrier-deck junction. Test results showed that the failure load of sample 1 was 165 kN as shown in Figure 4.28. As such associated flexural capacity of the barrier wall junction or anchorage capacity is taken as $165 \text{ kN} \times 0.99 \text{ m}$ applied load arm to the deck slab = 163.35 kN.m/m . According to CHBDC guidelines specified in Table 1.1 at inner portion of PL-3 barrier, the factored applied moment at the barrier deck junction is 83 kN.m/m . This leads to a factor of safety in design equal to 1.97. As such, the proposed barrier details shown in Fig. 1.3 are considered adequate for barrier-deck anchorage at interior location where vertical bar spacing is 300 mm. Figure 4.28 depicts the load-deflection history of the tested sample. One may not consider the importance of the deflection of the barrier and the deck since the design check is at the ultimate limit state.

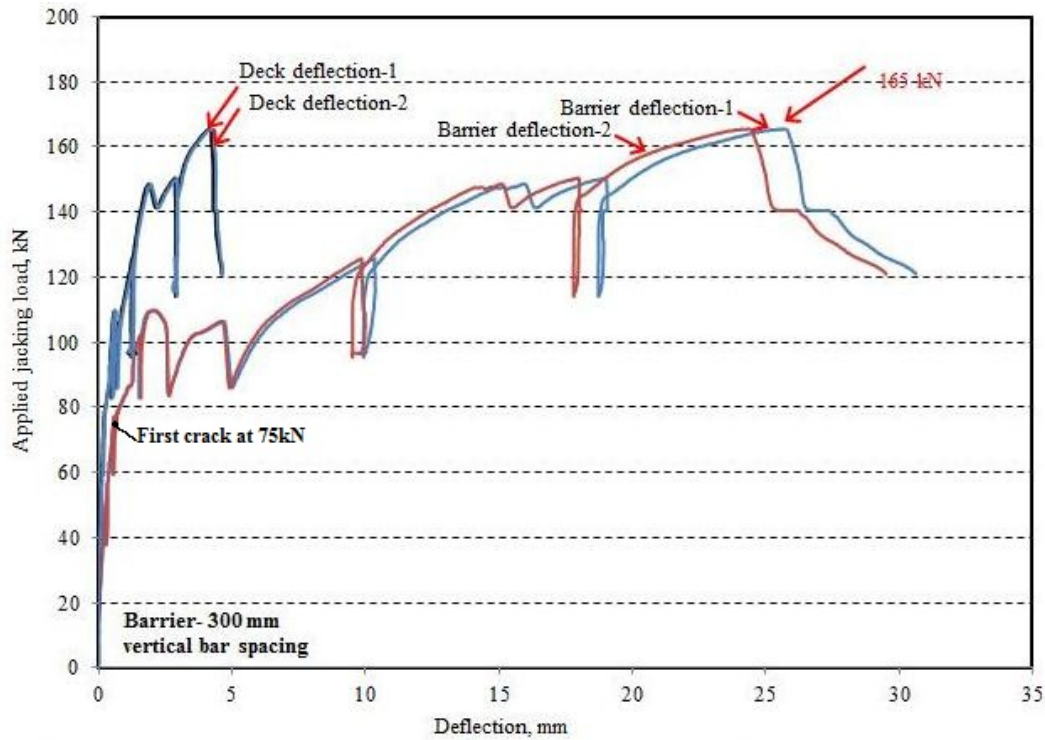


Fig. 4.28 Load-deflection relationship of the 1-m barrier wall

Sample2: Sample 2 was intended to examine the flexural capacity of the barrier wall at the bottom of the barrier as well as the anchorage capacity of the barrier-deck junction at end location where vertical bar spacing is 150 mm. Test results showed that the failure load of sample 1 was 189.5 kN as shown in Figure 4.29. As such associated flexural capacity of the barrier wall junction or anchorage capacity is takes as $189.5 \text{ kN} \times 0.99 \text{ m}$ applied load arm to the deck slab = 187.61 kN.m/m. According to CHBDC guidelines specified in Table 1.1 at end portion of PL-3 barrier, the factored applied moment at the barrier deck junction is 102 kN.m/m. This leads to a factor of safety in design equal to 1.84. As such, the proposed barrier details shown in Fig. 1.3 is considered adequate for barrier-deck anchorage at end location where vertical bar spacing is 150 mm. Figure 4.29 depicts the load-deflection history of the tested sample. One may not consider the importance of the deflection of the barrier and the deck since the design check is at the ultimate limit state. It should be noted that Sample 2 reached its ultimate load when failure in welding between the foundation anchors and steel bars of the deck cantilever. These steel anchors are shown in Fig. 4.30a, while they are shown welded to the top steel bars of the deck cantilever in Fig. 4.30b.

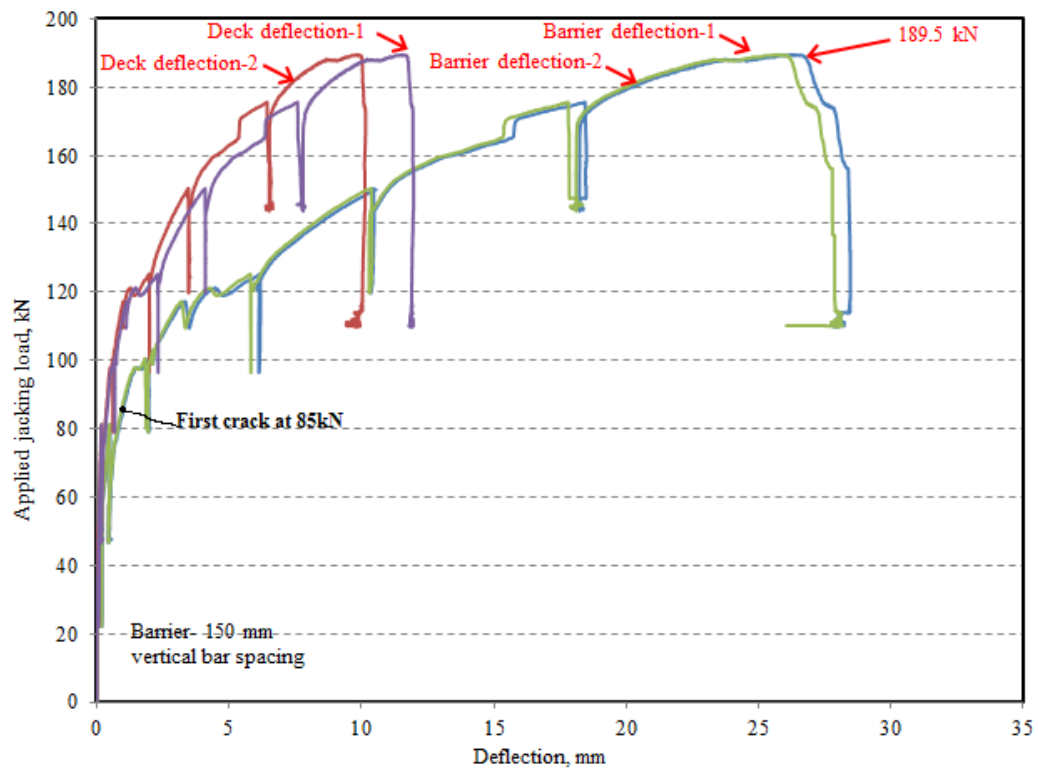


Fig. 4.29 Load-deflection relationship of the barrier wall of 150-mm spacing between vertical bars at the front face



(a)



(b)

Fig. 4.30 Views of (a) the projecting steel dowels from foundation wall that are (b) welded to deck cantilever steel reinforcement

Sample 3: sample 3 represented the end load location shown in Fig. 4.1. Figures 4.31 and 4.32 depict the load-deflection history of the barrier wall and deck slab, respectively. It can be observed that barrier wall has a maximum lateral deflection of 26.43 mm, decreasing to 16.92 mm at the inner side of the line load and 2.43 mm at a 2400 mm distance from the inner side of the line load. It can be observed that the crack pattern shown in Figure 4.23 contradicts with the AASHTO-LRFD crack pattern where the only one diagonal yield line is formed at the front face of the barrier extending from the barrier-deck junction at barrier end extending diagonally into the barrier wall as shown in Figure 4.1. Failure happened due to punching shear of the wall at 593 kN as shown in Fig. 4.31. According to CHBDC, end portion of PL-3 barrier should resist a factored applied transverse load of 357 kN, which gives a factor of safety of 1.66 in design. As such, the proposed barrier details shown in Fig. 1.3 are considered adequate to resist equivalent vehicle impact loading at end locations.

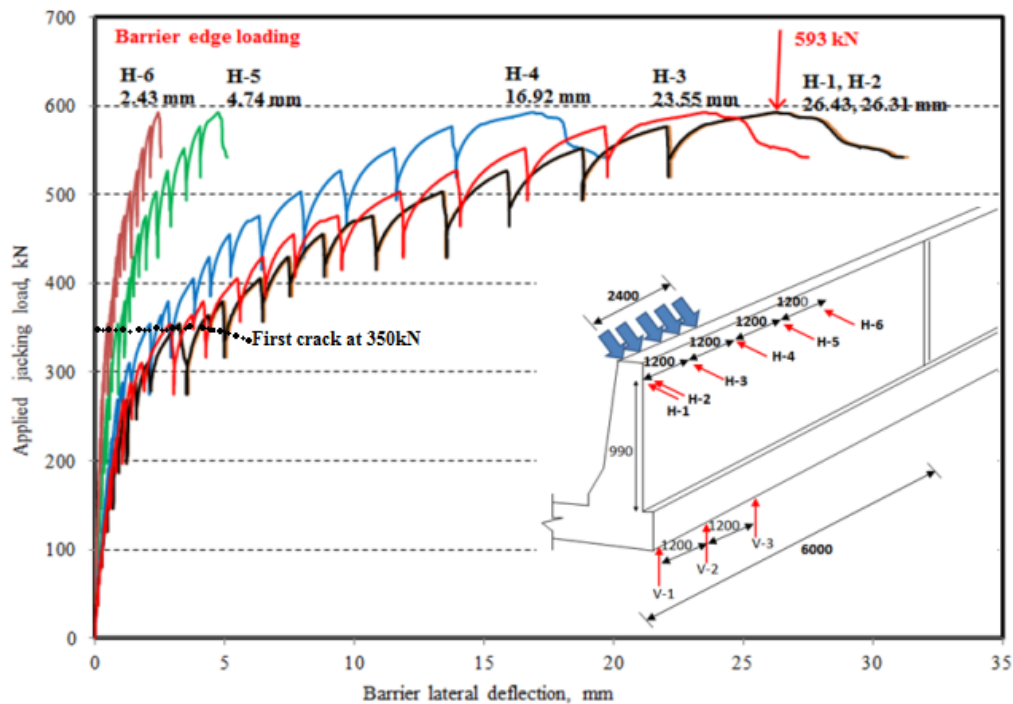


Fig. 4.31 Load-deflection relationship of the barrier wall loaded at end location

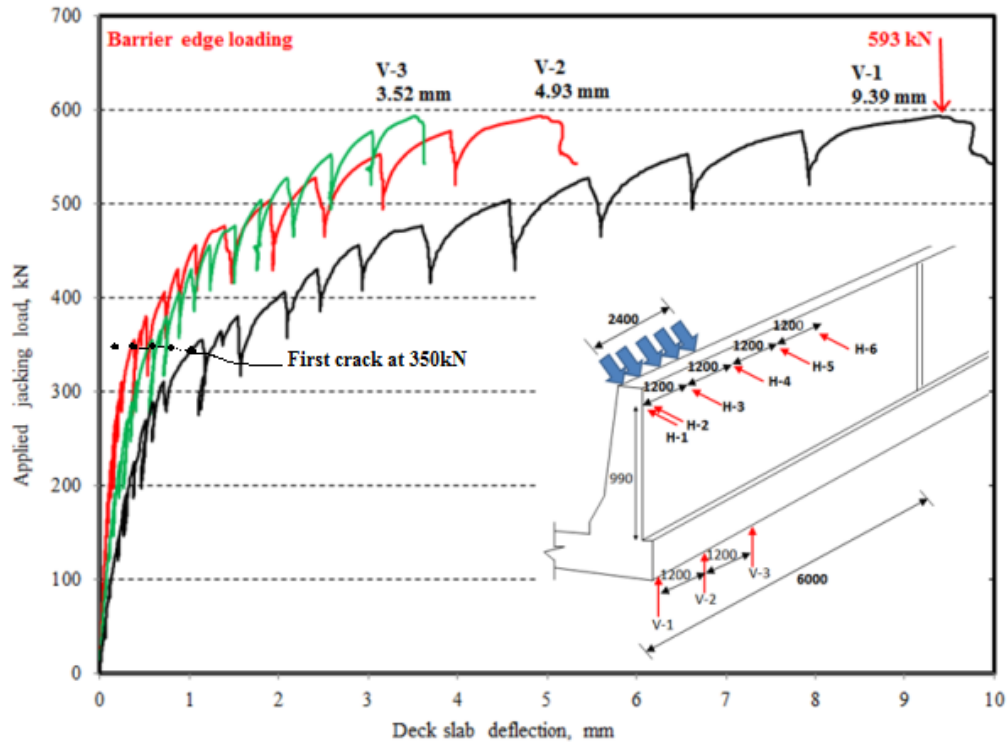


Fig. 4.32 Load-deflection relationship of the deck cantilever of the barrier wall loaded at its end

Sample 4: sample 4 represented the interior load location shown in Fig. 4.1 with the applied load centered at the control joint. Figures 4.33 and 4.34 depict the load-deflection history of the barrier wall and deck slab, respectively. It can be observed that barrier wall has a maximum lateral deflection of 11.04 mm which is very small to promote large deformations required to develop the AASHTO-LRFD yield-line pattern at failure. Also, it can be observed that the maximum deflection of the deck cantilever at failure was 0.73 mm which is very small indicating the deck slab cantilever was insignificantly affected by the maximum load reached experimentally, promoting the two-way slab action of the barrier wall at the load location. Failure of sample 4 happened due to punching of the wall at 607 kN transverse loading as shown in Figure 4.32. According to CHBDC, PL-3 Barrier should resist a factored applied transverse load of 357 kN, which leads to a factor of safety of 1.7 in design. As such, the proposed barrier details shown in Fig. 1.3 are considered adequate to resist equivalent vehicle impact loading at interior locations.

The crack pattern reported for sample 4 in Fig. 4.26 contradicts with the AASHTO-LRFD crack pattern where the two diagonal yield lines at the front face of the barrier meet at the barrier-deck slab junction located at the centre line of the line loading as shown in Figure 4.1. In addition, a

hair vertical crack appeared through the control joint at the back face of the barrier wall at a load of 200 kN. However, this flexural crack did not open enough to form a vertical yield-line similar to that shown in Fig. 4.1a. This is evident by the horizontal strain readings shown in Fig. 4.35. To measure the horizontal strains at the back face of the barrier wall, two Pie gauges were installed to the concrete surface at 25 mm from the top surface of the barrier wall and 50 mm apart, as shown in the sketch inserted in Fig. 4.35. It can be observed that strain readings were not significant till a load of about 320 kN, then strains increased almost linearly with increase of load till the barrier failed due to punching shear. The recorded strain at failure was in the order of 0.76×10^{-6} which is very small compared to the strain forming the yield-line pattern.

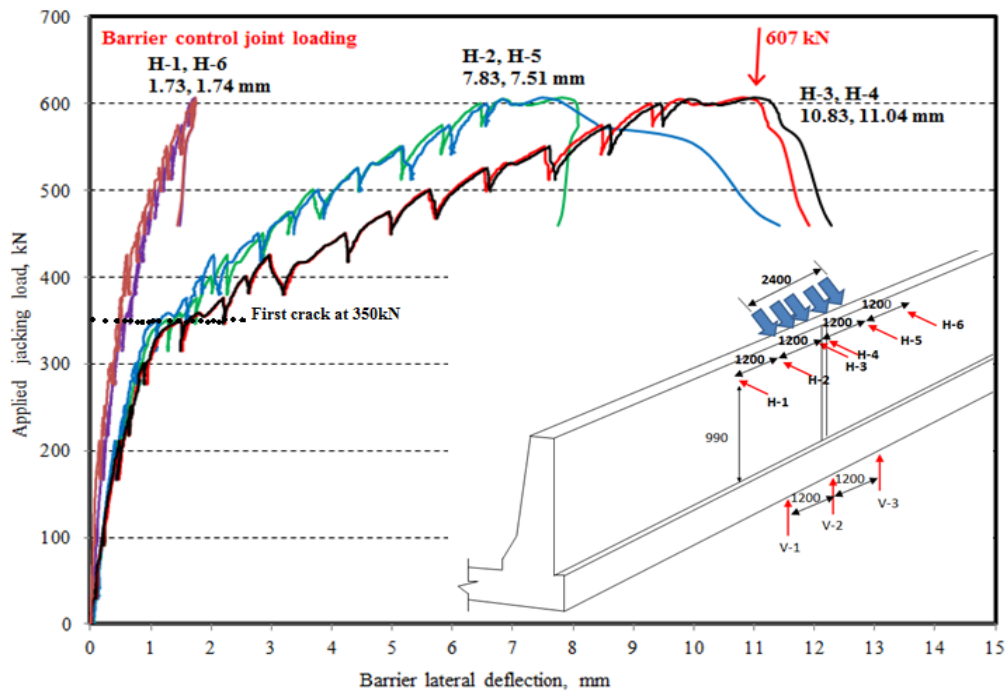


Fig. 4.33 Load-deflection relationship for barrier segment loaded at control joint

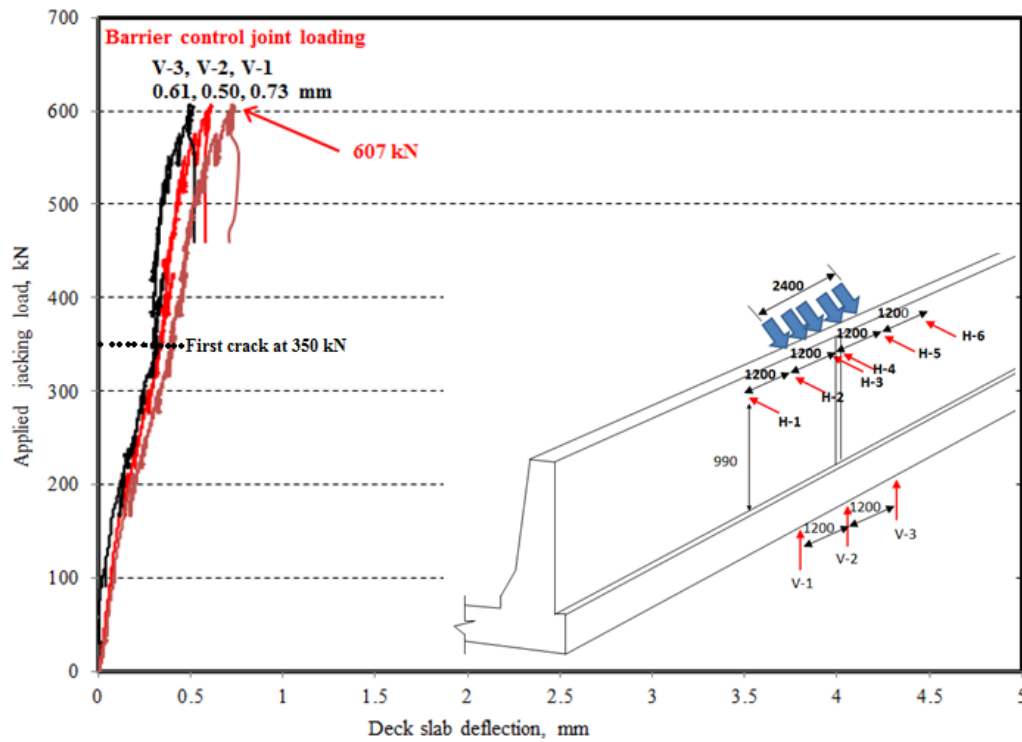


Fig. 4.34 Load-deflection relationship for the deck cantilever of barrier segment at control joint

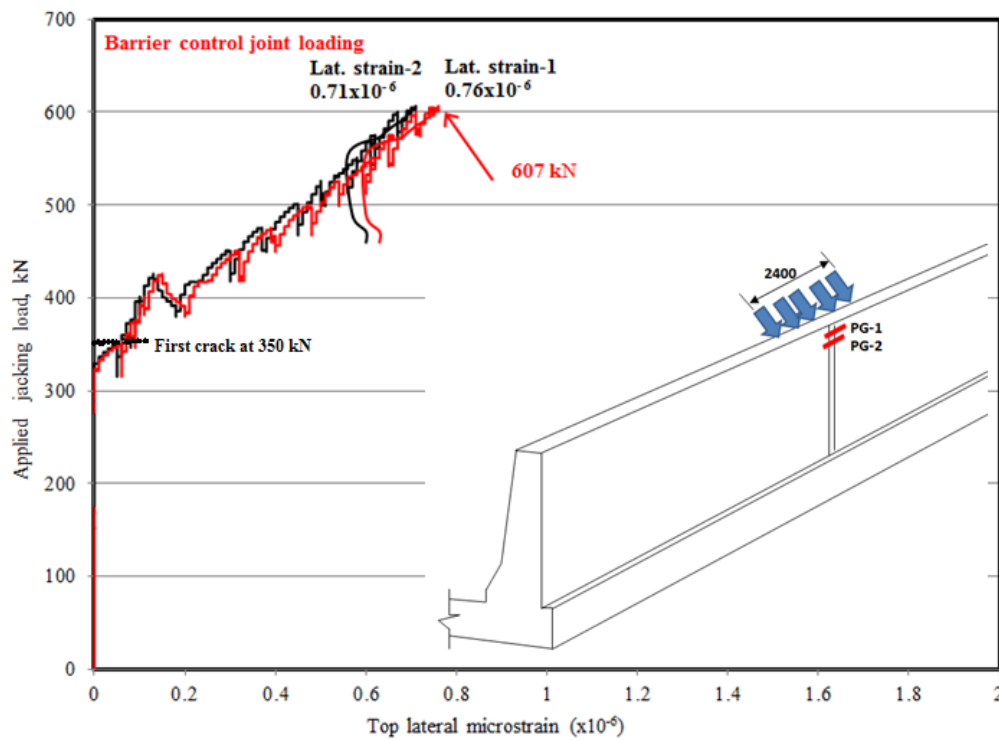


Fig. 4.35 Load-horizontal strain relationship at the top level of the barrier at control joint

Sample 5: Sample 5 represented the interior load location shown in Fig. 4.1 with the applied load centered at the mid-distance between two consecutive control joints. Figures 4.36 and 4.37 depict the load-deflection history of the barrier wall and deck slab, respectively. It can be observed that barrier wall has a maximum lateral deflection of 10.83 mm which is very small to promote large deformations required to develop the AASHTO-LRFD yield-line pattern at failure. Also, it can be observed that the maximum deflection of the deck cantilever at failure was 0.61 mm which is very small indicating the deck slab cantilever was insignificantly affected by the maximum load reached experimentally, promoting the two-way slab action of the barrier wall at the load location.

Failure happened due to punching of the wall at a load of 620 kN as shown in Fig. 4.36. According to CHBDC, interior portion of PL-3 barrier should resist factored applied transverse load of 357 kN. This lead to a factor of safety of 1.74 in design. As such, the proposed barrier details shown in Fig. 1.3 are considered adequate to resist equivalent vehicle impact loading at interior locations. One may observe that the failure load in samples 4 where the load was applied at the control joint and sample 5 where the load was applied at mid-distance between two consecutive control joints were 607 and 620 kN, respectively. So, the presence of the control joint reduced the load carrying capacity by only 2%.

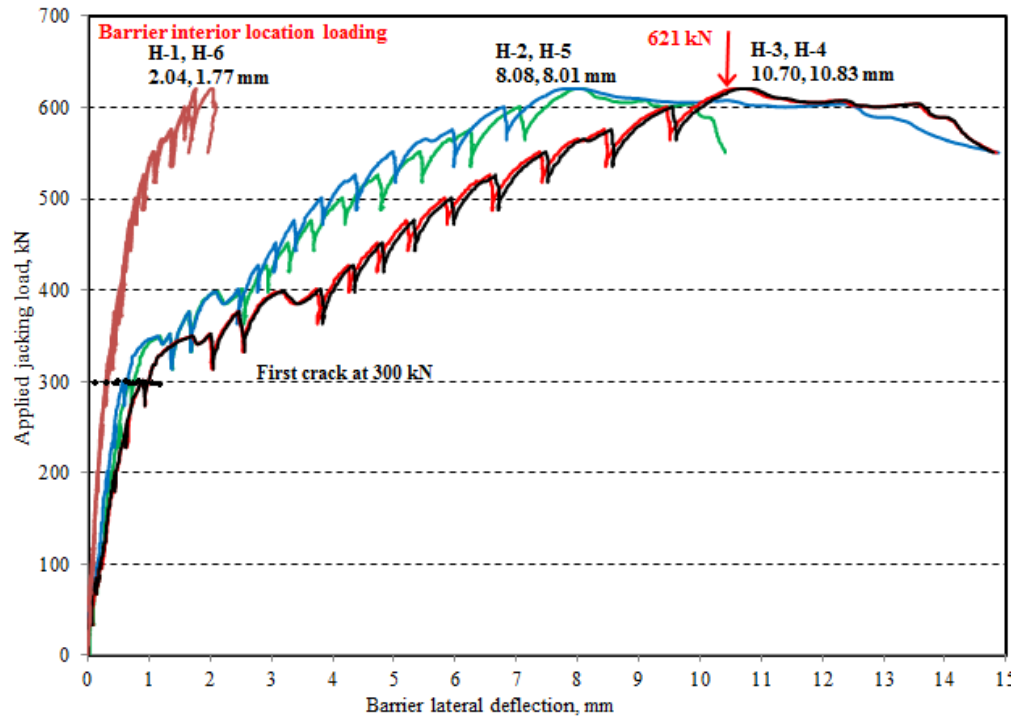


Fig. 4.36 Load-deflection relationship for barrier segment loaded at mid-length between two control joints

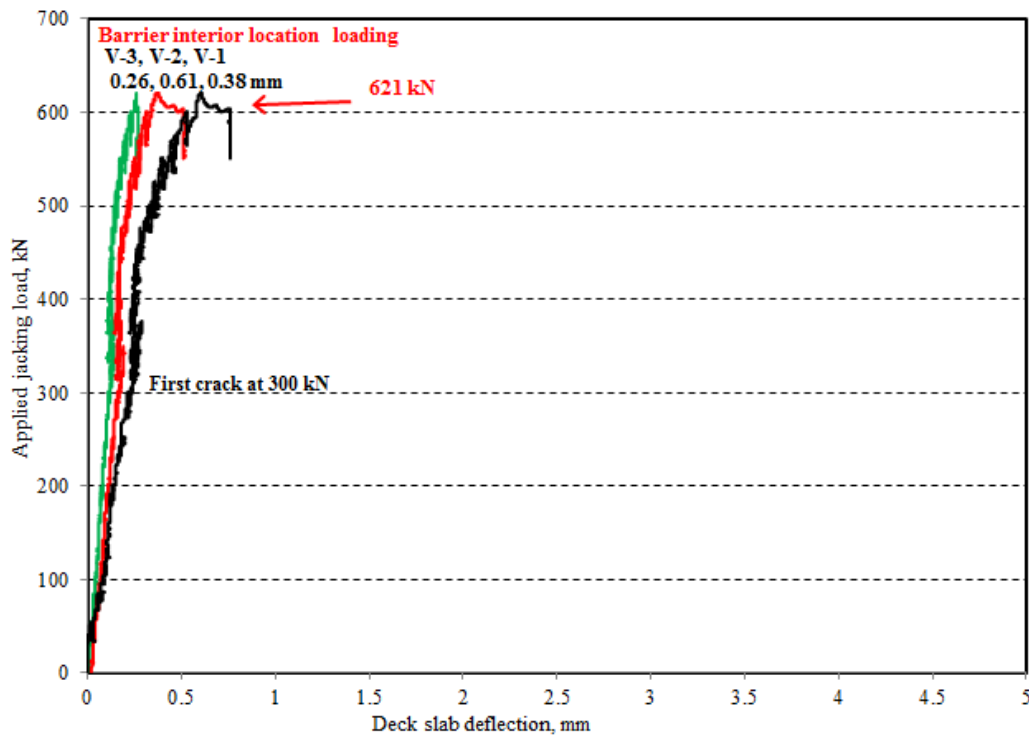


Fig. 4.37 Load-deflection relationship for the deck cantilever of barrier segment at mid-length between two control joints

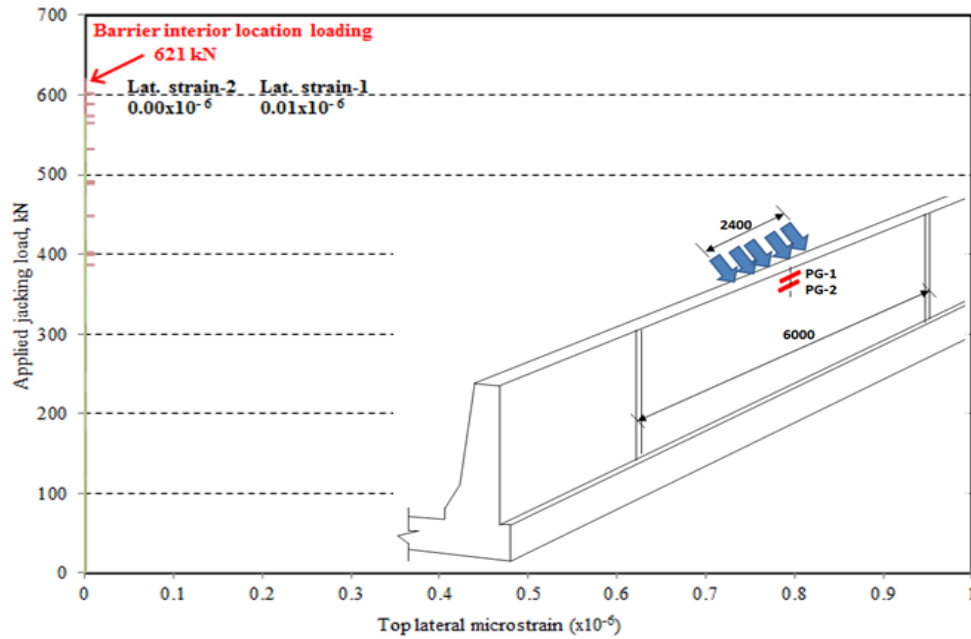


Fig. 4.38 Load-horizontal concrete strain relationship at the back face of the for barrier segment loaded at mid-length between two control joints

4.9 Analytical Investigation of Punching Shear Failure of the Samples

In two-way reinforced concrete slabs the punching shear resistance is provided by the shear resistance of the concrete, V_c . This shear resistance acts over the area equal to the length of a “critical perimeter” multiplied by the effective depth of the section, d . The critical perimeter is identified by the letter u and a subscript that represents the distance that the critical perimeter is offset from the perimeter of the area of the concentrated load, as a multiple of the effective depth, d . For example, $u_{0.5}$ is the critical perimeter measured at a distance $0.5d$ from the edge of the loaded area. Figure 4.36 and 4.37 are representing critical perimeter for barrier wall samples. The following sections consider several models for V_c . The selected models were used to predict capacities for the test samples 3 to 5, which were then compared to actual test ultimate capacities.

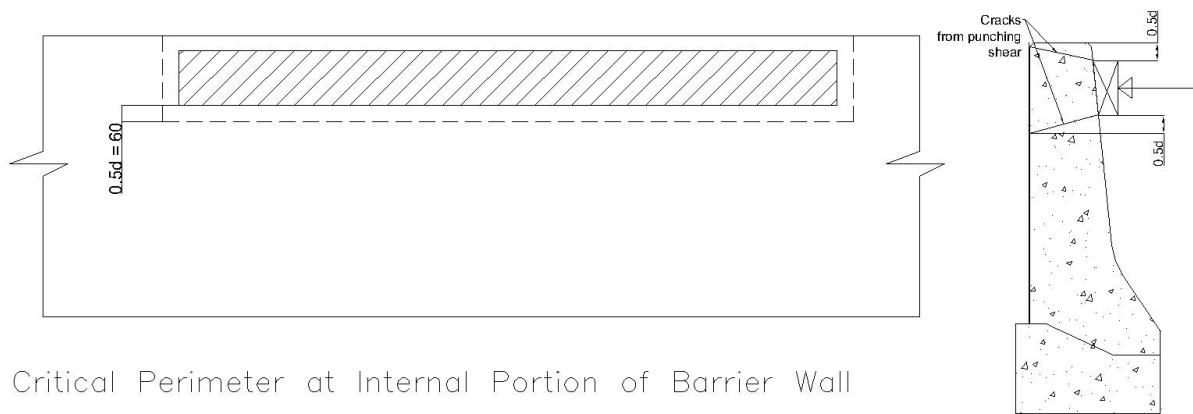


Fig. 4.39 Critical perimeter at internal portion of the barrier wall



Fig. 4.40 Critical perimeter at the end portion of the barrier wall

4.9.1 Punching Shear Models

A number of design standards provide punching shear design equations, typically for use with decks having steel reinforcement. Less is known about the punching shear behavior in concrete decks having FRP grid reinforcement systems. Similar to work performed by Banthia et al. (1995), Matthys and Taerwe (2000), El-Ghandour et al. (1997, 2003), Ospina et al. (2003), Jacobson et al. (2005), and Hassan et al. (2012), an attempt is made to determine the best punching shear prediction model for the FRP grid-reinforced concrete barrier wall at interior and end locations. Figures 4.39 and 4.40 show elevation of the 200x2400 mm loaded area on the

front face of the barrier wall at in interior and end location, respectively, assuming the punching shear plane at $d/2$ from the sides of the applied load.

CHBDC (CSA.S6-06)

For two-way action in a slab reinforced with steel bars, CHBDC specifies the following equation for punching shear strength:

$$V_r = (\phi_c f_{cr}) b_o d \quad (4.5)$$

Where:

b_o = perimeter of the critical section for slabs, mm;

ϕ_c = concrete resistance factor;

f_{cr} = the cracking strength of concrete, $f_{cr} = 0.4\sqrt{f'_c}$, for normal density concrete, MPa; and

d = effective depth (being the distance from extreme compression fibre to the centroid of the tensile force), mm.

CAN/CSA 23.3 (2004)

For two-way action in a slab reinforced with steel bars, CSA 23.3 specifies the punching shear strength, V_r , as the smallest of the following equations:

$$V_r = \left(1 + \frac{2}{\beta_c}\right) 0.19\lambda\phi_c \sqrt{f'_c} \quad (4.6)$$

Where

β_c = ration of the long side to short side of the column or concentrated load, or reaction area

$$V_r = \left(\frac{\alpha_c d}{b_o} + 0.19\right) \lambda\phi_c \sqrt{f'_c} \quad (4.7)$$

Where

α_c = 4 for interior columns, 3 for edge columns and 2 for corner column;

$$V_r = 0.38\lambda\phi_c \sqrt{f'_c} \quad (4.8)$$

CAN/CSA S806-11

CSA S806-11 (2011) specifies the punching shear strength of GFRP-reinforced slab as the smallest of the following equations. It can be noticed that those equations are those specified in CSA A23.3-04 equations with modifications to account for the FRP bars instead of steel bars.

For two-way action:

Shear resistance, V_r , shall be the smallest of:

$$a) V_r = \left(1 + \frac{2}{\beta_c}\right) 0.028 \lambda \phi_c \sqrt[3]{E_f \rho_f f'_c} b_o d \quad (4.9)$$

Where β_c = ration of the long side to short side of the column or concentrated load, or reaction area

$$b) V_r = \left(\frac{\alpha_c d}{b_o} + 0.028\right) \lambda \phi_c \sqrt[3]{E_f \rho_f f'_c} b_o d \quad (4.10)$$

Where α_c = 4 for interior columns, 3 for edge columns and 2 for corner columns

$$c) V_r = 0.06 \lambda \phi_c \sqrt[3]{E_f \rho_f f'_c} b_o d \quad (4.11)$$

Where λ is a factor to account for density of concrete; α_s is a factor that adjusts V_c for support conditions; and β_c is the ratio of long side to short side of the concentrated load or reaction area.

ACI-440.1R-06 (2006)

The ACI 440.1R-06 specifies the following equation for calculating the punching-shear strength of FRP-reinforced concrete slabs (calculations in imperial units):

$$V_c = 10k \sqrt{f'_c} b_o d \quad (4.12)$$

Where, $k = \sqrt{2\rho_f n_f + (\rho_f n_f)^2} - \rho_f n_f$

ρ_f is FRP reinforcement ratio (A_f/bd) ; and n_f is the modular ratio (E_f/E_c)

4.9.2 Comparison between Predicted and Experimental Results

Table 4.1 presents the ratio of experimental capacity of the barrier wall for punching shear to the predicted capacity based on the above-mentioned equations. It should be noted that ratios of 1.0 perfectly predict the test capacity, while ratios higher than 1.0 show some level of conservativeness in design for punching shear. Ratios below 1.0 show that the theoretical punching shear model overestimates the shear capacity of the deck slab which makes the design unsafe. By inspection of results in Table 4.1, it can be observed that the results from the ACI 440 and CSA 806 punching shear equations correlate very well with the experimental findings for barrier loaded at interior location and overestimate the response for barriers loaded at end

locations. This may most likely be attributed to the fact that barrier end location exhibited larger deflection than interior locations so that interaction of torsion, punching shear and flexure deformation occur at failure.

Table 4.1 Ratio of test result-to-predicted punching shear capacity

Sample No.	Load _{test} (kN)	Tested-to-predicted punching shear ratio, $V_{\text{test}}/V_{\text{pred}}$			
		V _{CHBDC}	V _{CSA 23.3}	V _{CSA 806}	V _{ACI 440}
3	593	0.41	0.64	0.9	0.89
4	607	0.41	0.74	1.03	1.07
5	621	0.42	0.75	1.05	1.09

CHAPTER 5

FINITE-ELEMENT MODELING OF BARRIER-DECK SYSTEM

5.1 General

Traffic Barrier is classified in CHBDC according to its performance level. There are 3 performance levels related to barrier's capacity to absorb impact loads, namely: PL-1, PL-2 and PL-3. The specified traffic loads are based on vehicular impact at the performance level. These loads create straining actions in the barrier wall in the form of bending moment and shear force and in the deck slab in the form of bending moment and tensile forces. Transverse moments in cantilever slabs at the barrier-deck junction due to horizontal loads are presented in the CHBDC Commentary (CAN/CSA-S6-06). The magnitudes of unfactored loads that are to be applied to various performance level barrier and/or railing systems for the determination of the force effects in the deck slab and barrier anchorage and the length of load application on the barrier and the location or height of load application above the roadway are specified in CHBDC Clause 12.5.2.4 and stated earlier in this thesis.

The load application and the length of load application as well as the resulting bending moment and tensile force in the deck slab at the deck-barrier junction on PL-3 and PL-2 barriers are summarized in CHBDC Table C 5.4 which is Table 1.1. An important characteristic of the finite-element model used to develop this table is the length of deck cantilever on which barrier is placed. A constant length of slab at the exterior edge or face of barrier equal to 1.50 m was used for determining moment intensity resulting from horizontal concentrated loads on barriers. The hypothesis in this thesis is that the magnitude of maximum moment intensity resulting from horizontal barrier loading is sensitive to geometrical feature of the deck slab supporting the barrier wall. The barrier wall may be connected to the deck slab cantilever projecting from slab-on-girder bridges or box-girder bridges, with a deck slab thickness in the order of 200 to 300 mm. Also, it can be connected to a stiff deck slab, representing solid or voided slab bridge superstructure with a total thickness ranging from 0.5 to 1.0 m. The latter may lead to considering the barrier wall fixed to a rigid base. These geometrical features are believed to influence the dispersal of moment intensity in the deck resulting from horizontal load on the barrier. As such

the objective of this study is to examine, using the finite-element modeling, the applied factored moments and tensile forces at the barrier-deck junction available in the CHBDC Commentary as affected by selected geometrical parameters.

5.2 Parametric Study

5.2.1 Key Parameters

The key parameters of the barrier-deck geometrical features considered in this study are: (i) length of the deck slab cantilever as opposed to the case of fixed base; (ii) type of the barrier wall based on the performance level; and (iii) barrier length in the direction of traffic.

Length of deck cantilever: Design of the GFRP decks is more stiffness driven rather than strength driven unlike traditional decks. Cantilever in GFRP deck tends to be much more heavily reinforced due to lower Young's modulus of GFRP bars in comparison to steel bars. To keep the same deflection limit for GFRP deck overhang, around 2.5 to 5 times more reinforcing bar area is required, depending on the modulus of elasticity of the GFRP bar. Therefore, longer cantilever length will result in heavier reinforced deck and less economical use of GFRP bar. As bars are not used in full strength, the design becomes costly and congestion of the bars would complicate construction. To end up with more economical solution the length of the cantilever needs to be optimized in design of GFRP decks. In practice, most GFRP bridge decks have cantilever length less than 1.5 m. In this study, variation of the length of the deck cantilever varied from fixed support to 1.5 m, taken in 0.5-m increments. In total, 4 different variations for length of deck cantilever were considered, namely: Fixed, 0.5, 1 and 1.5 m. In the first case, the barrier wall was considered fixed at the base.

Type of the Barrier: The parametric study was performed for PL-2 parapet with constant thickness, PL-2 barrier with tapered face and PL-3 barriers. Dimensions and the loads are specified in Table 1.1 and as presented in Chapter 4.

Barrier Length: In order to relate moments to the barrier wall longitudinal length, different barrier wall lengths were considered, namely: 3, 4, 5, 6 m. The 6-m long barrier expects to represent the continuous barrier in bridges since the aspect ratio of the wall is too large. On the

other hand, the 3-m long barrier is a short barrier used in multi-barrier segments, separated with construction joints, as the case in the Province of Alberta. This barrier expects to act as a cantilever promoting the one-way action of the wall in lieu of the two-way action of the long barrier wall.

Impact load location: Since transverse loading simulating vehicle impact creates the critical load carrying capacity, both the longitudinal and vertical loads were not considered as mentioned earlier in this thesis. Position of the horizontal load is also important, as the load applied at end locations of the barrier wall would create higher moments between the barrier wall and the deck junction than those induced at interior locations in the barrier wall subjected to similar impact loading. Table 1.1 shows the load scenario in case of end and interior locations of applied transverse loading.

5.3 FEM SAP2000 Modeling

General description of the model

In this analysis, linear elastic 3D model was used incorporating shell elements. Concrete material used was plain concrete with following properties: Compressive strength = 23.6 MPa, Modulus of Elasticity = 24.8 GPa and Poisson's ratio = 0.2. No reinforcement is considered in the modeling. End conditions of the cantilever or the deck slab included fixed joints by restraining all degrees of freedom at nodes along the support line.

PL-2 Parapet: Three-dimensional finite-element modeling, using SAP2000 software was performed on PL-2 parapet with constant thickness of 250 mm and total height of 915 mm. A factored horizontal load of 170 kN was applied over a length of 1050 mm and a height of load application of 700 mm above the deck. The deck slab thickness was taken 225 mm. The height of application of the line load was 790 mm as the asphalt thickness is 90 mm above the deck. However, due to FEA element size of 50x50 mm, the load was distributed over 2 rows of elements for the length of 1050 mm at a height of application of 800 mm in lieu of 790 mm. This would change the results by 1.25% which is considered negligible. Figure 5.1 shows elevation of the FEA model of the barrier wall along with the location of the line load at the end location of

the barrier. While Fig. 5.2 shows plan of the FEA modeling of the deck slab. It should be noted that 50x50 mm shell elements were used in the modeling to increase accuracy of results.

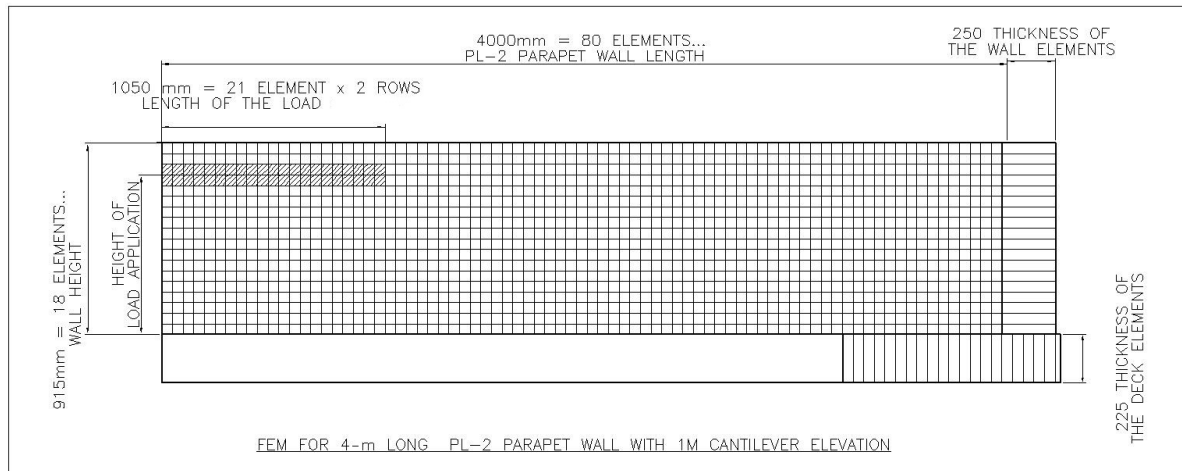


Fig. 5.1 Elevation and Section of PL-2 Parapet FE Model

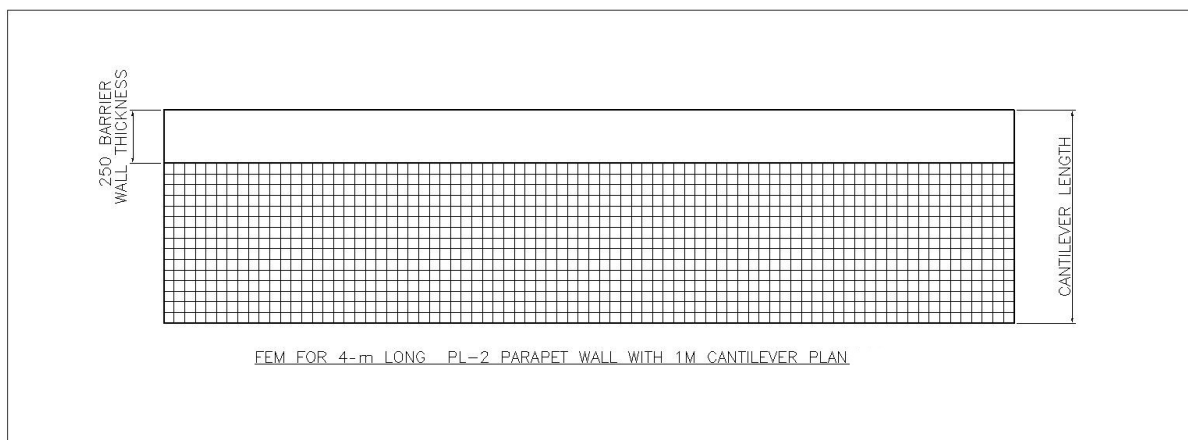


Fig. 5.2 Plan view of the PL-2 Parapet FE Model

PL-2 Barrier with Tapered face: The FEA modeling for this barrier was identical to that for PL-2 parapet with constant thickness except that the thickness of the shell elements varied in order to best-fit the tapered cross-section shown in Table 1.1. Figure 5.3 shows view of the FEA modeling of the barrier wall along with the location of the line loading at the end location of the barrier. The applied transverse loading was identical to that applied on PL-2 parapet with constant thickness.

PL-3 Barrier: Three-dimensional finite-element modeling was performed on PL-r barrier with tapered face. The dimensions of the barrier wall are shown in Table 1.1. A factored horizontal load of 357 kN was applied over a length of 2400 mm and a height of load application of 900 mm above the deck. The deck slab thickness was taken 225 mm. The height of application of the line load was 990 mm as the asphalt thickness is 90 mm above the deck. However, due to FEA element size of 50x50 mm, the load was distributed over 2 rows of elements for the length of 2400 mm at a height of application of 1000 mm in lieu of 990 mm. This would change the results by 1% which is considered negligible. Figure 5.4 shows elevation of the FEA model of the barrier wall along with the location of the line load at the end location of the barrier.

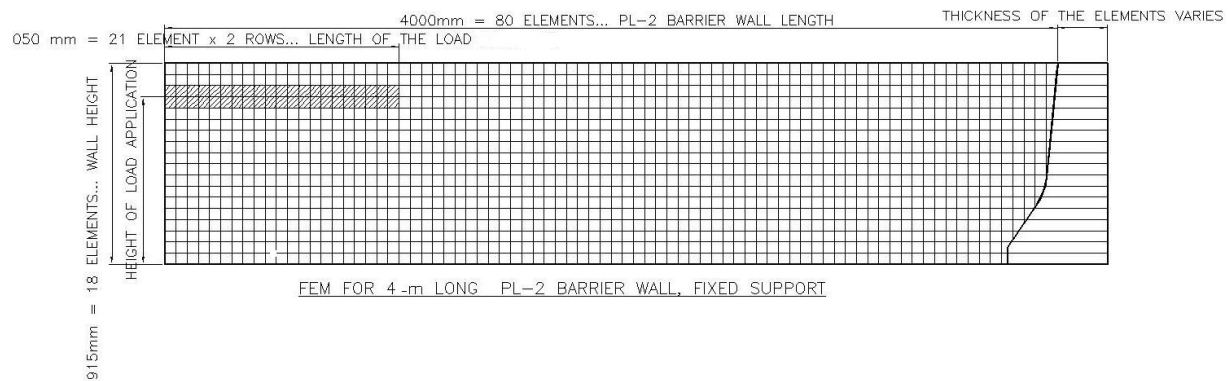


Fig. 5.3 Elevation of PL-2 Barrier wall FE Model

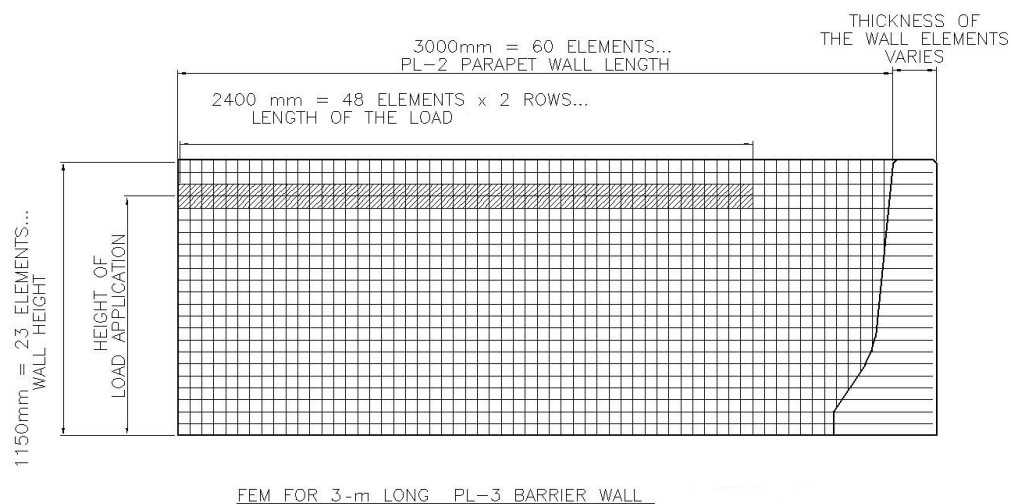


Fig. 5.4 Elevation of PL-3 Barrier Wall FE Model

5.4. FEA Results and Discussions

Tables 5.1 to 5.3 were created in the same manner as Table 1.1. Moment, shear and dispersal angles are schematically represented in Table 1.1. Two resultant moment diagrams are presented in Appendix A. One diagram result from load application in inner portion of the wall Fig. A.2 and second one shows moment results from load application at the end of the wall Fig. A.1.

5.4.1 PL-3 Barrier

Moment in inner portion of the deck per meter at face of the barrier (Table 5.1): As shown in Table 1.1, CHBDC Commentary specified this moment as 83 kN.m/m that was obtained using 1.5-m deck cantilever length. In the current study, such factored applied moment was 130 kN.m/m for barrier wall with fixed base. Also, this moment was obtained in this study as 80, 78, 77 and 74 kN.m/m for barrier lengths of 3, 4, 5 and 6 m, respectively, for 1.5-m length of deck cantilever. These values are observed to be less than that specified in the code. However, for 0.5-m length deck cantilever, this moment was obtained as 89, 87, 85 and 84 kN.m/m for barrier lengths of 3, 4, 5, and 6 m, respectively. This entails that the code value underestimates the response by a maximum of 7.2%. As such, it can be concluded that the CHBDC factored applied moment is conservative in case of barrier wall resting over a deck slab cantilever of length more than of equal 1 m, however it underestimates the factored applied moment by 57% for barrier wall connected to a rigid base and by a maximum of 7.2% for deck slab cantilever of 0.5 m or less. Shortening of the deck cantilever length result is a more rigid barrier-to-deck connection and therefore, result in higher factored applied moment. Dispersal angle for the barrier and the deck decreases with increase of cantilever length. As for the dispersal angle for barrier wall, it was observed that there are very close to those in the CHBDC, however deck dispersal angles are much smaller than the one defined in CHBDC. In any case, dispersal angle are not required in engineering design since the maximum moment per meter length of the barrier is identified.

Tensile force in inner portion of the deck at deck edge (Table 5.1): As shown in Table 1.1, CHBDC Commentary specified this tensile force in inner portion of the deck at the barrier-deck junction 144 kN/m that was obtained using 1.5-m deck cantilever length. In the current study, such factored applied tensile force was 140, 142, 143 and 144 kN/m for barrier lengths of 3, 4, 5

and 6 m, respectively, for 1.5-m length of deck cantilever. These values are observed to be almost similar to the specified in the code. However, for 0.5-m length deck cantilever, this factored tensile force was obtained as 161, 164, 166 and 169 kN/m for barrier lengths of 3, 4, 5, and 6 m, respectively. This entails that the code value underestimates the response by a maximum of 17.3%. Also, the factored tensile forces for a barrier length of 6 m, were 169, 158, and 144 kN/m for deck cantilever lengths of 0.5, 1 and 1.5 m, respectively. Thus, the tensile force in the deck increases with decrease of deck cantilever length. One may observe that the dispersal angles for the tensile forces in the barrier and the deck slab increase significantly with decrease of cantilever length.

Moment in end portion of the deck per meter at face of the barrier (Table 5.1): As shown in Table 1.1, CHBDC Commentary specified this moment as 102 kN.m/m that was obtained using 1.5-m deck cantilever length. In the current study, such factored applied moment was obtained as 144.5, 144, 143.5 and 143 kN.m/m for barrier wall with fixed base for barrier lengths of 3, 4, 5 and 6 m, respectively. This means that the CHBDC value underestimates the design moment by about 42%. It should be noted that barrier length has insignificant effect on the factored applied moment when the barrier is fixed at its base. Also, this moment was obtained in this study as 126, 114, 106 and 103 kN.m/m for barrier lengths of 3, 4, 5 and 6 m, respectively, for 1.5-m length of deck cantilever. So, one may conclude that the shorter the cantilever length, the greater the level of underestimation in code value. The maximum underestimation in code value in this case is $126/102 = 23.5\%$. Also, it can be observed that the applied factored moments for a 6-m long barrier were 118, 106 and 103 kN.m/m for deck slab lengths of 0.5, 1 and 1.5 m, respectively. As such, the factored applied moment increases with decrease in cantilever length.

Tensile force in end portion of the deck at deck edge (Table 5.1): As shown in Table 1.1, CHBDC Commentary specified this tensile force in end portion of the deck at the barrier-deck junction 161 kN/m that was obtained using 1.5-m deck cantilever length. In the current study, such factored applied tensile force was 157, 158, 160 and 160 kN/m for barrier lengths of 3, 4, 5 and 6 m, respectively, for 0.5-m length of deck cantilever. Also, for 1.5-m length deck cantilever, this factored tensile force was obtained as 135, 137, 139 and 140 kN/m for barrier lengths of 3, 4,

5, and 6 m, respectively. This entails that the code value overestimates the response which is considered safe in engineering design.

5.3.2 PL-2 barrier with tapered face and PL-2 Parapets with constant thickness

Tables 5.2 and 5.3 summarize results from the parametric study for PL-2 barrier with tapered face and PL-2 parapet with constant thickness. By inspection of data, it was observed that both barrier have similar trend and very close results. As such, for the same of analyzing the data, the following paragraphs discuss the results only for PL-2 barrier with tapered face.

Moment in inner portion of the deck per meter at face of the barrier (Tables 5.2 and 5.3): As shown in Table 1.1, CHBDC Commentary specified this moment as 38 kN.m/m that was obtained using 1.5-m deck cantilever length. In the current study, such factored applied moment was 75 kN.m/m for barrier wall with fixed base. Also, this moment was obtained in this study as 42, 41, 40 and 39.5 kN.m/m for barrier lengths of 3, 4, 5 and 6 m, respectively, for 1.5-m length of deck cantilever. These values are observed to be greater than the specified value in the code. As such, code value underestimates the response by 3.9 to 10.5% based on the length of the barrier wall. However, for 0.5-m length deck cantilever, this moment was obtained as 45.5, 44.5, 44 and 44 kN.m/m for barrier lengths of 3, 4, 5, and 6 m, respectively. This entails that the code value underestimates the response in the order of 17%. Shortening of the deck cantilever length result is a more rigid barrier-to-deck connection and therefore, result in higher factored applied moment.

Tensile force in inner portion of the deck at deck edge (Tables 5.2 and 5.3): As shown in Table 1.1, CHBDC Commentary specified this tensile force in inner portion of the deck at the barrier-deck junction 100 kN/m that was obtained using 1.5-m deck cantilever length. In the current study, such factored applied tensile force was 74, 75, 76, and 76 kN/m for barrier lengths of 3, 4, 5 and 6 m, respectively, for 1.5-m length of deck cantilever. These values are observed to be smaller than the specified value in the code. However, for 0.5-m length deck cantilever, this factored tensile force was obtained as 69, 67, 66.5, and 66 kN/m for barrier lengths of 3, 4, 5, and 6 m, respectively. This entails that the code value overestimates the response by about 32.5%. Also, the factored tensile forces for a barrier length of 6 m, were 66, 58 and 51 kN/m for deck

cantilever lengths of 0.5, 1 and 1.5 m, respectively. Thus, the tensile force in the deck increases with decrease of deck cantilever length.

Moment in end portion of the deck per meter at face of the barrier (Tables 5.2 and 5.3): As shown in Table 1.1, CHBDC Commentary specified this moment as 52 kN.m/m that was obtained using 1.5-m deck cantilever length. In the current study, such factored applied moment was obtained as 53, 52, 51, and 51 kN.m/m for barrier wall with fixed base for barrier lengths of 3, 4, 5 and 6 m, respectively, for 1.5-m length of deck cantilever, which are very similar to the CHBDC-specified value. This moment was obtained in this study for barrier wall fixed at the base as 99, 98.5, 98 and 97.5 kN.m/m for barrier lengths of 3, 4, 5 and 6 m, respectively. This means that CHBDC-specified value underestimates the response in barrier wall with fixed base by 90%. Also, it can be observed that the applied factored moments for a 6-m long barrier were 66, 58, and 51 kN.m/m for deck slab lengths of 0.5, 1 and 1.5 m, respectively. As such, the factored applied moment increases with decrease in cantilever length.

Tensile force in end portion of the deck at deck edge (Tables 5.2 and 5.3): As shown in Table 1.1, CHBDC Commentary specified this tensile force in end portion of the deck at the barrier-deck junction 142 kN/m that was obtained using 1.5-m deck cantilever length. In the current study, such factored applied tensile force was 151, 156, 158, and 158 kN/m for barrier lengths of 3, 4, 5 and 6 m, respectively, for 0.5-m length of deck cantilever. The means that code value underestimate the tensile force by about 9%. Also, for 1.5-m length deck cantilever, this factored tensile force was obtained as 158, 151, and 137 kN/m for barrier lengths of 3, 4, 5, and 6 m, respectively. This entails that the code value overestimates the response which is considered safe in engineering design.

5.5 Summary of the Findings

The parametric study conducted on PL3 and PL-2 barrier-deck system resulted in the following findings:

- 1- Overall results for factored applied moment and tensile force at the barrier-deck junction are very similar to the CHBDC specified values for the deck cantilever length of 1.5 m.

Small differences most likely come from variations in finite-element modeling and engineering judgment.

- 2- For cantilever lengths less than 1.5 m, the factored applied moment and tensile forces increase with decrease in cantilever length.
- 3- The barrier wall with fixed base, representing the case of rigid deck slab, exhibited very much larger factored applied moments than those specified in the code, in the order of 57 and 43% in case of PL-3 barrier, 97 and 90% in case of PL-2 barrier with tapered face, and 61 and 65% in case of PL-parapet with constant thickness.

Table 5.1 Finite-element results for PL-3 barrier

WALL LENGTH	3m				4m				5m				6m			
CANTILEVER	FIXED	0.5M	1 M	1.5M	FIXED	0.5M	1M	1.5M	FIXED	0.5M	1M	1.5M	FIXED	0.5M	1M	1.5M
Moment in inner portions of the deck kN/m per meter at face of barrier	130	89	82	80	130	87	81	78	130	85	79	77	130	84	78	74
Dispersal Angle for barrier	42	56	60	50	42	56	60	50	42	58	60	50	42	50	56	48
Dispersal Angle for Deck		26	21	26		18	21	26		34	21	26		34	11	26
Tensile Force in Inner Portion of Deck at Deck Edge,kN	195	161	152	140	195	164	155	142	195	166	156	143	195	169	158	144
Dispersal Angle for Barrier		34	31	0		30	31	0		30	31	0		30	31	0
Dispersal Angle for Deck		14	7	7		18	7	7		18	7	7		18	11	7
Moment in End Portion of Deck kN/m per meter at Face of Barrier	144.5	128	127	126	144	120	118	114	143.5	118	107	106	143	118	106	103
Dispersal Angle for Barrier	45	55	25	63	45	55	56	63	45	55	56	62	45	55	56	57
Dispersal Angle for Deck		25	34	20		25	34	20		25	34	20		26	34	18
Tensile Force End Portion of Deck at Deck Edge, kN	159	157	120	135	159	158	138	137	159	160	139	139	159	160	140	140
Dispersal Angle for Barrier		0	0	0		0	0	0		0	0	0		0	0	0
Dispersal Angle for Deck		1	0.5	0		1	0.5	0		1	0.5	0		1	0.5	0

Table 5.2 Finite-element results for PL-2 barrier with tapered face

WALL LENGTH	3 m				4 m				5 m				6 m			
CANTILEVER	FIXED	0.5M	1M	1.5M	FIXED	0.5M	1M	1.5M	FIXED	0.5M	1M	1.5M	FIXED	0.5M	1M	1.5M
Moment in inner portions of the deck kN/m per meter at face of barrier	75	45.5	44	42	75	44.5	43	41	75	44	43	40	75	44	42	39.5
Dispersal Angle for barrier	41	42	40	34	41	40	39	33	41	38	38	31	41	36	37	31
Dispersal Angle for Deck		48	40	38		49	40	37		50	40	36		50	40	35
Tensile Force in Inner Portion of Deck at Deck Edge, kN	130	112	96	74	130	113	97	75	130	113	97	76	130	114	98	76
Dispersal Angle for Barrier		0	18	0		0	19	0		0	20	0		0	22	22
Dispersal Angle for Deck		9	11	6		10	12	6		11	13	6		11	14	16
Moment in End Portion of Deck kN/m per meter at Face of Barrier	99	69	60	53	98.5	67	58.5	52	98	66.5	58	51	97.5	66	58	51
Dispersal Angle for Barrier	46	60	54	50	46	60	54	50	45	60	54	50	44	60	54	49
Dispersal Angle for Deck		34	52	52		34	52	52		34	52	52		34	52	51
Tensile Force in End Portion of Deck at Deck Edge,kN	149	147	145	120	149	150	148	130	149	153	149	137	149	153	151	137
Dispersal Angle for Barrier		0	3	7		0	3	7		0	3	7		0	3	7
Dispersal Angle for Deck		1	4	4		1	4	4		1	4	4		1	4	4

WALL LENGTH	3m				4m				5m				6m			
CANTELIEVER	FIXED	0.5M	1M	1.5M	FIXED	0.5M	1M	1.5M	FIXED	0.5M	1M	1.5M	FIXED	0.5M	1M	1.5M
PL-2 PARAPET																
Moment in inner portions of the deck kN/m per meter at face of barrier	61	46.5	45	41.5	61	46	44	41	61	45.5	43	40.5	61	45	42	40
Dispersal Angle for barrier	33	52	56	60	33	52	56	62	33	52	56	56	33	52	56	59
Dispersal Angle for Deck		18	16	14		18	16	14		18	16	14		18	16	14
Tensile Force in Inner Portion of Deck at Deck Edge,kN	120	100	91	80	120	101	93	80	120	103	95	81	120	104	96	82
Dispersal Angle for Barrier		20	20	20		20	20	20		20	20	20		20	20	20
Dispersal Angle for Deck		18	16	14		10	16	12		10	16	12		10	16	12
Moment in End Portion of Deck kN/m per meter at Face of Barrier	86	70	65	60	86	68	63	59	86	67	61	58	86	65	60	58
Dispersal Angle for Barrier	51	60	58	60	51	60	56	54	51	56	52	51	51	56	51	50
Dispersal Angle for Deck		16	25	26		16	26	24		14.5	7	24		14	9	22
Tensile Force in End Portion of Deck at Deck Edge,kN	151	147	140	139	151	148	144	141	151	150	145	143	151	154	146	144
Dispersal Angle for Barrier		0	0	7		0	0	7		0	0	7		0	0	7
Dispersal Angle for Deck		0.5	8	7		0.5	7	7		0.5	7	7		0.5	7	7

Table 5.3 Finite-element results for PL-2 parapet wall with constant thickness

Based on the data generated from the parametric study, Table 5.4 is proposed for the design of barrier-deck joint subjected to vehicle impact. Equations in Table 5.4 were developed using least squares method, using statistical option for curve fit in Excel software, take into account the change in the factored applied factored moment and tensile force with change in deck cantilever length as well as barrier length. The method of least squares assumes that the best-fit curve of a given type is the curve that has the minimal sum of the deviations squared (least square error) from a given set of data.

Table 5.4 Proposed design table for barrier-deck joint

		PL-3 barrier	PL-2 barrier	Pl-2 Parapet
Moment in inner portions of the deck per meter at face of barrier, kNm/m	Fixed	130	75	61
	Cantilever	$89 L_b^{-0.045} L_c^{-0.08}$	$47 L_b^{-0.07} L_c^{-0.08}$	$47 L_b^{-0.04} L_c^{-0.07}$
Tensile force in inner portion of deck at deck edge, kN/m	Fixed	175	130	120
	Cantilever	$165 L_b^{0.01} L_c^{-0.01}$	$92 L_b^{0.03} L_c^{-0.33}$	$92 L_b^{0.03} L_c^{-0.01}$
Moment in end portion of deck per meter at face of barrier, kNm/m	Fixed	144	99	86
	Cantilever	$129 L_b^{-0.01} L_c^{-0.01}$	$64 L_b^{-0.06} L_c^{-0.23}$	$68 L_b^{-0.04} L_c^{-0.13}$
Tensile force end portion of deck at deck edge, kN/m	Fixed	159	149	151
	Cantilever	$130 L_b^{0.01} L_c^{-0.16}$	$130 L_b^{0.1} L_c^{-0.16}$	$129 L_b^{0.12} L_c^{-0.13}$

Notes:

- 1- L_b = barrier length and L_c = deck cantilever length
- 2- For barrier length greater than 6 m, use values for $L_b = 6$ m.
- 3- For cantilever length greater than 1.5 m, use $L_c = 1.5$ m.

CHAPTER 6

CONCLUSIONS AND RECOMMENDATIONS FOR FUTURE RESEARCH

6.1 General

Glass fibre reinforced polymer (GFRP) bars are increasingly being used in construction as an alternative to conventional steel bar that corrode due to the use of de-icing salt in the winter times in Canada. This thesis investigates the application of GFRP bars in bridge barrier as a non-corrosive alternative to conventional steel reinforcement. A new barrier reinforcement layout was proposed to replace steel bend bars with GFRP bars with with anchorage heads. In order to design such GFRP reinforcement, CHBDC and AASHTO-LRFD design provisions were used, however no design provisions or research data in the literature were found to design the anchorage at barrier-deck slab junction. As such, pullout tests were conducted on GFRP bars with straight and headed ends, embedded in concrete slabs and concrete blocks, to determine their bonding properties. Also, testing to-collapse of full-scale bridge barrier was conducted to determine its load carrying capacity under simulated vehicle impact. In addition, finite element analysis of the barrier wall and deck slab portion was performed in order to examine the level of accuracy of the specified factored applied moments due to vehicle impact at the barrier-deck junction. The experimental findings qualified the proposed GFRP-reinforced barrier detailing when subjected to simulated vehicle impact loading. The following sections summarize the conclusions of this research as well as recommendations for further research.

6.2 Conclusions

The experimental findings on the pullout tests on GFRP bars embedded in reinforced concrete slab and concrete blocks can be summarized as follows:

1. For straight bars of 12 and 16 mm diameters, the pullout failure was always due to bond failure in the interface between outer surface of the bars and concrete.
2. For headed bars, the head has a larger contact area with concrete, which can lead to concrete conical failure at shallower embedment depths. In order to avoid conical failure of concrete, minimum embedment length can be calculated using available equation in

Chapter 12 of the Concrete Design Handbook quoted from CSA A23.3-04 Standard. The equation is based on tensile breakout capacity of the concrete. Minimum embedment length would ensure that pullout failure of headed anchor will be due to failure of the head, and therefore result in the maximum possible pullout strength of the headed anchor.

3. Results show that the larger bar diameter produces larger bond stresses. This conclusion was based on the unconfined pullout tests, because results from the tests that had a confinement effect would lead to opposite conclusions.
4. For headed bar pullout capacity, it is recommended to consider maximum pullout capacity as a pullout capacity of the head only. In order to reach failure of the head, minimum embedment length needs to be calculated or obtained by testing. It is suggested to use the pullout equation specified in CSA A23.3 Standard for tensile concrete breakout capacity. Theoretically, once the minimum embedment length is obtained for a specific head capacity for a specific concrete strength, further increase in embedment length should not increase pullout capacity of the headed anchor. This conclusion can be made mainly for the normal strength concrete.

The experimental findings on the static tests to-collapse on the proposed PL-3 GFRP-reinforced barrier can be summarized as follows:

- 1- The experimental ultimate load carrying capacities at the interior load and end load locations were observed to be far greater than the factored design loads specified in AASHTO-LRFD Specifications and CHBDC.
- 2- It was observed that the failure mode of the GFRP-reinforced barrier wall is punching shear at the location of the impact loading. As such, the AASHTO-LRFD yield-line failure equations cannot be applied to the design of GFRP-reinforced barrier wall.
- 3- As punching shear caused failure in the barrier under equivalent vehicle impact loading, analytical investigation was performed in order to find the best available in the codes punching shear equation. This equation can be used to estimate load carrying capacity of the PL-3 barrier wall. Based on the correlation of experimental finding and available code punching shear capacity, it is recommended to use punching shear equations in CSA 806-11 and ACI 440-1R-06 Standard to predict the barrier resistant to equivalent vehicle impact loading.

- 4- Testing 1-m length of the barrier wall at locations where vertical GFRP bars are spaced at 300 mm at interior portions and at 150 mm at end portion of the barrier revealed that the proposed anchor details shown in Fig. 1.3, incorporated GFRP bars with headed end in lieu of bent bars, are adequate to resist factored anchorage forces and moments specified in CHBDC by a significant margin.

The parametric study conducted, using the finite-element modeling, on PL3 and PL-2 barrier-deck system resulted in the following findings:

1. Overall results for factored applied moment and tensile force at the barrier-deck junction are very similar to the CHBDC specified values for the deck cantilever length of 1.5 m. Small differences most likely come from variations in finite-element modeling and engineering judgment.
2. For cantilever lengths less than 1.5 m, the factored applied moment and tensile forces increase with decrease in cantilever length.
3. The barrier wall with fixed base, representing the case of rigid deck slab, exhibited very much larger factored applied moments than those specified in the code, in the order of 57 and 43% in case of PL-3 barrier, 97 and 90% in case of PL-2 barrier with tapered face, and 61 and 65% in case of PL-parapet with constant thickness.
4. Based on the data generated from the parametric study, a design table was deduced for the design of barrier-deck joint subjected to vehicle impact, taking into account the change in the factored applied factored moment and tensile force with change in deck cantilever length, barrier length and whether the barrier is fixed to a rigid deck slab.

Recommendations for Future Research

Bases on the results from this thesis, the following recommendations can be considered for future research.

1. It is recommended to conduct pullout tests of headed GFRP bars, similar to those conducted in this thesis, at higher concrete strength in the order of 60 MPa as well as in ultra-high performance concrete.

2. It is recommended to use unconfined test method in testing pullout strength. Cube Pullout test results have much higher stresses than slab pullout results. It is also recommended to investigate the magnitude of confinement effect present in cube pullout test and then construct a finite-element model to estimate realistic bond stresses.
3. Evaluate, using the finite element modeling, the factored resistance force to be carried by the barrier wall subjected to line loading simulating vehicle impact, considering both material and geometric nonlinearity.

APPENDIX A

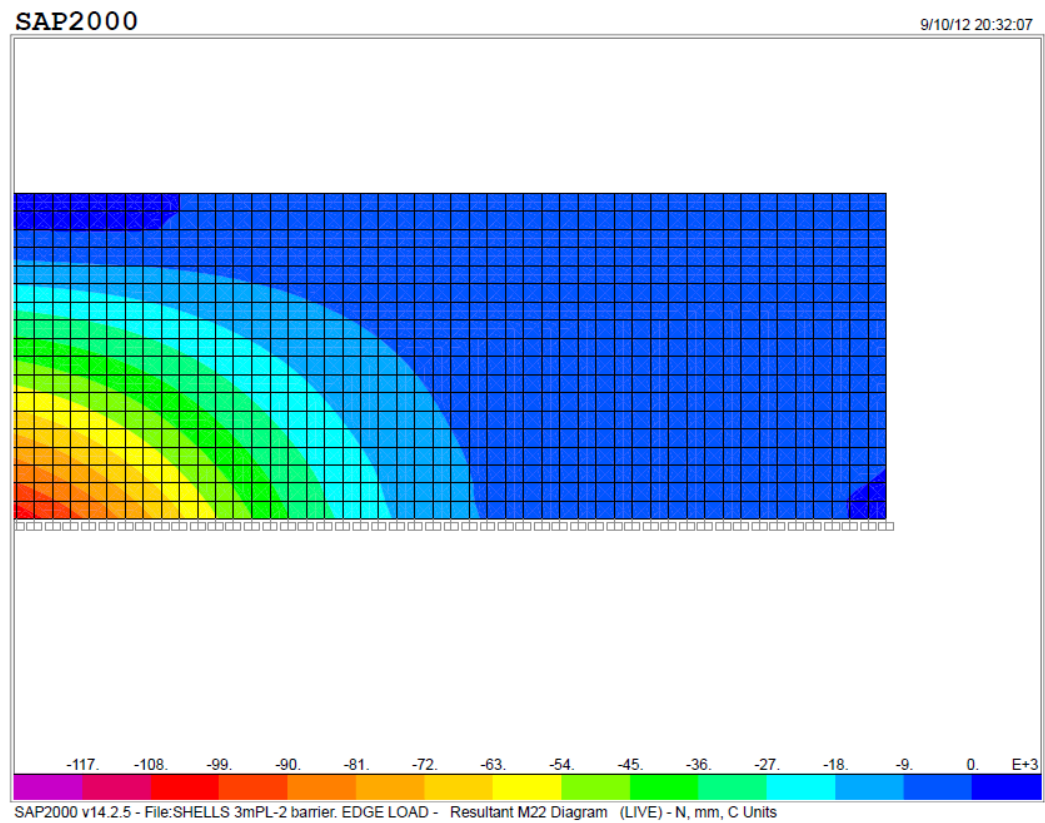


Figure A.1 Moment Diagram for PL-2 Barrier Wall with load application at the end of the wall.

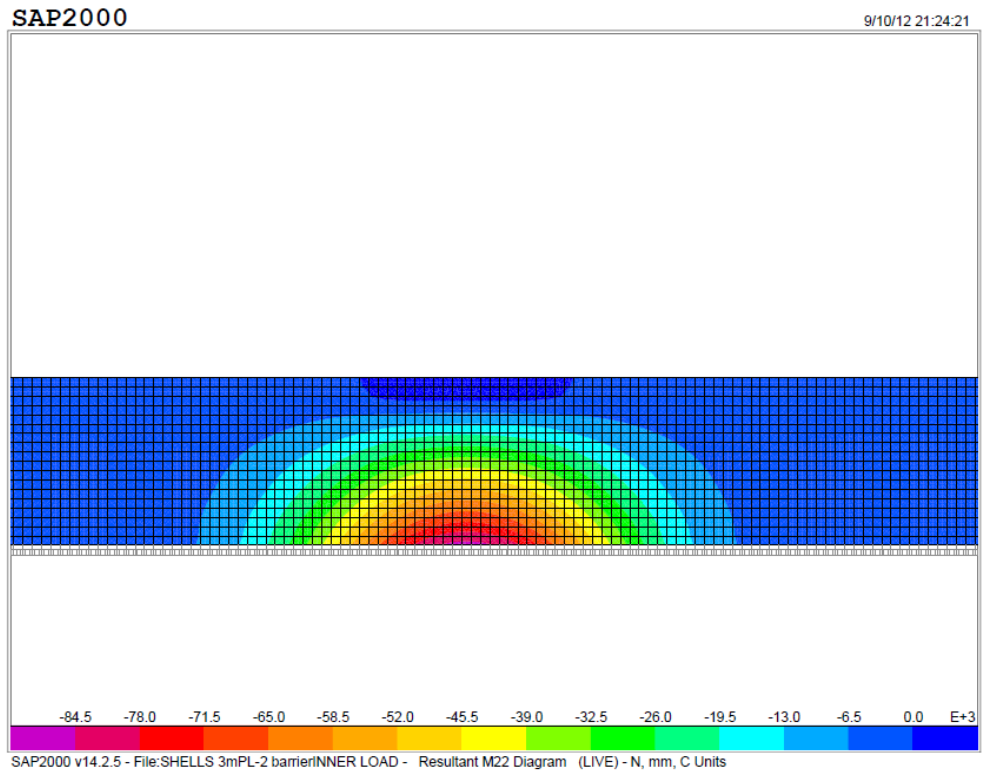


Figure A.2 Moment Diagram for PL-2 Barrier Wall. Load application at inner portion of the wall.

APPENDIX B

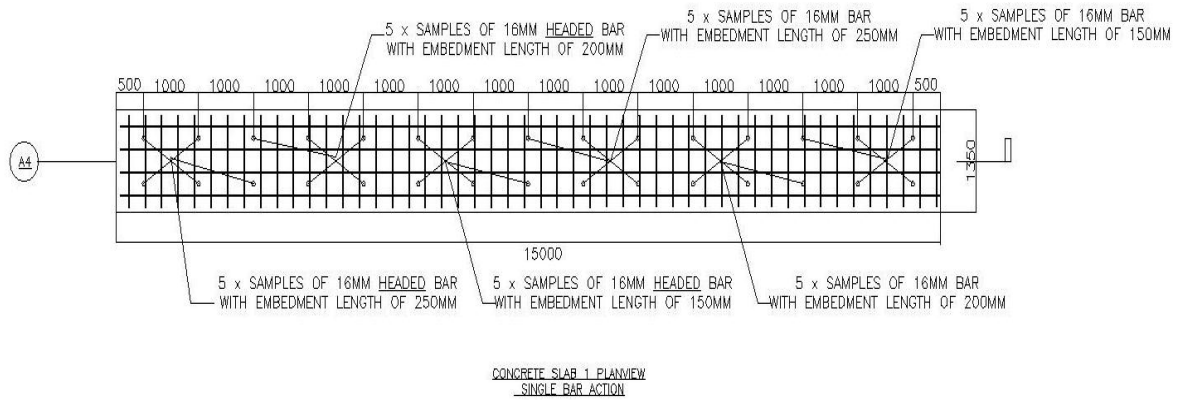


Figure B.1 16M bar position in concrete slab, casted for pullout tests and dimensions of the casted slab.

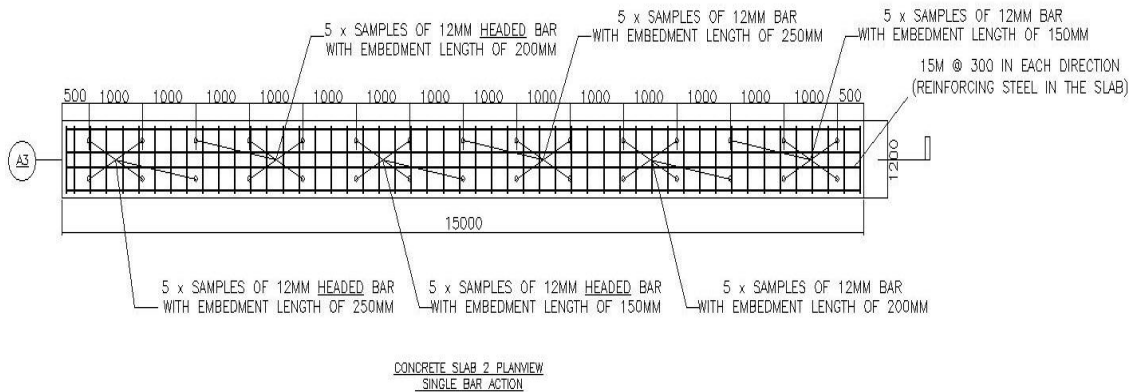


Figure B.1 12M bar position in concrete slab, casted for pullout tests and dimensions of the casted slab.

REFERENCES

- AASHTO. (1977). AASHTO Guide for Selecting, Locating, and Designing Traffic Barriers, American Association of State Highway and Transportation Officials, Washington DC, USA.
- AASHTO. (1989). AASHTO Guide Specifications for Bridge Railings, American Association of State Highway and Transportation Officials, Washington DC, USA.
- AASHTO. (2012). AASHTO-LRFD Bridge Design Specifications. American Association of State Highway and Transportation Officials, Washington D.C.
- Ametrano, D., Bond Characteristics of Glass Fibre Reinforced Polymer Bars Embedded In High Strength And Ultra-High Performance Concrete. M.A.SC. Thesis, Civil Engineering Department, Ryerson University, Toronto, Ontario, Canada.
- Achillides, Z., Pilakoutas, K. (2004), “Bond Behavior of Fiber Reinforced Polymer Bars under Direct Pullout Conditions”, ASCE Journal of Composites for Construction, Vol. 8, No. 2, March-April 2004.
- Alberson, D., Williams, W., Boyd, C., and Bloshock, M. (2005). Analysis and Testing of the Florida Jersey Safety Shaped Bridge Rail. TRB 2005 Annual Meeting, Transportation Research Board, pp. 1-24.
- Alunno Rossetti, V., Galeota, V., and Giammatteo, M. M. (1995). Local bond stress-slip relationships of glass fibre reinforced plastic bars embedded in concrete. Materials and Structures, 28 (6), 340-344.
- Aly, R. S., & Benmokrane, B. (2005). Flexural Behaviour of Lap Splicing CFRP Bars in Concrete: Bundled Bars. Proceedings of the Third International Conference on Composites in Constructions, (pp. 807-814). Lyon.
- Aly et al. (2005) Bond splitting strength of lap splicing of GFRP bars in concrete. Proc., 33rd Annual General Conference of the Canadian Society for Civil Engineering, (pp. 1- 10). Toronto.
- Aly, R., Benmokrane, B., and Ebead, U. (2006). Tensile lap splicing of fibre-reinforced polymer reinforcing bars in concrete. ACI Structural Journal, 103 (6), 857-864.

- Al-Zaharani, M.H., Nanni, A., Al-Dulaijan, S.U., and akis C. E. (1996. Bond of FRP to Concrete in Reinforcement Rods with Axisymmetric Deformations”. Proc., 2nd Int. Conf. on Advanced Composite Materials in Bridge Structures.
- American Concrete Institute (2006). Guide For The Design And Construction of Concrete Reinforced With FRP Bars”, ACI 440.1R-07, American Concrete Institute, Farmington Hills,Mi.
- Baena, M., Torres, L., Turon, A., and Barris, C. (2009). Experimental study of bond behaviour between concrete and FRP bars using a pull-out test. Composites:Part B , 40 (8), 784-797.
- Bank, L., Yin, J., and Gentry, T. (1997). Pendulum Impact Tests on Steel W-Beam Guardrails. Journal of Transportation Engineering, 124(4): 319-325.
- Banthia, N., Al-Asaly, M., and Ma, S. (1995). “Behavior of Concrete Slabs Reinforced with Fiber-Reinforced Plastic Grid,” Journal of Materials in Civil Engineering, Vol. 7 , No. 4, pp. 252-257.
- Benmokrane, B., and Masmoudi, R. (1996). FRP C-bar as reinforcing rod for concrete structures. Proceedings of the 2nd Intern. Conf. on Advanced Composite Materials in Bridges and Structures (ACMBS II), Canadian Society of Civil Engineering, Montreal, pp. 181-188.
- Bielenberg, B., Faller, R., Reid, J., Rohde, J., and Sicking D. (2003). Design and Testing of Tie-Down Systems for Temporary Barriers”. Transportation Research Board, 82nd Annual Meeting, CD-ROM Paper No. 03-3146: 1-25.
- Bisby, L. A. (2006). ISIS Canada Educational Module No. 2: FRP Composites for Construction. ISIS Canada Corporation, Winnipeg, Manitoba, Canada.
- Bisby, L. A. (2006). ISIS Canada Educational Module No. 3: FRP Composites for Construction. ISIS Canada Corporation, Winnipeg, Manitoba, Canada,
- Buth, C., Menges, W., and Williams, W. (2000). Test Level 4 Bridge Rails. Transportation Research Record 1720, 80-94.
- Chaallal, O., and Benmokrane, B. (1993). Pullout and bond of glass fibre rods embedded in concrete and cement grout. Materials and Structures , 26 (3), 167-175.
- Consenza E, Manfredi G, and Realfonzo R. (1997). Behavior And Modeling of Bond of FRP Rebars to Concrete. Journal of Composites for Construction, May 1997, p.40-51

- Consolazio, G., Chung, J., and Gurley, K. (2003). Impact Simulation and Full Scale Crash Testing of a Low Profile Concrete Work Zone Barrier. *J. of Computers & Structures*, 81: 1359-1374.
- CSA. (2006a). Canadian Highway Bridge Design Code, CAN/CSA-S6-06. Canadian Standard Association, Toronto, Ontario, Canada.
- CSA. (2006b). Commentaries of the Canadian Highway Bridge Design Code, Canadian Standard Association, Toronto, Ontario, Canada.
- CSA. (2002). Design and Construction of Building Components with Fibre Reinforced Polymers, CAN/CSA S806-02. Canadian Standards Association, Toronto, Ontario, Canada.
- CSA (2005). Design of Concrete Structures, CSA-A23.3-05. Cement Association of Canada.
- Darwin, D., Tholen, M. L., Idun, E. K., and Zuo, J. (1996). Splice Strength of High Relative Rib Area Reinforcing Bars. *ACI Structural Journal*, 93 (1), 95-107.
- Darwin, D., and Graham, E. K. (1993). Effect of Deformation Height and Spacing on Bond Strength of Reinforcing Bars. SL Report, University of Kansas Center for Research, Lawrence, Kans.
- Deitz D, Harik I., Gesund H.,and Zatar W. (2004). Barrier Wall Impact Simualtion of Reinforced Concrete Decks with Steel and Glass Fiber Reinforced Polymer Bars. *Journal of Composites for Construction*,8(4): 369-373.
- El-Gamal, S., Tobbi, H., El-Sayed, A., and Benmokrane, B. (2007). Impact Testing of Concrete Bridge Barriers Reinforced with New GFRP Bars (Types 201 and 301). Technical Report submitted to Ministry of Transportation of Quebec, October.
- Ehsani, M. R., Saadatmanesh, H., and Tao, S. (1996). Bond Behavior and Design Recommendations for Fiber-Glass Reinforcing Bars. *Proceedings of the First International Conference on Composites in Infrastructure*, Tucson, Ariz, pp. 466-476.
- Ehsani, M. R., Saadatmanesh, H., and Tao, S. (1995). Bond of hooked glass fibre reinforced plastic (GFRP) reinforcing bars to concrete. *ACI Materials Journal*, 92 (4), 391-400.
- Eligehausen, R. (1979). Bond in Tensile Lapped Splices of Ribbed Bars with Straight Anchorages. German Institute for Reinforced Concrete. Berlin: Publication 301.
- El-Ghandour, A.W., Pilakoutas, K., Waldron, P. (1997). "Behavior of FRP Reinforced Concrete Flat Slabs," in *Third International RILEM Symposium on Non-Metallic (FRP) Reinforcement for Concrete Structures (FRPRCS-3)*, pp. 567-574.

- El-Ghandour, A.W., Pilakoutas, K., Waldron, P. (2003). "Punching Shear Behavior of Fiber Reinforced Polymers Reinforced Concrete Flat Slabs: Experimental Study," *Journal of Composites for Construction*, Vol. 7, No. 3, pp. 258-265.
- El-Salakawy, E., Masmoudi, R., Benmokrane, B., Brière, F., and Desgagne, G. (2005). "Pendulum Impacts on Concrete Bridge Barriers Reinforced with Glass Fiber-Reinforced Polymer Composite Bars". *Canadian Journal of Civil Engineering*, 31: 539- 552.
- El-Salakawy E., Masmoudi R., Benmokran B., Briere F., and Desgagne G.,(2003) Concrete Bridge Barriers Reinforced with Glass Fibre-Reinforced Composite Bars, *ACI Structural Journal*, Vol. 100, No.6, Nov.-Dec., pp.815-824.
- Hao, Q., Wang, Y., He, Z., and Ou, J. (2009). Bond strength of glass fiber reinforced polymer ribbed rebars in normal strength concrete. *Construction and Building Materials* , 23 (2), 865-871.
- Harajli, M. H., Hamad, B. S., and Rteil, A. A. (2004). Effect of Confinement on Bond Strength between Steel Bars and Concrete. *ACI Structural Journal*, 101(5), 595-603.
- Hassan M., Ahmed E.A., and Benmokrane, B. (2012) Punching Shear Strength Prediction of FRP Reinforced Flat Slabs, 6th International Conference on Advanced Composite Materials in Bridges and Structures, Kingston, pp. 1-8.
- Itoh, Y., Liu, C., and Suzuki, S. (2000). Impact Performance and Safety of Steel Highway Guard Fences. *Structural Failure and Plasticity*, Elsevier Science Ltd, pp. 79-85.
- Jacobson D.A., Bank L.C., Oliva M.G., and Russel J.S. (2005). Punching Shear Capacity of Double Layer FRP Grid Reinforced Slabs. *Proceedings of the 7th International Symposium on Fiber-Reinforced (FRP) Polymer Reinforcement for Concrete Structures*, paper No. SP-230-49, pp. 857-876.
- Johnson, David (2009) Investigation of Glass Fibre Reinforced Polymer Reinforcing Bars as Internal Reinforcement for Concrete Structures M.A.SC. Thesis,Civil Engineering Department, University of Toronto, Toronto, Ontario, Canada.
- Larralde, J., and Silva-Rodriguez, R. (1993). Bond and slip of FRP reinforcing bars in concrete. *Journal of Materials in Civil Engineering*, 5(1), 30-40.
- Maheu, J. and Bakht, B. (1994). A New Connection Between Concrete Barrier Walls and Bridge Decks," *Proceedings of the CSCE Annual Conference*, Winnipeg, Manitoba, 224-229.

- Mak, K., Gripne, D., and McDevitt, C. (1994). Single-Slope Concrete Bridge Rail. Transportation Research Record, 1468: 25- 33.
- Marzougui, D., Buyuk, M., Kan, C., and Opeila, K. (2008). Safety Performance Evaluation of Portable Concrete Barriers. TRB 2008 Annual Meeting CD-ROM, 1-20.
- Matthys, S., and Taerwe, L., 2000, "Concrete Slabs Reinforced with FRP Grids: One-Way Bending," Journal of Composites for Construction, V. 4, Aug., pp. 145-153.
- Mosley, C. P., Tureyen, A. K., and Frosch, R. J. (2008). Bond Strength of Nonmetallic Reinforcing Bars. ACI Structural Journal, 105 (5), 634-642.
- Newhook, J., & Svecova, D. (2006). Reinforcing Concrete Structures with Fibre-Reinforced Polymers. ISIS Canada Corporation, Winnipeg, Manitoba, Canada.
- Okelo, R., and Yuan, R. L. (2005). Bond strength of fibre reinforced polymer bars in normal strength concrete. Journal of Composites for Construction, 9 (3), 203-213.
- Okelo, R. (2007). Realistic bond strength of FRP bars in NSC from beam specimens. Journal of Aerospace Engineering, 20 (3), 133-140.
- Orangun, C. O., Jirsa, J. O., and Breen, J. E. (1977). Reevaluation of Test Data on Development Length and Splices. ACI Proceedings, 74 (3), 114-122.
- Ospina, C. E.; Alexander, S. D. B.; and Cheng, J. J. R., 2003, "Punching of Two-Way Concrete Slabs with Fiber- Reinforced Polymer Reinforcing Bars or Grids," ACI Structural Journal, V. 100, No. 5, Sept.-Oct., pp. 589-598.
- Pahn, M. (2008). Monitoring of Bond Test and Pull-out Tests for ComBar G16 Provided with Headed Stud Connectors 2008, Technical Report for Schoeck Bauteil GmbH, Technische Universität Kaiserslautern, Germany, pp. 1-17.
- Pefeifer, B. and Sickling, D. (1997). Development of a Metal-Cutting Guardrail Terminal. Transportation Research Record 1258, 1-10.
- Plaxico, C., Ray, M., and Hiranmayee, K. (2000). Comparison of the Impact Performance of the G4(1W) and G4(2W) Guardrail Systems under NCHRP Report 350 Test 3-11 Conditions. TRB Annual Meeting, 1-32.
- Plaxico, C. A., Patzner, G. S., and Ray, M. H. (1998). Response of Guardrail Posts under Parametric Variation of Wood and Soil Strength. Transportation Research Board, 1- 27.

- Ranzo, A., and Bonin, G. (2005). Dynamic Actions on Bridge Slabs due to Heavy Vehicle Impact on Roadside Barriers. TRB 2005 Annual Meeting, Transportation Research Board, pp. 1-11.
- Ray, M., and Patzner, G. (1997). A Finite-Element Model of the Modified Eccentric Loader Breakaway Cable Terminal (MELT). FHWA Vehicle Crash Anal. Annual Conf. Proc., pp. 33-53.
- RCCAO. (2007). Ontario's Bridges Bridging the Gap. Report prepared by MMM Group for Residential and Construction Alliance of Ontario, RCCAO, 56 pages.
- Ross, H., Sicking D, Zimmer R, and Michie J. (1993). NCHRF Report 350: Recommended Procedures for the Safety Performance Evaluation of Highway Features". TRB, National Research Council, Washington, D.C.
- Schoeck Canada Inc. 2011. ComBAR Technical Information. www.schoeck-canada.com.
- Sennah K., Tropynina E., Mahmoud Z. (2012). Ultimate Load Tests on PL-3 Bridge Barrier Reinforced with GFRP bars with Ribbed Surface and Headed Ends, 3rd International Specialty Conference, Edmonton.
- Sennah K., Juette B., Weber A., and Witt C. (2011). Vehicle Crash Testing of a GFRP-Reinforced PL-3 Concrete Bridge Barriers. Proceedings of the 4th International Conference on Durability & Sustainability of Fibre Reinforced Polymer Composites for Construction and Rehabilitation, Quebec City, Quebec, pp. 417- 424.
- Shield, C. K., French, C. W., and Retika, A. (1997). Thermal and mechanical fatigue effects on GFRP rebar- concrete bond. Proc., Third Int. Symp. on Non-Metallic Reinforcement for Concrete Structures, (pp. 381- 388). Sapporo, Japan.
- Tam, S., Sheikh, S. (2008). Behavior Of Fibre Reinforced Polymer (FRP) And FRP Bond Under Freeze Thaw Cycles And Sustained Load", Fourth International Conference on Composites in Civil Engineering (CICE 2008), Zurich, Switzerland.
- Tang, B.E. (1997). Fibre Reinforced Polymer Composites Applications in USA. First Korea USA Road Workshop Proceedings, FHWA, January 28-29.
- Tepfers, R. (1973). A Theory of Bond Applied to Overlapping Tensile Reinforcement Splices for Deformed Bars. Chalmers University of Technology, Division of Concrete Structures, Goteborg.

- Thomson, R., Romilly, D., and Navin, F. (1999). Two-Dimensional Modeling of Collision Dynamics of Deflecting Concrete Barriers. *Transportation Research Record*, 1690: 103-109.
- Tighiouart, B., Benmokrane, B., and Gao, D. (1998). Investigation of bond in concrete member with fibre reinforced polymer (FRP) bars. *Construction and Building Materials*, 12, 453-462.
- Tropynina, E., and Goremyk, S. (2009). Experimental Study of PL-3 Bridge Barrier Wall Reinforced With GFRP Bars. Undergraduate Thesis Project, Department of Civil Engineering, Ryerson University, Toronto, Ontario, Canada.
- Uddin, W. and Hackett, R. (1998). Simulation of Vehicle Impact and Crashworthiness Analysis of a Modified Thrie-Beam Guardrail. *TRB Annual Meeting*, 1-28.
- Untrauer, R. E. (1965). Development Length for Large High Strength Reinforcing Bars. *ACI Journal*, 62 (9), 1153-1154.
- Wambeke, B. W. (2003). Development length of glass fibre reinforced polymer bars in concrete. MS Thesis, University of Minnesota, Minneapolis.
- Wambeke, B. W., and Shield, C. K. (2006). Development length of glass fibre-reinforced polymer bars in concrete. *ACI Structural Journal*, 103 (1), 11-17.
- Wekezer, J., Wuttrich, R., and Ramaley, M. (2000). Performance Problems and Structural Retrofit Analysis of Existing BCT's. *Journal of Performance of Constructed Facilities*, 14(3): 118-125.
- Zaouk, A., N. Bedewi, and L. Meczowski. (1998). Development and Validation of Detailed Chevrolet C-1500 Pickup Truck Model for Multiple Impact Applications. Presented at 77th Annual Meeting of the Transportation Research Board, Washington, D.C.